

Washington University in St. Louis  
**Washington University Open Scholarship**

---

Engineering and Applied Science Theses &  
Dissertations

McKelvey School of Engineering

---

Winter 12-15-2015

# Clinical Application of Electrocardiographic Imaging in Patients with Ischemic Cardiomyopathy, Early Repolarization Syndrome and Brugada Syndrome

Junjie Zhang

*Washington University in St. Louis*

Follow this and additional works at: [https://openscholarship.wustl.edu/eng\\_etds](https://openscholarship.wustl.edu/eng_etds)



Part of the [Engineering Commons](#)

---

## Recommended Citation

Zhang, Junjie, "Clinical Application of Electrocardiographic Imaging in Patients with Ischemic Cardiomyopathy, Early Repolarization Syndrome and Brugada Syndrome" (2015). *Engineering and Applied Science Theses & Dissertations*. 144.  
[https://openscholarship.wustl.edu/eng\\_etds/144](https://openscholarship.wustl.edu/eng_etds/144)

This Dissertation is brought to you for free and open access by the McKelvey School of Engineering at Washington University Open Scholarship. It has been accepted for inclusion in Engineering and Applied Science Theses & Dissertations by an authorized administrator of Washington University Open Scholarship. For more information, please contact [digital@wumail.wustl.edu](mailto:digital@wumail.wustl.edu).

WASHINGTON UNIVERSITY IN ST. LOUIS

School of Engineering and Applied Science

Department of Biomedical Engineering

Dissertation Examination Committee:

Yoram Rudy, Chair

Jianmin Cui

Richard B. Schuessler

Timothy W. Smith

Pamela K. Woodard

Clinical Application of Electrocardiographic Imaging

in Patients with Ischemic Cardiomyopathy,

Early Repolarization Syndrome and Brugada Syndrome

by

Junjie Zhang

A dissertation presented to the  
Graduate School of Arts & Sciences  
of Washington University in  
partial fulfillment of the  
requirements for the degree  
of Doctor of Philosophy

December 2015

St. Louis, Missouri

# Table of Contents

List of Figures .....	v
List of Tables .....	vii
Acknowledgments.....	viii
Abstract .....	xi
Chapter 1: Introduction.....	1
1.1 The ECGI Methodology.....	2
1.2 Validation of ECGI in Animal Models and Human Studies.....	3
1.3 Dissertation Organization.....	4
Chapter 2: Noninvasive High-Resolution Cardiac Mapping in Ischemic Cardiomyopathy Patients: the Electrophysiological Substrate in Relation to Ventricular Arrhythmias and Arrhythmic Risk.....	6
2.1 Abstract .....	6
2.2 Introduction .....	7
2.3 Methods.....	9
2.3.1 Patient Population .....	9
2.3.2 Noninvasive Mapping.....	9
2.3.3 Data Analysis .....	10
2.3.4 Statistical analysis .....	12
2.4 Results .....	13
2.4.1 Characteristics of Abnormal EP Substrate .....	14
2.4.2 Relationship between Ventricular Arrhythmias and EP Substrate.....	19
2.4.3 Comparison of EP Substrate Properties between VT Patients and Non-VT patients .....	21
2.5 Discussion .....	23
2.5.1 Key Findings.....	23
2.5.2 The EP Scar Substrate.....	24
2.5.3 Substrate Mapping and Ablation.....	25
2.5.4 ECGI-recorded Scar EGMs and Far-field Deflections .....	25
2.5.5 Scar-related Arrhythmias .....	26
2.5.6 Risk Stratification for VT .....	27

2.5.7	Limitations .....	28
2.6	Conclusions .....	29
2.7	Supplemental Material .....	29
2.7.1	Maps of EP Substrate and Activation Sequence for VT Patients .....	29
2.7.2	Maps of EP Substrate for Non-VT Patients .....	47
2.7.3	Video Files (available in the attached CD): ECGI Activation Movies .....	62
Chapter 3: The Electrophysiological Substrate of Early Repolarization Syndrome: Noninvasive Mapping in Patients .....		
3.1	Abstract .....	63
3.2	Introduction .....	64
3.3	Methods .....	65
3.3.1	Patient Population .....	65
3.3.2	Noninvasive Mapping .....	66
3.3.3	Data Analysis .....	66
3.3.4	Statistical Analysis:.....	67
3.4	Results:.....	69
3.4.1	EGM Characterization and Localization.....	69
3.4.2	Epicardial Activation .....	71
3.4.3	Epicardial Repolarization.....	74
3.4.4	Ventricular Arrhythmias .....	75
3.5	Discussion: .....	77
3.6	Conclusions:.....	83
Chapter 4: The Cardiac Electrophysiologic Substrate Underlying the ECG Phenotype and Electrogram Abnormalities in Brugada Syndrome Patients .....		
4.1	Abstract .....	84
4.2	Introduction .....	85
4.3	Methods .....	87
4.3.1	Patient Population .....	87
4.3.2	Noninvasive Mapping .....	87
4.3.3	Simulation .....	91
4.3.4	Statistical Analysis.....	91

4.4	Results .....	92
4.4.1	BrS Abnormal EGM Characteristics and Localization .....	92
4.4.2	BrS Activation .....	94
4.4.3	BrS Repolarization.....	96
4.4.4	Effects of Increased HR in BrS.....	96
4.4.5	Comparison between BrS and Non-BrS RBBB.....	98
4.5	Discussion .....	100
4.5.1	Abnormal EGM Characteristics and Localization .....	101
4.5.2	Substrate for Abnormal Conduction .....	101
4.5.3	Substrate for Abnormal Repolarization .....	104
4.5.4	Examining the Coexistence of Conduction and Repolarization Substrates Using Increased HR.....	106
4.5.5	Comparison to Non-BrS RBBB.....	107
4.5.6	Limitations .....	107
4.6	Conclusions .....	108
Chapter 5:	Concluding Remarks and Future Work .....	110
5.1	Concluding Remarks .....	110
5.2	Future Work .....	111
References	.....	113
Appendix: Case Reports	.....	125
A1.	Continuous ECGI Mapping of Spontaneous VT Initiation, Continuation and Termination with Antitachycardia Pacing .....	125
A2.	Electrophysiologic Mechanism of Deteriorating Cardiac Function in a Patient with Inappropriate CRT Indication and Frequent Ventricular Ectopy .....	127
Curriculum Vitae	.....	130

## List of Figures

Figure 1-1: ECGI Procedure .....	3
Figure 2-1: Far-field Potential Identification. ....	11
Figure 2-2: Representative Electrograms (EGMs).....	14
Figure 2-3: The abnormal electrophysiological substrate in a non-VT patient (control) with an inferior infarct.....	16
Figure 2-4: The abnormal electrophysiological substrate in a VT patient (case) .....	17
Figure 2-5: The electrophysiological substrate in relation to ventricular arrhythmias. ....	18
Figure 2-6: Comparison of the electrophysiological substrate properties between VT patients (case) and non-VT patients (control).....	21
Figure 2-7: Patient #1: VT patient; inferior myocardial infarction.....	30
Figure 2-8: Patient #2: VT patient; inferior myocardial infarction.....	31
Figure 2-9: Patient #3: VT patient; apical myocardial infarction .....	32
Figure 2-10: Patient #4: VT patient; apical myocardial infarction .....	33
Figure 2-11: Patient #5: VT patient; apical myocardial infarction .....	34
Figure 2-12: Patient #6: VT patient; inferior myocardial infarction.....	35
Figure 2-13: Patient #7: VT patient; inferior and infero-lateral myocardial infarction .....	36
Figure 2-14: Patient #8: VT patient; anterior myocardial infarction .....	37
Figure 2-15: Patient #9: VT patient; inferior and infero-lateral myocardial infarction .....	38
Figure 2-16: Patient #10: VT patient; inferior and apical myocardial infarction .....	39
Figure 2-17: Patient #11: VT patient; anterior and apical myocardial infarction.....	40
Figure 2-18: Patient #12: VT patient; anterior and apical myocardial infarction.....	41
Figure 2-19: Patient #13: VT patient; anterior, lateral and inferior myocardial infarction .....	42
Figure 2-20: Patient #14: VT patient; anterior myocardial infarction .....	43
Figure 2-21: Patient #15: VT patient; lateral, inferior and apical myocardial infarction .....	44
Figure 2-22: Patient #16: VT patient; anterior and apical myocardial infarction.....	45
Figure 2-23: Patient #17: VT patient; inferior and apical myocardial infarction .....	46
Figure 2-24: Patient #18: Non-VT patient; inferior myocardial infarction .....	47
Figure 2-25: Patient #19: Non-VT patient; apical, inferior and infero-lateral myocardial infarction .....	48
Figure 2-26: Patient #20: Non-VT patient; apical and inferior myocardial infarction .....	49
Figure 2-27: Patient #21: Non-VT patient; inferior myocardial infarction .....	50
Figure 2-28: Patient #22: Non-VT patient; inferior myocardial infarction .....	51
Figure 2-29: Patient #23: Non-VT patient; apical and inferior myocardial infarction .....	52
Figure 2-30: Patient #24: Non-VT patient; apical and inferior myocardial infarction .....	53
Figure 2-31: Patient #25: Non-VT patient; apical myocardial infarction.....	54
Figure 2-32: Patient #26: Non-VT patient; inferior myocardial infarction .....	55

Figure 2-33: Patient #27: Non-VT patient; inferior myocardial infarction .....	56
Figure 2-34: Patient #28: Non-VT patient; apical myocardial infarction.....	57
Figure 2-35: Patient #29: Non-VT patient; inferior myocardial infarction .....	58
Figure 2-36: Patient #30: Non-VT patient; anterior, apical and inferior myocardial infarction.....	59
Figure 2-37: Patient #31: Non-VT patient; anterior and apical myocardial infarction.....	60
Figure 2-38: Patient #32: Non-VT patient; anterior and apical myocardial infarction.....	61
Figure 3-1: Epicardial J-wave Distribution and Magnitude .....	70
Figure 3-2: Activation Isochrone Maps .....	71
Figure 3-3: Recovery Time (RT) Maps.....	72
Figure 3-4: Activation-recovery Interval (ARI) Maps.....	73
Figure 3-5: The electrophysiological substrate in relation to premature ventricular contractions (PVCs).....	76
Figure 4-1: ECGI Procedure and Parameters .....	89
Figure 4-2: Abnormal Epicardial Electrograms (EGMs) Characteristics and Localization .....	93
Figure 4-3: Activation and Repolarization during Sinus Rhythm.....	94
Figure 4-4: Effects of Increased Heart Rate (HR).....	97
Figure 4-5: Comparison between BrS and Non-BrS RBBB.....	100
Figure 4-6: Computer Simulation of BrS Effects on a Human RVOT Action Potential .....	105
Figure A-1: Continuous ECGI Mapping of Spontaneous VT Initiation, Continuation and Termination with Antitachycardia Pacing.....	125
Figure A-2: Activation Isochrone Maps during Native Sinus Rhythm and BiV Pacing .....	128
Figure A-3: PVC Activation Isochrone Maps with and without Pacing .....	129

## List of Tables

Table 2-1: Cumulative Patient Characteristics .....	13
Table 2-2: Comparison between VT Patients and Non-VT Patients .....	23
Table 3-1: Clinical Characteristics of the ERS Patients .....	69
Table 3-2: Comparison of ECGI Parameters between ERS Patients and Normal Subjects .....	75
Table 4-1: BrS Patient Demographics .....	88
Table 4-2: Cumulative Subject Characteristics.....	89
Table 4-3: EGM Properties for BrS Patients .....	92
Table 4-4: Activation and Repolarization Parameters for BrS Patients .....	95
Table 4-5: Effects of Increased Heart Rate (HR) in BrS Patients.....	98
Table 4-6: A Comparison of ECGI Parameters between BrS and Non-BrS RBBB Patients .....	99



## Acknowledgments

This dissertation would not have been possible without the generous help from many people. First and foremost, I would like to express my sincere gratitude to my advisor Dr. Yoram Rudy for his extraordinary guidance and ceaseless support. Over the past few years, Dr. Rudy has helped me grow as a scientist and as a person.

I would like to thank the dissertation committee members Dr. Jianmin Cui, Dr. Richard B. Schuessler, Dr. Timothy W. Smith, Dr. Pamela K. Woodard and former committee member Dr. Igor Efimov, for sharing their knowledge and providing valuable comments.

This work benefited from the ideas and suggestions from our clinical collaborators. Barnes-Jewish Hospital: Dr. Daniel H. Cooper, Dr. Phillip S. Cuculich, Dr. Mitchell N. Faddis, Dr. Jennifer Silva and Dr. Pamela K. Woodard; UCSF: Dr. Kurt Hoffmayer and Dr. Melvin Scheinman; Bordeaux University Hospital: Dr. Michel Haïssaguerre, Dr. Mèze Hocini and Dr. Frédéric Sacher.

I had the opportunity to work with and learn from a team of bright young scientists in the Rudy Laboratory. Thanks to them, my time in the lab was enjoyable and gratifying. ECGI group: Ramya Vijayakumar, Christopher Andrews, Dr. Subham Ghosh, Dr. Yong Wang and Dr. Kavita Desouza; Modeling group: Smiruthi Ramasubramanian, Jiajing Xu, Dr. Ashwin Mohan, Dr. Jordi Heijman, Dr. Pan Li, Dr. Namit Gaur, Dr. Tom O'Hara, Dr. Keith Decker, Dr. Ali Nekouzadeh and Dr. Leonid Livshitz. I would also like to thank our lab administrators Maya Bera, Huyen Nguyen, Kimberly Smith and Li Li for providing excellent assistance.

**Funding Sources:**

This work was supported by NIH–National Heart, Lung, and Blood Institute grants R01-HL-033343 and R01-HL-049054 (to Dr. Yoram Rudy) and by Washington University Institute of Clinical and Translational Sciences grant UL1-TR000448 from the National Center for Advancing Translational Sciences of the NIH.

Junjie Zhang

*Washington University in St. Louis*

*August 2015*

To my family

for their relentless support

# ABSTRACT OF THE DISSERTATION

## Clinical Application of Electrocardiographic Imaging In Patients with Ischemic Cardiomyopathy, Early Repolarization Syndrome and Brugada Syndrome

by

Junjie Zhang

Doctor of Philosophy in Biomedical Engineering

Washington University in St. Louis, 2015

Professor Yoram Rudy, Chair

Electrocardiographic Imaging (ECGI) is a noninvasive modality for human application in both research and clinical settings. It is an important tool for investigation of abnormal electrophysiological (EP) substrates and arrhythmias in patients. Multi-channel body surface potential recordings and the patient-specific heart-torso geometry from ECG gated computed tomography are processed by ECGI algorithms to reconstruct epicardial potentials, electrograms and patterns of activation and repolarization. ECGI is able to continuously generate high-resolution, panoramic EP maps of the entire heart on a beat-by-beat basis, which cannot be achieved with invasive catheter mapping.

ECGI was applied in ischemic cardiomyopathy patients to characterize the abnormal EP substrate associated with myocardial infarction. In patients who developed ventricular tachycardia during the study, the arrhythmia activation pattern and site of origin were correlated with the EP

substrate to identify components of the reentry circuit. The study subjects included patients with and without a history of clinical ventricular arrhythmias. The properties of scar EP substrate were compared between the two groups to determine whether substantial differences exist. This differentiating capability of ECGI was examined as a potential tool for arrhythmic risk stratification in this population.

In a separate clinical study, ECGI was applied in a group of patients with early repolarization syndrome, which has been recently shown to be associated with an increased risk of ventricular fibrillation. The ventricular activation and repolarization patterns during sinus rhythm were characterized and compared with data from normal controls. This study aimed to provide insights into the mechanisms of the early repolarization ECG pattern and the related arrhythmogenesis.

ECGI was also applied in patients with Brugada syndrome to image the EP substrate and to study the underlying mechanisms of the Brugada ECG pattern and abnormal epicardial electrograms. Heart rate change protocol in selected patients helped unmask the coexistence of abnormal conduction and abnormal repolarization in the EP substrate. Brugada syndrome patients were also compared with patients with right bundle branch block (generally considered benign) to determine whether the substrate was specific to Brugada syndrome, and whether ECGI can differentiate between these two pathologies with similar ECG patterns.

The above studies demonstrated the feasibility and clinical importance of ECGI for noninvasive diagnosis, pre-procedural guidance and arrhythmic risk stratification in human subjects.

## **Chapter 1: Introduction**

Cardiac electrical activity is a complex process. Each cardiac cycle starts with fast depolarization of the myocytes in the sinoatrial node. The electrical impulse spreads to the myocardium via the cardiac conduction system. The ordered and rhythmic excitation of the myocardium during each cardiac cycle ensures efficient contraction of the heart. Immediately after the depolarization phase, the myocardial cells start to repolarize, a relatively slow process that brings the membrane potential back to the resting voltage.

Pathological changes can affect the membrane excitability (by down-regulating the sodium current), change the tissue structure (by causing fibrosis or by affecting gap-junction expression and distribution), and modify myocardial refractoriness (by disturbing current balance during the repolarization phase). These electrophysiological (EP) and structural changes can lead to slow, discontinuous propagation of the action potential through the cardiac tissue and steep gradients of myocardial repolarization, creating abnormal EP substrates that support initiation and maintenance of fatal reentrant arrhythmias.

The 12-lead ECG is the only routine noninvasive tool for diagnosis and detection of cardiac rhythm disorders. Since its first introduction in 1902 by Einthoven, the 12-lead ECG has become a major clinical tool in assessing the function of the heart. However, in clinical practice, it is difficult to relate the ECG signals directly to the actual electrical activation and recovery processes in the heart. Each ECG electrode on the body surface records a signal that reflects integrated electrical activity over the entire heart. The ECG recordings are also smoothed by the torso-volume conductor. Therefore, the conventional 12-lead ECG lacks spatial resolution, sensitivity and specificity.

Electrocardiographic Imaging (ECGI)<sup>1-20</sup> is a noninvasive modality for human application in both research and clinical settings. It has become an important tool for investigation of arrhythmogenic substrates and arrhythmias in patients. ECGI overcomes the limitations of conventional ECG by providing physiologically relevant information about cardiac electrical activity and reconstructing the actual spatial properties on the surface of the heart.

## 1.1 The ECGI Methodology

The electric potential field  $\phi$ , generated by excitation of the heart in the surrounding torso volume between the epicardium and the body surface, obeys Laplace's equation. Torso surface potentials ( $\phi_T$ ) can be measured by electrodes placed on the body surface.  $\phi_E$ , epicardial potentials, is the unknown variable to be solved for. Application of Green's second theorem and discretization of the epicardial and torso surfaces into triangular elements yields the following matrix equation relating  $\phi_T$  to  $\phi_E$ :<sup>21</sup>

$$\mathbf{A} \phi_E = \phi_T \quad 1.1$$

The transfer matrix  $\mathbf{A}$  contains the heart-torso geometric information. The objective of ECGI is to compute  $\phi_E$  from a known  $\phi_T$ , a procedure that constitutes the inverse problem of electrocardiography. The inverse problem is ill-posed<sup>22-23</sup> in the sense that direct inversion of transfer matrix  $\mathbf{A}$  leads to unstable solution. Two different computational schemes have been applied to suppress errors in the inverse solution: Tikhonov regularization<sup>22-23</sup> (a method that imposes constraints on  $\phi_E$ ) and the generalized minimal residual (GMRes) iterative technique.<sup>9, 24</sup>

The ECGI procedure is shown in Figure 1-1. To obtain  $\phi_T$ , multi-electrode strips are applied to the patient's torso; up to 256 electrocardiograms are recorded simultaneously. To obtain transfer matrix  $\mathbf{A}$ , the patient-specific heart-torso geometry is acquired via ECG-gated computed

tomography. These two sets of data are processed by ECGI algorithms to reconstruct epicardial potentials, unipolar electrograms (EGMs), and high-resolution maps of activation and repolarization. The reconstruction is performed during a single beat and does not require accumulating data from multiple identical beats. This property makes it possible to image non-sustained and polymorphic arrhythmias, and arrhythmias that are not hemodynamically tolerated.

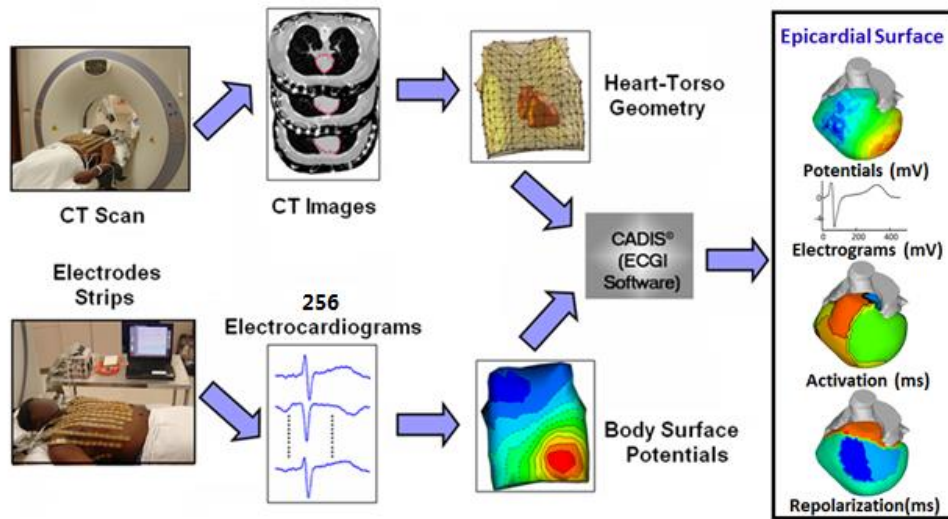


**Figure 1-1: ECGI Procedure**

The noninvasive ECGI procedure. Body surface potential recordings (256 electrodes) and gated, non-contrast thoracic computed tomography scan are processed mathematically to obtain epicardial potentials, 1500 unipolar electrograms, and maps of epicardial activation and repolarization.

## 1.2 Validation of ECGI in Animal Models and Human Studies

Validation experiments in animal models showed that ECGI can reconstruct EGMs with good accuracy, including in infarcted hearts, where EGMs inside the scar region display low potentials and fractionation.<sup>1-2, 4-5</sup> ECGI was also shown to accurately reconstruct repolarization properties and to localize areas of increased dispersion of repolarization.<sup>6</sup> Later, ECGI was validated in human subjects with direct intra-operative mapping during open-heart surgery.<sup>11</sup> It



was shown that ECGI-reconstructed isochrones captured sites of earliest activation, areas of slow conduction, and the general excitation pattern. In addition, ECGI demonstrated a high spatial resolution of 6 mm for determining initiation sites (induced by pacing).

Recently, ECGI was applied to study patients with a history of myocardial infarction.<sup>16</sup> The location, size and shape of the electrical scar imaged by ECGI co-localized to the anatomic scar imaged by late gadolinium enhancement MRI or single-photon emission computed tomography with high accuracy. In a separate study, diverse ventricular arrhythmia activation patterns, mechanisms, and sites of origin in human subjects have been described in detail using ECGI.<sup>17</sup> These studies in humans showed great promise and paved the way for further clinical application of this novel technique as presented in this dissertation.

### **1.3 Dissertation Organization**

**Chapter 2: Application of ECGI in ischemic cardiomyopathy (ICM) patients.** Scar-related ventricular arrhythmias are the most common cause of rhythm disorders and sudden cardiac death (SCD) in patients who suffered myocardial infarction. Catheter ablation utilizing activation mapping and substrate mapping has evolved to treat scar-related ventricular arrhythmias. However, this invasive mapping procedure is difficult, time consuming and involves substantial risk. Given the increased risk of SCD associated with scar-related arrhythmias, the implantable cardioverter-defibrillator (ICD) has been prescribed for ICM patients. The clinical criterion for ICD implantation in these patients is based almost exclusively on reduced left ventricular ejection fraction. However, only a small percentage of ICM patients who undergo device implantation receive appropriate shocks, making the reactive therapy with ICD unsatisfactory. In this study, noninvasive ECGI is used to map the EP substrate and VT circuits with high resolution and to stratify arrhythmic risk in ICM patients.

### **Chapter 3: Application of ECGI in early repolarization syndrome (ERS) patients:**

The ER pattern is a common ECG finding. Recent studies established a definitive clinical association between ER and fatal ventricular arrhythmias. Although ER has been extensively studied at the molecular and cellular levels, information on the EP substrate and arrhythmic behaviors of the intact human heart in vivo, where arrhythmias occur, is missing. With limited sensitivity, specificity and spatial resolution, the ECG characteristics are inadequate measures of the underlying activation and repolarization properties. The aim of this study is to characterize the epicardial EP substrate in ERS patients and to investigate how ERS predisposes patients to an increased risk of ventricular arrhythmias.

**Chapter 4: Application of ECGI in Brugada syndrome (BrS) patients:** BrS is a highly arrhythmogenic cardiac disorder, associated with an increased incidence of SCD. It is estimated that BrS causes approximately 20% of SCD in cardiac patients with structurally normal heart. Understanding its pathophysiological mechanisms is essential for improving risk stratification, diagnosis and treatment to prevent SCD. While much is known at the molecular and cellular scales, understanding the cause of the BrS ECG pattern and associated arrhythmias requires detailed characterization of the EP substrate in the intact hearts of BrS patients. The goal of this study is to characterize the EP substrate in BrS patients using high-resolution panoramic EP maps generated by ECGI, in an effort to provide insight into the mechanistic origin of the BrS phenotype.

**Chapter 5** finishes the dissertation with concluding remarks and a discussion of future work that can be done to improve the work presented here.

## **Chapter 2: Noninvasive High-Resolution Cardiac Mapping in Ischemic Cardiomyopathy Patients: the Electrophysiological Substrate in Relation to Ventricular Arrhythmias and Arrhythmic Risk**

### **2.1 Abstract**

Ventricular tachycardia (VT) occurs frequently in the setting of myocardial infarction. Additional methods are needed for mapping the electrophysiological (EP) substrate and VT circuits with high resolution and for stratifying VT risk in ischemic cardiomyopathy (ICM) patients.

Noninvasive epicardial mapping with Electrocardiographic Imaging (ECGI) was performed in 32 patients with ICM (17 with clinical VT, 15 without VT). Abnormal EP scar substrate was determined based on low electrogram voltage (as percentage of maximal peak-to-peak voltage over the entire ventricular epicardium; total scar-TS <30%; dense scar-DS <15%). Scar burden was defined as the ratio of the scar size to the total epicardial surface area. Scar heterogeneity was characterized by presence of electrogram fractionation. Late potentials (LPs) were deflections that occurred after completion of global epicardial activation. Patients with VT had higher scar burden (TS:  $51.0 \pm 9.3\%$  vs.  $36.5 \pm 5.4\%$ ,  $p < 0.05$ ; DS:  $29.5 \pm 7.3\%$  vs.  $16.8 \pm 6.8\%$ ,  $p < 0.05$ ) with lower unipolar electrogram voltage (TS:  $1.34 \pm 0.34$  vs.  $1.91 \pm 0.39$  mV,  $p < 0.05$ ; DS:  $0.91 \pm 0.29$  vs.  $1.22 \pm 0.33$  mV,  $p < 0.05$ ), greater prevalence of fractionated electrograms (TS:  $44.1 \pm 10.6\%$  vs.  $26.8 \pm 6.3\%$ ,  $p < 0.05$ ; DS:  $50.8 \pm 10.8\%$  vs.  $30.9 \pm 7.0\%$ ,  $p < 0.05$ ) and LPs (TS:  $26.8 \pm 10.7\%$  vs.  $15.8 \pm 5.3$ ,  $p < 0.05$ ). VTs were mapped in 8 patients; the reentry circuits were closely related to the EP substrate.

ECGI identifies scar EP properties that underlie abnormal conduction and VT in ICM patients. It also correlates VT activation patterns with the scar EP substrate. ECGI can potentially be used for VT risk stratification in ICM patients.

## **2.2 Introduction**

Scar-related ventricular arrhythmias are the most common cause of rhythm disorders and sudden cardiac death (SCD) in patients who suffered myocardial infarction (MI). Healed infarcts can produce abnormal electrophysiological (EP) substrates that support arrhythmogenicity. With inexcitable scar tissue separating islands of surviving myocardial fibers, the EP substrate tends to have an inhomogeneous structure.<sup>25-26</sup> This heterogeneity is associated with slow discontinuous conduction, direction-dependent conduction blocks and the presence of conducting channels within the scar, which can ultimately facilitate the formation and maintenance of reentrant arrhythmias.<sup>27-29</sup>

Catheter ablation utilizing activation mapping (complemented by entrainment and pace-mapping) has evolved to treat scar-related VT with up to 75% success rate after successful mapping procedures.<sup>30</sup> However, non-sustained, non-inducible, or hemodynamically unstable VTs cannot be mapped by this technique. Alternatively, substrate mapping can be performed during sinus rhythm (SR), which does not require prolonged periods of ventricular tachycardia (VT). This procedure identifies the EP substrate associated with myocardial scars. In the scar, regions with low-voltage, fractionated electrograms (EGMs), slow conduction and late potentials (LPs) are considered critical components for reentrant arrhythmias.<sup>31-33</sup> This information is used to guide substrate-based ablation for interruption of the reentry circuit and elimination of VT. However, the invasive mapping procedure is difficult, time consuming and involves substantial risk. Moreover, it only maps the substrate, instead of the actual reentry circuit. Due to the point-by-point sampling

nature of catheter mapping, some critical sites might be missed. Thus, a need exists to develop alternative techniques to map both the VT circuits and the EP substrate with high resolution.

Given the increased risk of SCD associated with scar-related arrhythmias, the implantable cardioverter-defibrillator (ICD) has been prescribed for ischemic cardiomyopathy (ICM) patients. The clinical criterion for ICD implantation in these patients is based almost exclusively on reduced left ventricular ejection fraction (LVEF). However, approximately 20% of ICM patients who undergo device implantation receive appropriate shocks, making the reactive therapy with ICD unsatisfactory.<sup>34</sup> Clearly, new methods and better criteria are needed for arrhythmia risk stratification of ICM patients.

Recent developments in noninvasive Electrocardiographic Imaging (ECGI; also called ECG mapping, ECM) have demonstrated its clinical usefulness in studying the EP properties and mechanisms of a variety of pathologies in the intact human heart. ECGI provides panoramic, high-resolution EP data with up to 1,500 unipolar epicardial EGMs that cover both ventricles, from which epicardial maps of activation and repolarization can be generated.<sup>1, 5, 10, 13, 16-17, 20</sup> Important to this study, ECGI can identify and characterize the abnormal EP substrate (low-voltage, fractionated EGMs and the presence of LPs) on the epicardial aspect of myocardial scars.<sup>5, 16</sup> The location, size and shape of the electrical scar imaged by ECGI co-localized to the anatomic scar imaged by late gadolinium enhancement MRI (LGE-MRI) or single-photon emission computed tomography (SPECT) with high accuracy.<sup>16</sup> In addition, ECGI mapping is accomplished during a single beat, making it capable of mapping premature ventricular contractions (PVCs), and polymorphic and unstable VTs. Diverse VT activation patterns, mechanisms, and sites of origin in human subjects have been described in detail using ECGI.<sup>17</sup> In the current study, based on high-resolution ECGI data recorded during sinus rhythm (SR), we characterize the EP substrate in ICM

patients. We correlate the activation pattern and site of origin during VT (if present) with the EP substrate map to identify components of the reentry circuit. We also compare the EP substrate between ICM patients with and without VT, to determine whether substantial differences in EP properties exist. This differentiating capability of ECGI is examined as a potential tool for arrhythmic risk stratification in ICM patients.

## **2.3 Methods**

### **2.3.1 Patient Population**

The control group consisted of ICM patients with (1) history of MI (at least 6 months elapsed since the most recent MI), (2) systolic dysfunction with left ventricular ejection fraction (LVEF)  $\leq 35\%$ , (3) an implantable cardioverter-defibrillator (ICD) inserted based on primary prevention criteria, and (4) no history of clinical ventricular arrhythmias, syncope or cardiac arrest for at least 48 months since ICD insertion. The case group shared criteria (1) and (2) with the control group. In addition, the case group patients experienced at least one episode of clinical VT post-MI. These patients may have an ICD inserted for the primary prevention of SCD, but it was not required. Patients with the following conditions were excluded:<sup>35</sup> (1) Surgical or percutaneous revascularization within the last 6 months; (2) Decompensated cardiac failure within the last month; (3) Uncontrolled hypertension; (4) Active cerebrovascular disease (or stroke within the last 6 months); (5) Electrolyte abnormalities. All protocols were approved by the Institutional Review Boards at Washington University; written informed consent was obtained from all patients.

### **2.3.2 Noninvasive Mapping**

ECGI methodology was described previously.<sup>1, 5, 10, 13, 16-17, 20</sup> Multi-channel body surface potential mapping with 256 electrodes was performed during SR in all patients and during

arrhythmic period in patients who developed VT or PVCs at the time of the study. Patient-specific heart-torso geometry was obtained via non-contrast ECG-gated computed tomography. The heart-torso geometrical information was combined with the body surface potential data to noninvasively reconstruct epicardial potentials, unipolar electrograms, and high-resolution maps of activation, repolarization and EP substrate associated with myocardial scar. The method was validated extensively for reconstruction of EGMs,<sup>1,5</sup> activation<sup>10,13</sup> and repolarization.<sup>13</sup>

Clinical noninvasive cardiac imaging, including LGE-MRI (2 patients) and myocardial perfusion imaging with SPECT (30 patients), was available for comparing anatomical scar to ECGI-reconstructed electrical scar.

### **2.3.3 Data Analysis**

Characteristics of the abnormal EP substrate associated with MI were analyzed by using data recorded during SR. EGM magnitude was measured peak-to-peak during the EGM QRS. Because the absolute EGM magnitude was influenced by patient-specific factors such as body habitus and heart-torso geometry, the EP substrate was defined based on EGM magnitude as a percentage of the maximal EGM magnitude of all EGMs reconstructed over the entire epicardium for each patient (total scar: <30%; dense scar: <15%; peripheral scar: between 15% and 30%). Scar burden was defined based on the size of total scar, dense scar and peripheral scar as a percentage of total epicardial surface area.

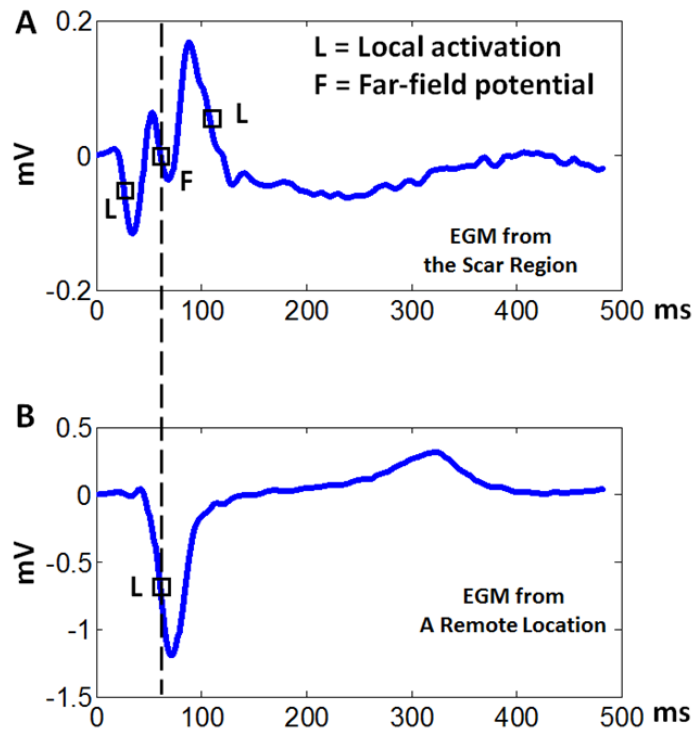


**Figure 2-1: Far-field Potential Identification.**

Panel A shows a unipolar EGM reconstructed in the scar region. It is of low voltage and includes 3 deflections (squares). The timing of the second deflection matches the activation time of a remote EGM (Panel B, about 2 cm away). Therefore, it was considered far-field potential and was excluded from fractionation analysis.

The spatial resolution of ECGI was about 2 to 6 mm.<sup>12</sup> The degree of scar heterogeneity was quantified by EGM fractionation. Fractionation was expressed as the number of intrinsic, sharp deflections ( $dV/dt < -0.05$  V/s) per EGM. Each EGM reflected the electrical activity in cardiac tissue beneath and adjacent to the EGM location. For fractionated EGMs, deflections due to far-field activities were identified if the timing of the deflections matched the timing of deflection(s) in neighboring EGMs, remote EGMs, or both (Figure 2-1). Far-field deflections were marked and excluded for fractionation analysis. The remaining deflections were considered local activations. The sharpest local activation with the maximal negative slope was used to create the



global activation isochrone map. LPs were defined as local activations with magnitude above the ambient electrical noise level that occurred after the completion of global epicardial activation.

The presence of conducting channels within abnormal EP substrate was inferred if a continuous region of higher amplitude signals within the substrate could be observed after adjusting the threshold and color scale of the EGM voltage map.

Activation time (AT) was determined by the maximal negative slope of the EGM during QRS inscription. All ATs were referenced to the beginning of QRS in ECG lead II. Epicardial activation isochrone maps were created from ATs. Lines of conduction block were inferred if adjacent ATs differed by more than 50 ms. Slow conduction was represented by crowded isochrones.

Local recovery time (RT), which reflects the sum of local AT and local action potential duration (APD), was determined from the maximal positive slope of the EGM T-wave. For a given activation sequence, RT determines spatial voltage gradients during repolarization. Activation-recovery interval (ARI) was defined as the difference between RT and AT. ARI is independent of AT and a surrogate for local APD.

ECGI analyzed ventricular arrhythmias from a single beat and did not require accumulating data from multiple identical beats. Each arrhythmia was characterized and analyzed based on the global activation isochrones, properties of local EGMs, and patterns of wavefront propagation and its relationship to the EP substrate.

#### **2.3.4 Statistical analysis**

All continuous data are presented as mean  $\pm$  SD. Categorical data were analyzed by the chi-square test (or Fisher's exact test). Continuous variables were analyzed by unpaired t-test. The

Satterthwaite modified t-test was used for variables with unequal variances. The Mann-Whitney U test was used for variables with non-normal distribution. All tests with  $P < 0.05$  were considered statistically significant. Statistical analysis was performed by using SPSS v19.

<b>Characteristics</b>		<b>Case Group: VT Patients</b>	<b>Control Group: Non-VT Patients</b>	<b>P Value</b>
<b>N</b>		17	15	
<b>Age, years</b>		70±10	68±15	NS
<b>Male</b>		16(94%)	13(87%)	NS
<b>Left ventricular ejection fraction, %</b>		24±6	25±5	NS
<b>QRS duration, ms</b>		135±22	142±25	NS
<b>Mean time since MI, months</b>		90±31	96±21	NS
<b>Infarct Location</b>	Anterior	6(35%)	3(20%)	NS
	Inferior	9(53%)	11(73%)	NS
	Apical	10(59%)	8(53%)	NS
<b>Beta-blocker</b>		17(100%)	15(100%)	NS
<b>ACE/ARB</b>		17(100%)	15(100%)	NS
<b>Amiodarone</b>		14	0	<0.001
<b>Other antiarrhythmic drugs</b>		6	0	<0.001

**Table 2-1: Cumulative Patient Characteristics**

Data are presented as mean±SD or number (percentage). ACE= angiotensin-converting enzyme inhibitors; ARB= angiotensin receptor blockers; MI= myocardial infarction; NS= not significant; VT= ventricular tachycardia.

## 2.4 Results

Between March 2010 and March 2014, 32 ICM patients were enrolled in this study, including 15 patients with no history of clinical ventricular arrhythmias (control group) and 17 patients with spontaneous VT (case group). Patient characteristics are provided in Table 2-1. Overall, the two groups had similar characteristics in terms of age, gender, LVEF, QRS duration,

time since MI and infarct distribution. All patients were treated by beta-blocker and angiotensin-converting enzyme inhibitors/ angiotensin receptor blockers. All case group patients were treated by antiarrhythmic drugs, whereas none of the control patients were on antiarrhythmic drugs.

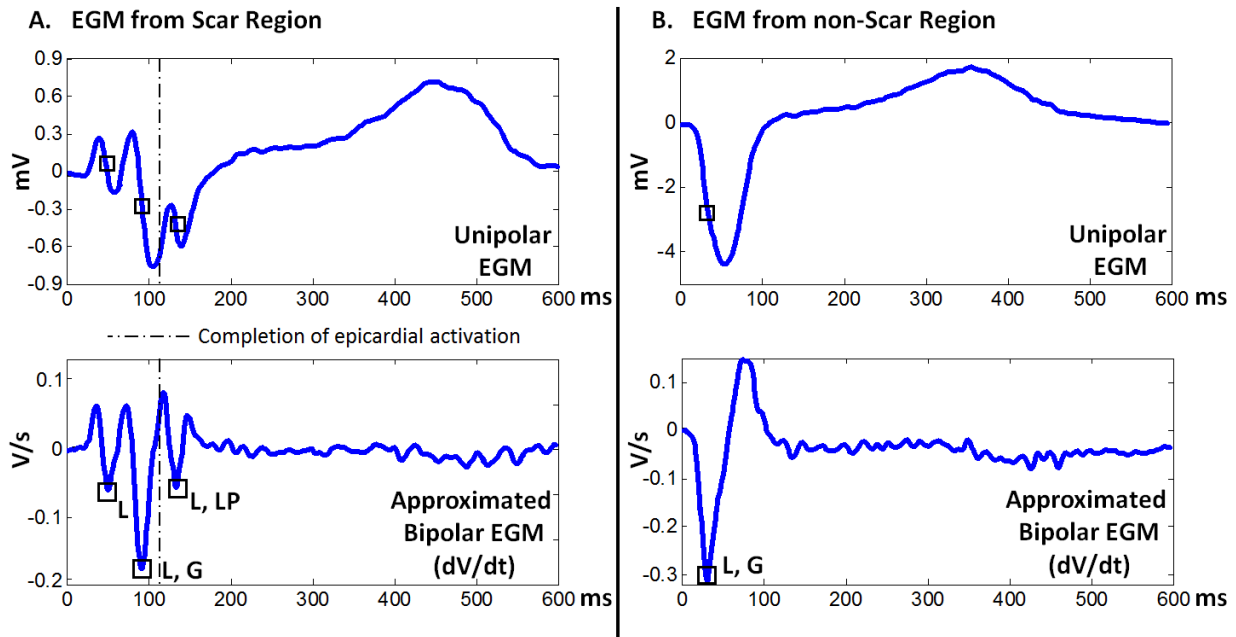


**Figure 2-2: Representative Electrograms (EGMs)**

Panel A: EGM from scar region. Panel B: EGM from non-scar region. Each panel shows a reconstructed unipolar EGM (top) and the corresponding time derivatives ( $dV/dt$ ; bottom). The time derivative approximates a bipolar EGM and emphasizes fractionation. Squares indicate intrinsic sharp deflections (steep negative  $dV/dt$ ), reflecting local activation. The dashed line indicates the time when global epicardial activation has been completed. L= local activation, G= global activation, LP= late potential. Note that the EGM from the scar region has a low voltage and multiple deflections.

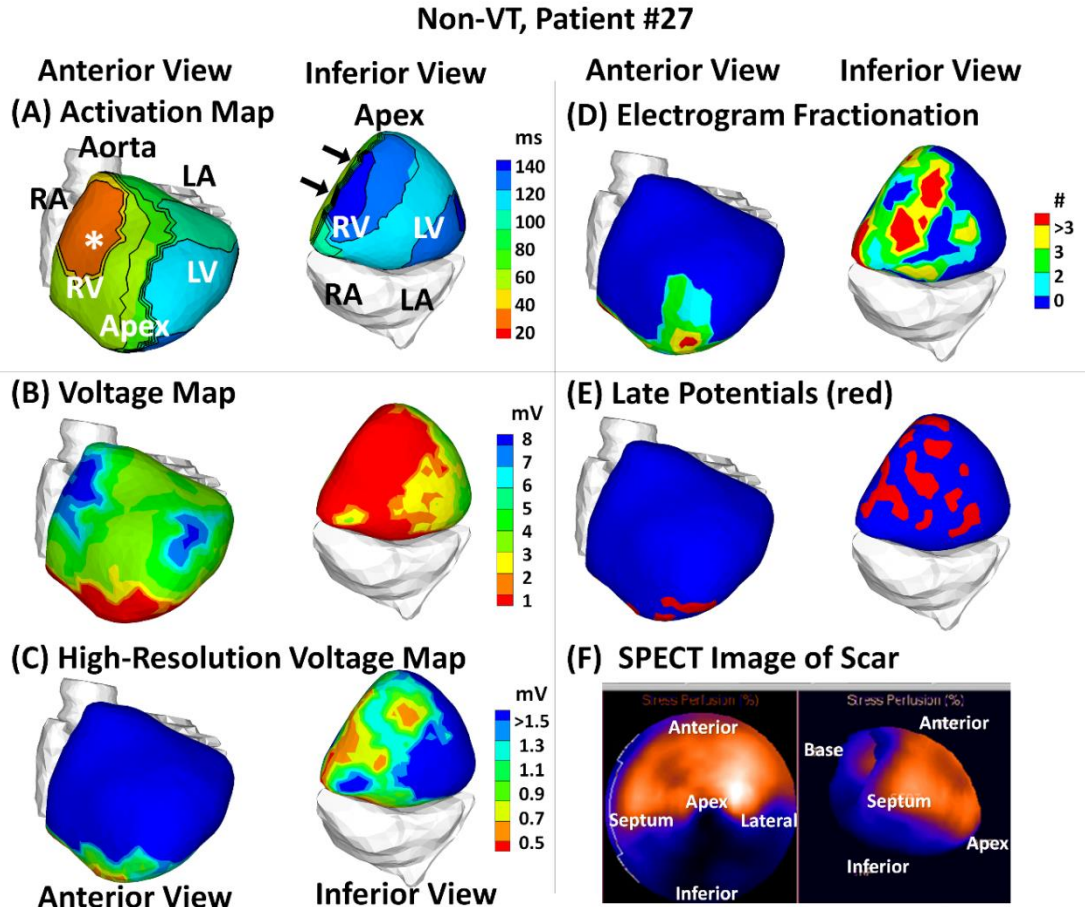
### 2.4.1 Characteristics of Abnormal EP Substrate

Figure 2-2A shows a reconstructed epicardial unipolar EGM (top) and its time derivatives ( $dV/dt$ ; bottom) from inside a scar. The time derivative approximates a bipolar EGM and helps to emphasize fractionation. In this example, the EGM has low voltage and 3 deflections, reflecting 3 local activation events. The second deflection has the sharpest negative slope and was taken as the AT for constructing the global isochrone map. The third deflection occurred after the completion of global epicardial activation (the latest activation over both ventricles) and was considered a LP.

A normal EGM at a site remote from the scar and its derivative are shown in Figure 2-2B for reference.

Examples of abnormal EP substrate in a non-VT patient and a VT patient are shown in Figure 2-3 and Figure 2-4, respectively. Data for all patients are shown in the supplemental material (Section 2.7, Figure 2-7 to Figure 2-38). EP substrate for a non-VT patient is shown in Figure 2-3. Patient #27 was a 69 year-old male with LVEF of 28%. After suffering MI in 2006, he received a pacemaker/ICD device for primary prevention of SCD. He never had any arrhythmic event since the ICD insertion. Based on SPECT images (Panel F), large irreversible perfusion abnormality of marked severity involved the entire inferior, infero-lateral and infero-septal walls. The voltage map identified the electrical scar on the inferior wall (Panel B, red). By adjusting the threshold and color scale of the voltage map, the scar architecture could be observed and studied with high-resolution. The dense scar (Panel C, orange) separated strands of tissue with preserved voltage (Panel C, cyan). Fractionated EGMs (Panel D, yellow, red) and late potentials (Panel E, red) were seen inside the electrical scar. Normal human epicardial activation during SR was reported previously.<sup>13</sup> In general, ventricular epicardial activation starts with right ventricular (RV) breakthrough, then propagates smoothly and uniformly towards the basal lateral left ventricle (LV). Activation isochrone map in this patient (Panel A) showed that the epicardial activation pattern during SR was altered by the presence of the inferior scar. After the normal RV breakthrough (asterisk), the activation wavefront could not proceed towards the inferior RV (line-of-block at the scar border, black arrows). This forced activation of the inferior wall in a left-to-right pattern, leaving the inferior RV the latest region to activate. The scar burden in this patient was: total scar =30%, dense scar =14%, peripheral scar =16% of total epicardial surface area. Prevalence of fractionated EGM was 28% in the total scar, 32% in the dense scar and 25% in the

peripheral scar. Prevalence of LP was 10% in the total scar, 12% in the dense scar and 9% in the peripheral scar.



**Figure 2-3: The abnormal electrophysiological substrate in a non-VT patient (control) with an inferior infarct.**

Panel A: Activation isochrone map. Panel B Global voltage map; magnitude of unipolar electrograms. Panel C: High-resolution scar voltage map with adjusted threshold and color scale. Panel D: Electrogram fractionation; number of intrinsic deflections per electrogram. Panel E: Late potentials; regions with late potentials shown in red. Panels A-E display the heart in anterior view (left) and inferior view (right). Panel F: Single-photon emission computed tomography (SPECT) anatomic scar in a standard "bullseye" configuration or apical view (left) and long-axis view (right). In panel A, epicardial breakthrough is indicated by an asterisk, isochrones are depicted with thin black lines, and black arrows point to conduction block at the border of the inferior infarct. LA= left atrium; LV= left ventricle; RA= right atrium; RV= right ventricle.

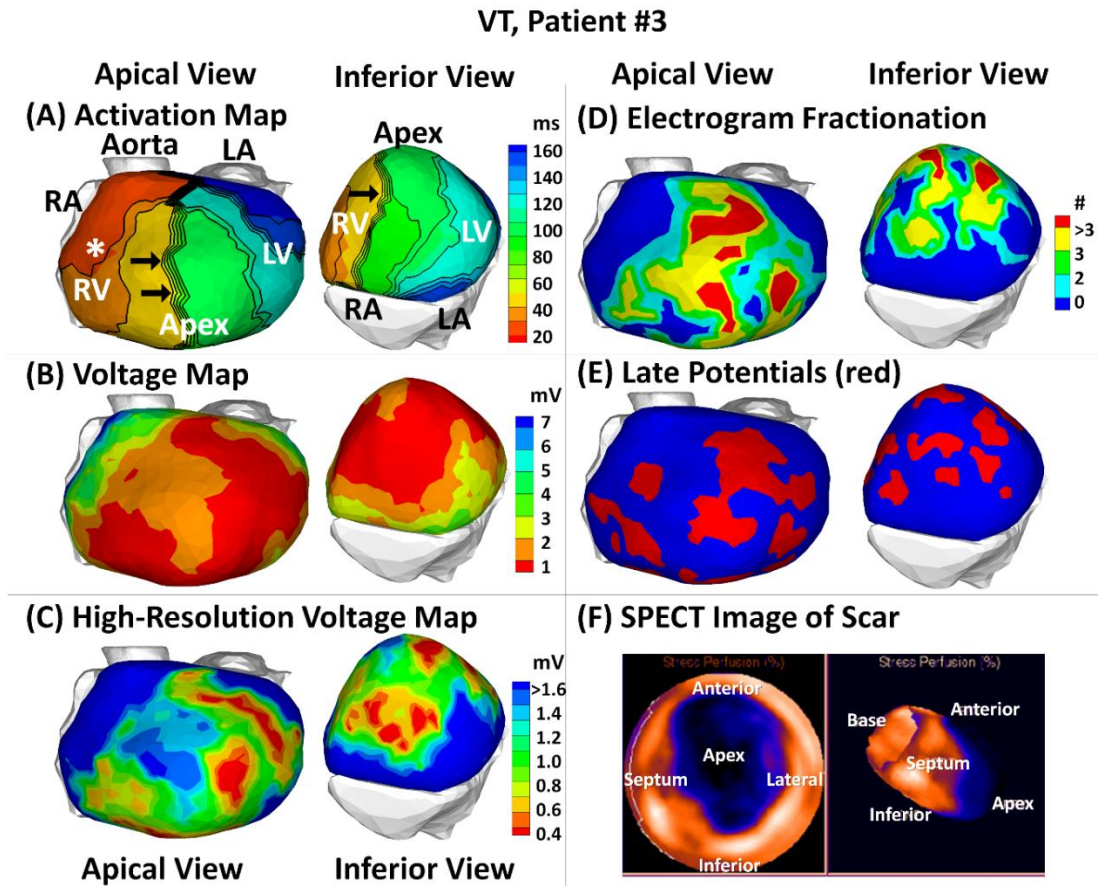


**Figure 2-4: The abnormal electrophysiological substrate in a VT patient (case)**

This patient had a large apical infarct, extending anteriorly and inferiorly. Same format as Figure 2-3. In panel A, black arrows point to conduction block along the septum.

Figure 2-4 shows the EP substrate in a VT patient. Patient #3 was a 72 year-old male with LVEF of 27%. He had multiple episodes of MI in 1980, 1987 and 1990, complicated by VTs. SPECT images (Panel F) suggested the presence of large, severe infarct involving the anterior, inferior, septal, and lateral walls and centering on the apex. ECGI co-localized an extensive apical scar that extended into the mid-myocardium (Panel B, red and orange). The only region with normal-voltage EGMs was the ventricular base. High-resolution voltage map identified several corridors with higher voltage (Panel C, light blue, green; near apex, inferior wall and lateral wall)

that penetrated the dense scar. Fractionated EGMs (Panel D, yellow, red) and late potentials (Panel E, red) were seen inside the electrical scar. Activation isochrone map (Panel A) showed a delayed activation of the LV as a result of the extensive infarct. Lines-of-block (black arrows) were seen over the interventricular septum. Anterior and inferior LV base were the latest regions to activate, about 80 ms later than in normal hearts.<sup>13</sup> The scar burden in this patient was: total scar =67%, dense scar =44%, peripheral scar =23% of total epicardial surface area. Prevalence of fractionated EGM was 58% in the total scar, 59% in the dense scar and 56% in the peripheral scar. Prevalence of late potentials was 39% in the total scar, 31% in the dense scar and 43% in the peripheral scar.

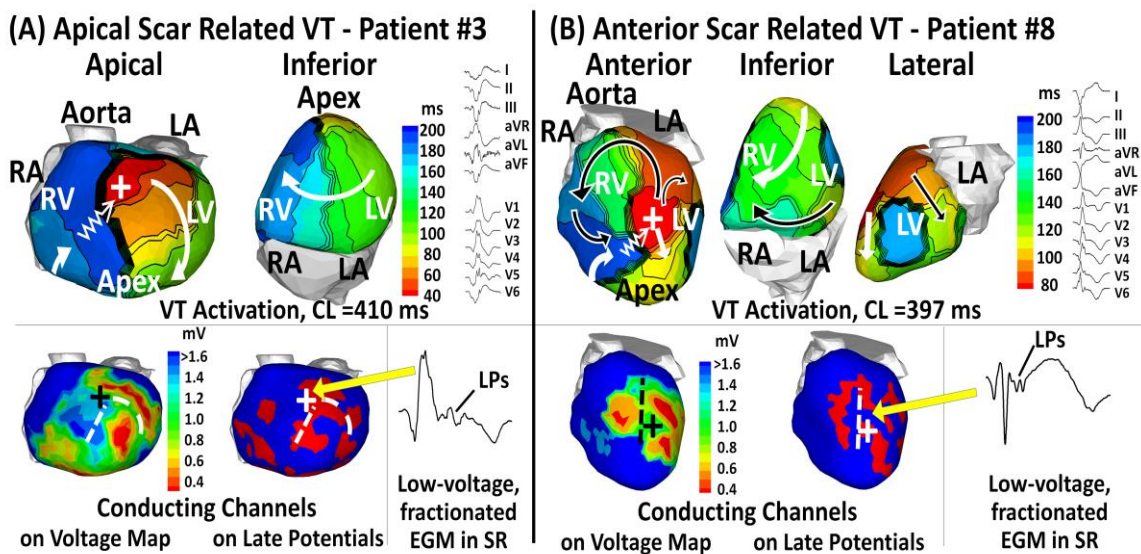


**Figure 2-5: The electrophysiological substrate in relation to ventricular arrhythmias.**

Panel A: Apical scar related ventricular tachycardia (VT) with a single reentrant loop. Panel B: Anterior scar related VT with a double-loop pattern. Each panel shows the VT activation map (top), possible conducting channels (dashed lines) that facilitated VT (bottom left), a fractionated electrogram (EGM) with late potentials (LPs) during sinus rhythm (SR) (bottom right; yellow arrows point to EGM location). The VT initiation sites are indicated by plus signs “+”. In top panels, zigzag arrows indicate very slow conduction that crossed the scar border and reentered the VT initiation site. In panel A, the white arrows indicate a clockwise apical loop. In panel B, the white arrows indicate propagation of the inferior wavefront and the black arrows indicate propagation of the superior wavefront. CL= cycle length. Activation movies for both VTs are provided in the attached CD (Movie 2-1 and Movie 2-2, respectively).

## 2.4.2 Relationship between Ventricular Arrhythmias and EP Substrate

Figure 2-5 presents two examples of scar-related reentrant VT. Panel A shows an apical scar related VT with a simple activation pattern from patient #3 (substrate shown in Figure 2-4). A short run of non-sustained VT with a cycle length (CL) of 410 ms was recorded and analyzed. The earliest epicardial activation was in the anterior mid wall near the septum (plus sign), a peripheral scar region based on the EGM voltage criterion. The activation wavefront exited the anterior wall at the beginning of the VT beat, then activated sequentially in a clockwise pattern the lateral LV, inferior wall and anterior RV (white arrows), and reentered to complete one VT cycle (zigzag arrow). A movie of the activation sequence is provided in the attached CD (Movie 2-1). Panel B presents an anterior scar related VT with a complex activation pattern from patient #8 (substrate shown in Figure 2-14, Page 37). The patient developed non-sustained VT (CL = 397 ms) during the ECGI procedure. The site of VT origin was located in the anterior mid wall near the apex, inside a region of the scar with preserved voltage (plus sign). The activation wavefront exited this region in two directions. The inferior wavefront propagated towards the apex (white arrows) then towards the inferior wall before it entered the anterior mid-RV, forming a clockwise apical loop. The superior wavefront propagated towards the base then bifurcated (black arrows). The left branch of the superior wavefront activated the LV base, and merged with the inferior wavefront at the inferior base. The right branch of the superior wavefront circumvented the dense scar, then propagated slowly into the superior RV in a counterclockwise fashion. The anterior mid-RV was the region where the right branch of the superior wavefront met the inferior wavefront, and was the latest region to activate in the VT cycle. From here, the VT wavefront slowly propagated through the anterior scar (zigzag arrow) and reentered the site of origin. A double-loop pattern could be seen in the anterior view of the VT activation map. The lateral LV activated late, because



the activation wavefront was blocked at the lateral dense scar. A movie of the activation sequence is provided in the attached CD (Movie 2-2).

For both cases, possible conducting channels that could have facilitated the VT formation and conduction were identified and labeled with dashed lines (Figure 2-5, bottom panels). EGMs with low voltage, fractionation and late potentials were recorded during SR at and near the site of VT origin (Figure 2-5, right of bottom panels), These EGMs reflected local diastolic activities at the scar border (zigzag arrows), indicating slow, discontinuous and non-uniform conduction through the scar.

Among 17 patients with a history of spontaneous VT, 8 developed ventricular arrhythmia during the ECGI procedure, including non-sustained VT in 6 patients and frequent PVCs in 2 patients. The site of origin was localized to the dense scar in 2 patients, to the peripheral scar in 5 patients, and to the non-scar region in 1 patient. SR EGMs at or near the VT/PVC site of origin showed fractionation and LPs in all 8 patients. Only one of these arrhythmias were originated from regions with latest SR activation.

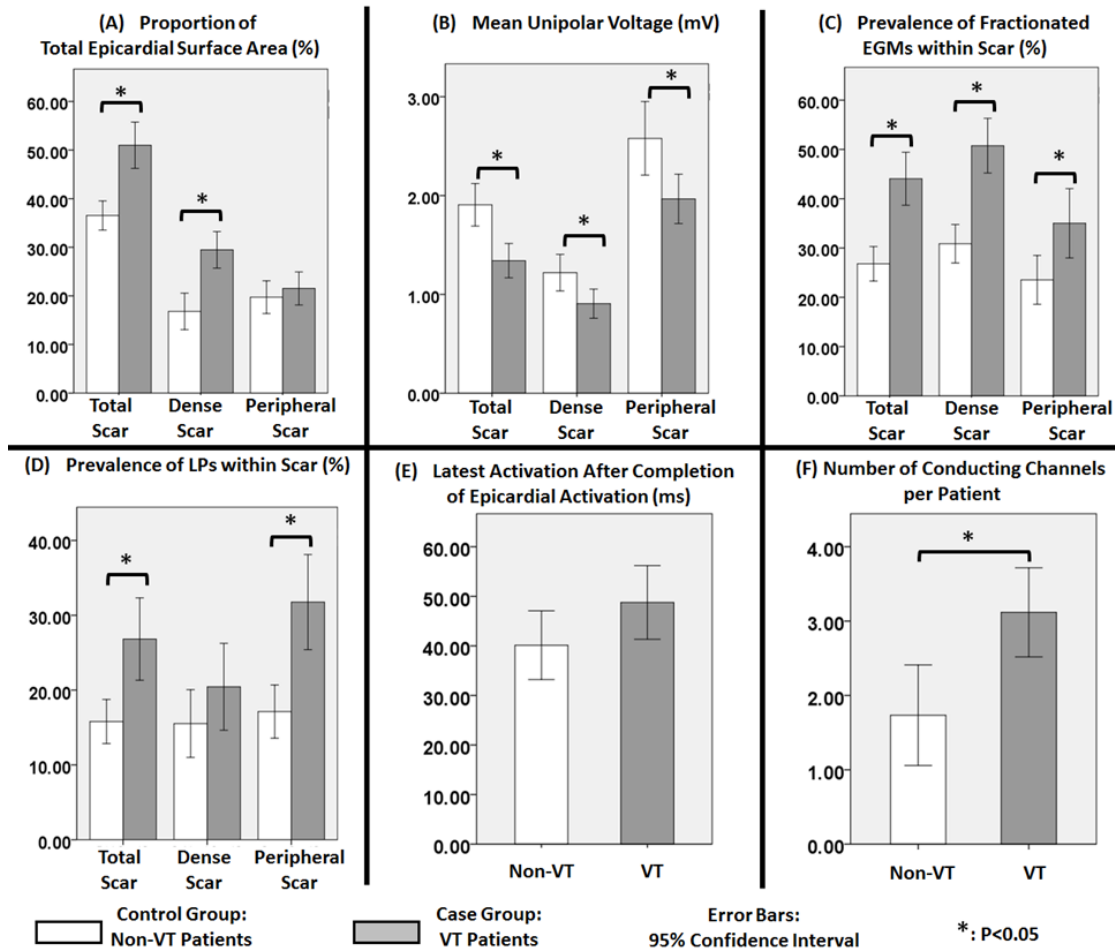


**Figure 2-6: Comparison of the electrophysiological substrate properties between VT patients (case) and non-VT patients (control)**

Panel A: Scar burden (scar size as percentage of total epicardial surface area). Panel B: Mean unipolar voltage. Panel C: Percentage of fractionated electrograms (EGMs) within total scar, dense scar and peripheral scar. Panel D: Prevalence of late potentials (LPs). Percentage of EGMs with LPs within total scar, dense scar and peripheral scar. Panel E: Latest activation detected after completion of global epicardial activation. Timing is referenced to the latest epicardial activation time. Panel F: Number of conducting channels per patient.  $P < 0.05$  is marked with an asterisk.

### 2.4.3 Comparison of EP Substrate Properties between VT Patients and Non-VT patients

Figure 2-6 summarizes the differences in the EP substrate between patients with VT (case) and patients without VT (control). When controlled for total epicardial surface area, VT patients had higher proportion of total scar ( $51.0 \pm 9.3\%$  vs.  $36.5 \pm 5.4\%$ ,  $p < 0.05$ ) and dense scar ( $29.5 \pm 7.3\%$  vs.  $16.8 \pm 6.8\%$ ,  $p < 0.05$ ) than non-VT patients (Panel A). There was no significant difference

between the groups with respect to the proportion of peripheral scar ( $21.5 \pm 6.6\%$  vs.  $19.7 \pm 6.1\%$ ,  $p=0.43$ ). The mean unipolar voltage (Panel B) was significantly lower in VT patients than in non-VT patients within the total scar ( $1.34 \pm 0.34$  vs.  $1.91 \pm 0.39$  mV,  $p<0.05$ ), the dense scar ( $0.91 \pm 0.29$  vs.  $1.22 \pm 0.33$  mV,  $p<0.05$ ) and the peripheral scar ( $1.97 \pm 0.49$  vs.  $2.58 \pm 0.67$ ,  $p<0.05$ ). Fractionated EGMs were observed in every patient. VT patients had higher percentage of fractionated EGMs within the total scar ( $44.1 \pm 10.6\%$  vs.  $26.8 \pm 6.3\%$ ,  $p<0.05$ ), the dense scar ( $50.8 \pm 10.8\%$  vs.  $30.9 \pm 7.0\%$ ,  $p<0.05$ ) and the peripheral scar ( $35.0 \pm 13.7\%$  vs.  $23.5 \pm 9.0\%$ ,  $p<0.05$ ), respectively (Panel C). LPs were observed in every patient also. VT patients had higher percentage of EGMs with LPs within the total scar ( $26.8 \pm 10.7\%$  vs.  $15.8 \pm 5.3$ ,  $p<0.05$ ) and the peripheral scar ( $31.8 \pm 12.3\%$  vs.  $17.1 \pm 6.4\%$ ,  $p<0.05$ ), respectively (Panel D). The 2 groups had similar prevalence of LPs within the dense scar ( $20.4 \pm 11.3\%$  vs.  $15.5 \pm 8.2\%$ ,  $p=0.17$ ). If LP was present in an EGM, the timing of each late component was measured in reference to the completion of epicardial activation. The mean value of latest activation was slightly higher for the VT group ( $48.8 \pm 14.5$  vs.  $40.1 \pm 12.5$  ms,  $p=0.08$ ), but the difference did not reach statistical significance (Panel E). Voltage channels were found in all VT patients and 10 non-VT patients. VT patients had more channels per patient than non-VT patients ( $3.1 \pm 1.2$  vs.  $1.7 \pm 1.2$ ,  $p<0.05$ ).

Global repolarization properties were measured and compared between the groups, including mean RT, mean ARI, RT dispersions and ARI dispersions. No significant differences were found in these parameters (Table 2-2).

ECGI-derived Parameters		Case Group: VT Patients	Control Group: Non-VT Patients	P Value
Scar Size (%)	Total Scar	51.0±9.3	36.5±5.4	<0.05
	Dense Scar	29.5±7.3	16.8±6.8	<0.05
	Peripheral Scar	21.5±6.6	19.7±6.1	0.43
Mean Unipolar Voltage (mV)	Total Scar	1.34±0.34	1.91±0.39	<0.05
	Dense Scar	0.91±0.29	1.22±0.33	<0.05
	Peripheral Scar	1.97±0.49	2.58±0.67	<0.05
Prevalence of Fractionated EGMs within (%)	Total Scar	44.1±10.6	26.8±6.3	<0.05
	Dense Scar	50.8±10.8	30.9±7.0	<0.05
	Peripheral Scar	35.0±13.7	23.5±9.0	<0.05
Prevalence of LP within (%)	Total Scar	26.8±10.7	15.8±5.3	<0.05
	Dense Scar	20.4±11.3	15.5±8.2	0.17
	Peripheral Scar	31.8±12.3	17.1±6.4	<0.05
Number of conducting channels		3.1±1.3	1.7±1.2	<0.05
Latest LP (ms)		48.8±14.5	40.1±12.5	0.08
Apex-to-base ARI Dispersion (ms)		43.7±9.8	49.3±10.3	0.13
Apex-to-base RT Dispersion (ms)		55.3±11.8	60.3±10.2	0.22
RV-to-LV ARI Dispersion (ms)		45.1±8.3	48.5±7.8	0.23
RV-to-LV RT Dispersion (ms)		59.3±9.5	62.2±10.9	0.43
Mean ARI (ms)		260.7±18.4	271.2±15.0	0.09
Mean RT (ms)		336.6±25.3	349.5±22.1	0.14

**Table 2-2: Comparison between VT Patients and Non-VT Patients**

Data are presented as mean±SD.

## 2.5 Discussion

### 2.5.1 Key Findings

Key findings of this study include: (1) With noninvasive ECGI, the epicardial EP substrate associated with MI was characterized by low-voltage and fractionated EGMs, the presence of LPs, and altered SR activation pattern; (2) By correlating substrate maps with VT activation maps,

critical substrate that supported the VT could be identified; (3) Repolarization abnormalities (such as steep dispersion of repolarization) were not present in the substrate, indicating that the mechanistic basis for conduction block and VT was structure-based abnormal propagation through the scar substrate; (4) Significant differences existed in the EP substrate between VT patients and non-VT patients: VT patients had greater epicardial scar burden, lower voltage in the scar, a higher prevalence of fractionated EGM and LPs, and more conducting channels. These observations explain to a certain extent the role of EP substrate in ventricular arrhythmia and the difference in VT incidence between the groups. Given these findings, the study constitutes a first step towards noninvasive arrhythmia risk stratification in ICM patients and pre-procedural guidance for scar-related VT ablation.

### **2.5.2 The EP Scar Substrate**

Following an ischemic event, a complex and progressive remodeling process occurs, which changes the EP properties of the heart.<sup>25</sup> In heterogeneous post-MI scars, strands of viable, excitable myocardial fibers are separated by necrotic myocardium. This creates sites of mismatched electrical properties with abrupt increases of electrical load that reduce the safety factor for conduction and increase spatial dispersion of excitability.<sup>27</sup> These changes can result in reduced conduction velocity, discontinuous propagation through the infarct substrate, and regions of conduction block - EP properties that promote reentrant arrhythmias. The scar-related abnormal EP properties are reflected in low-voltage and fractionated EGMs, as was shown in experimental, theoretical and clinical studies.<sup>29, 36-38</sup>

### **2.5.3 Substrate Mapping and Ablation**

Clinically, ICM patients are studied with invasive catheter mapping. If hemodynamically stable VT can be mapped, critical pathways for reentry are identified and ablated. However, extended period of VT cannot be tolerated by the majority of patients. Alternatively, substrate mapping is performed during SR to identify regions with low-voltage, fractionated and prolonged EGMs with LPs, as surrogate targets for ablation.

Recent substrate-based mapping and ablation studies suggested that complete LP abolition is an effective strategy that yields good procedural outcomes.<sup>39-42</sup> LPs identify excitable tissue that supports very slow, discontinuous conduction and possibly regions of block. Beyond ablation of the critical isthmus for VT, this approach requires ablation of all substrates that exhibit LPs to achieve scar homogenization. A difficulty with LP mapping is that far-field potentials due to depolarization of myocardial tissue remote from the recording electrode could be the source of some LPs. In fact, ablating regions with LPs that reflect far-field activity may contribute to failure of some substrate guided ablation procedures.<sup>39, 41</sup> A recent study combined EGM analysis with pace-capture to identify far-field potentials and refine identification of targets for substrate-based ablation.<sup>43</sup> In the present study, ECGI was used to identify directly far-field potentials in scar EGMs and eliminate them from considerations of EGM fractionation.

### **2.5.4 ECGI-recorded Scar EGMs and Far-field Deflections**

Previous validation studies demonstrated ECGI's ability to reconstruct characteristics of EGMs associated with post-MI scar in canine experiments.<sup>5</sup> In a recent study, ECGI was performed in 24 post-MI patients.<sup>16</sup> Globally, the abnormal EP substrate on the epicardial aspect of the scar was identified. It was characterized by low potentials, and presence of low-voltage fractionated EGMs and LPs. The epicardial electrical scar imaged by ECGI co-localized to LGE-

MRI or SPECT with high accuracy (sensitivity 89%, specificity 85%). The current study dissected the scar EP substrate with higher resolution and correlated it with the VT pattern. Because ECGI provides panoramic maps of activation times, it can identify far-field potentials in local scar EGMs by matching activation times in neighboring EGMs, remote EGMs, or both. This capability for direct detection and exclusion of far-field deflections improved the accuracy of EGM fractionation analysis. It enabled us to obtain high-resolution maps of voltage, EGM fractionation and LPs within the scar, providing detailed spatial EP maps of the scar substrate. By correlating the VT activation maps with the high-resolution ECGI images of the EP substrate obtained during SR, critical components of the VT circuit could be identified and localized in the scar. These included initiation sites, exit sites, and possible conducting channels.

### **2.5.5 Scar-related Arrhythmias**

Arrhythmic events in 8 patients were imaged and analyzed. The ECGI-imaged reentry circuits were closely related to the EP substrate with EGM fractionation and LPs. The data were consistent with the findings from clinical studies,<sup>31</sup> in which the isthmus for reentry circuit was confined to a region of viable myocardium surrounded by the scar tissue. In 7 of 8 cases, the site of origin was located near regions with LPs and low-voltage fractionated EGMs within the scar. In one patient, the PVCs were found to originate from a location with a normal EGM magnitude, but with fractionation and LP deflections. It is possible that this patient had a mild endocardial scar near the PVC site of origin (not detectable by SPECT) and that the ECGI reconstructed epicardial unipolar EGMs picked up diastolic activities from intramural locations. Since the epicardium remained largely viable, the epicardial EGMs yielded normal magnitude but fractionation and LPs. It is noteworthy that the majority of sites critical to reentry exhibited conduction slowing during SR based on the activation isochrone map, but only one of them was found in a region with latest

SR activation. The observation is consistent with invasive EP studies that suggested that regions with conduction delay during SR may be critical for VT maintenance, and that zones with the most delayed activation during SR may represent bystander sites irrelevant to the VT circuit.<sup>44</sup> Additionally, part of the inexcitable dense scar possibly served as an inert obstacle determinant of the reentry circuit. As shown in Figure 2-5, the wavefront propagated around the dense scar with high curvature after exiting from the site of origin.

### **2.5.6 Risk Stratification for VT**

Earlier studies<sup>45-46</sup> examining the EP substrate associated with MI provided initial insights into the differences between VT and non-VT patients. However, they did not provide detailed EP information due to limited endocardial sampling points. In a recent study, high-density endocardial mapping collected detailed data from the dense scar region, and was used to compare ICM patients with and without previous clinical ventricular arrhythmias.<sup>35</sup> VT patients were found to have markedly larger low-voltage zones, higher density of fractionated EGM, and more conducting channels, which were the key markers of the VT substrate. In the current study, using noninvasive ECGI, we compared the epicardial EP substrate between 17 ICM patients presenting with clinical VT and 15 ICM patients who had an ICD inserted for primary prevention of SCD and had been free from clinical episodes of VT for at least 48 months since ICD insertion. Despite the similar patient characteristics of the 2 groups, the ECGI mapping data revealed that the VT patients had a larger extent of total scar and dense scar EP substrate and lower voltage in the scar area. Furthermore, the prevalence of EGMs with fractionation and LPs was greater in the VT patients. The results add support to previous findings correlating substrate to VT incidence, and emphasize the fact that the EP substrate for VT may or may not be present in patients with similar LV function.



Not only the extent of the scar, but also its structural components that underlie spatial properties of the EP substrate are important determinants of VT incidence.

### **2.5.7 Limitations**

ECGI reconstructs potential maps and unipolar EGMs on the epicardial surface. These provide information not only on the epicardial substrate; they reflect properties in the myocardial depth as well.<sup>2</sup> A previous study demonstrated high correlation between ECGI and imaging with MRI and SPECT of transmural scars.<sup>16</sup> However, activation isochrone mapping with ECGI is limited to the epicardium. Scar-related reentry circuit may involve the endocardium, mid-myocardium and epicardium. The earliest epicardial activation of VT may not accurately identify the location of an endocardial circuit. Importantly, accumulating evidence demonstrates major involvement of the epicardium in VT. A recent study predicted scar transmural and the presence of LPs in the epicardium based on the extension and density of the endocardial scar, indicating possible requirement of an epicardial ablation procedure.<sup>40</sup> The presence of an epicardial substrate may be the reason for failure of a subset of endocardial procedures. A combined endocardial-epicardial ablation strategy is associated with fewer readmissions for VT and repeat ablations compared to only-endocardial ablation.<sup>47</sup>

The conducting channel in the scar was defined based on preserved EGM voltage during SR. This study showed relationship between the conduction channels and the VT entry and exit sites. However, slow conduction through the channel during VT cannot be directly mapped by ECGI due to limited spatial resolution.

The extent of the ECGI-derived EP scar was determined by the threshold for EGM magnitude. We adapted the threshold from a previous study, which correlated the EP scar to the

anatomical scar with good levels of specificity and sensitivity.<sup>16</sup> ECGI is also limited in its ability to image small amplitude deflections during the repolarization period (T wave). Therefore, the maps of LP distribution may not include all the LPs.

The generalizability of this study is limited by the relatively small number (32) of patients. Future large-scale ECGI studies should be conducted to establish the potential of the approach for noninvasive arrhythmic risk stratification in ICM patients prior to ICD implantation.

## **2.6 Conclusions**

EP mapping with ECGI can overcome certain limitations of catheter mapping. It can provide high-resolution maps of post-MI EP substrate together with panoramic maps of activation during SR and VT. Being noninvasive, it reduces the procedural risk and can be repeated in follow-up studies during the remodeling process. Due to its single-beat mapping capability, it can map polymorphic and unstable VT. It complements endocardial substrate mapping by providing high-resolution images of the epicardial EP substrate. To our knowledge, this is the first noninvasive EP mapping study in ICM patients that identifies key epicardial EP properties that may account for the difference in VT incidence between VT and non-VT patients. It also correlates scar-related arrhythmia patterns with high-resolution maps of spatial characteristics of the scar EP substrate obtained during SR. With larger-scale studies, ECGI has the potential to become a clinical tool for identification of ICM patients at high risk of arrhythmias for ICD indication and for pre-procedural guidance of substrate-base ablation.

## **2.7 Supplemental Material**

### **2.7.1 Maps of EP Substrate and Activation Sequence for VT Patients**

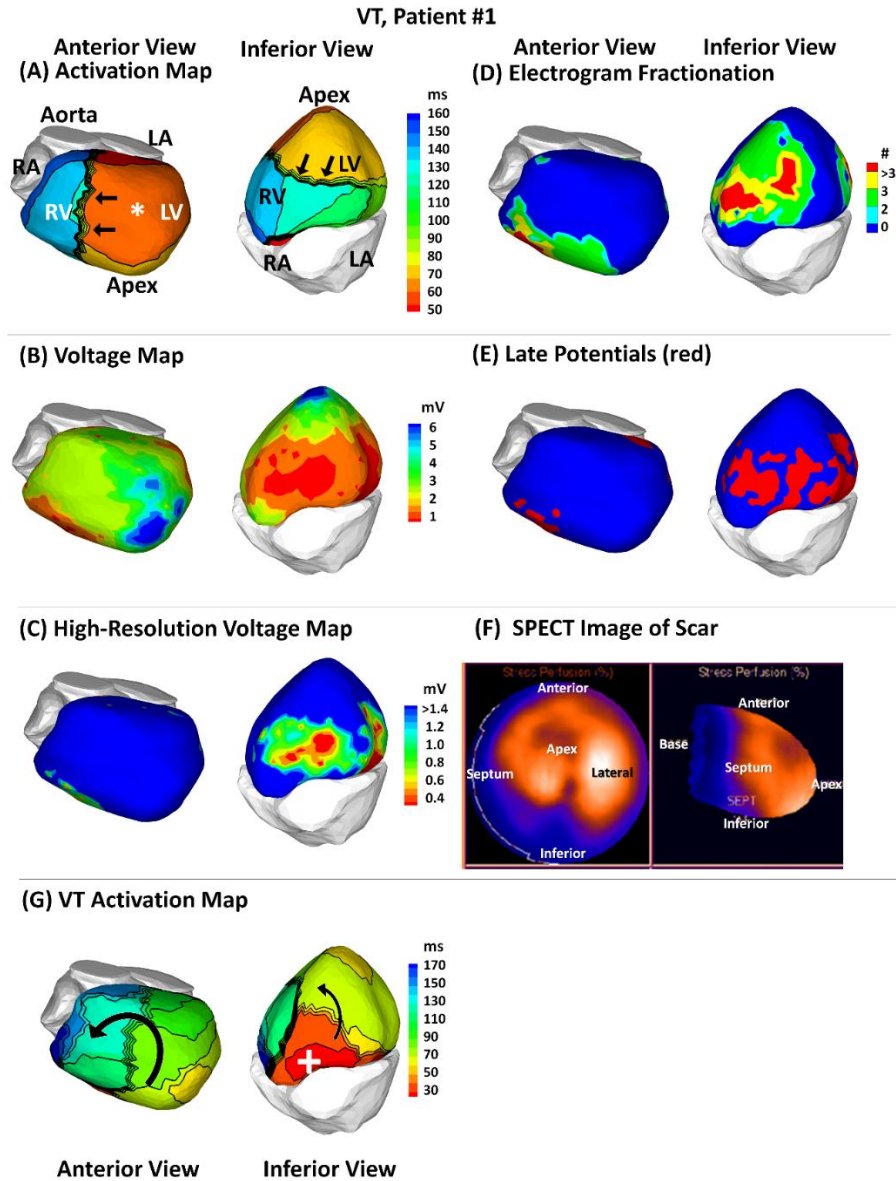


**Figure 2-7: Patient #1: VT patient; inferior myocardial infarction**

(A) Activation isochrone map. (B) Global voltage map; magnitude of unipolar electrograms. (C) High-resolution scar voltage map with adjusted threshold and color scale. (D) Electrogram fractionation; number of intrinsic deflections per electrogram. (E) Late potentials; regions with late potentials shown in red. (F) Single-photon emission computed tomography (SPECT) anatomic scar in apical view (left) and long-axis view (right); (G) VT activation map. Panels A-E and G display the heart in anterior view (left) and inferior view (right). In panel A, epicardial breakthrough is indicated by an asterisk “\*”, isochrones are depicted with thin black lines, and black arrows point to conduction block. In panel G, the VT site of origin is indicated by a plus sign “+”, curved arrows indicate propagation of the VT wavefront.

The VT site of origin was localized to the peripheral scar near the inferior base.

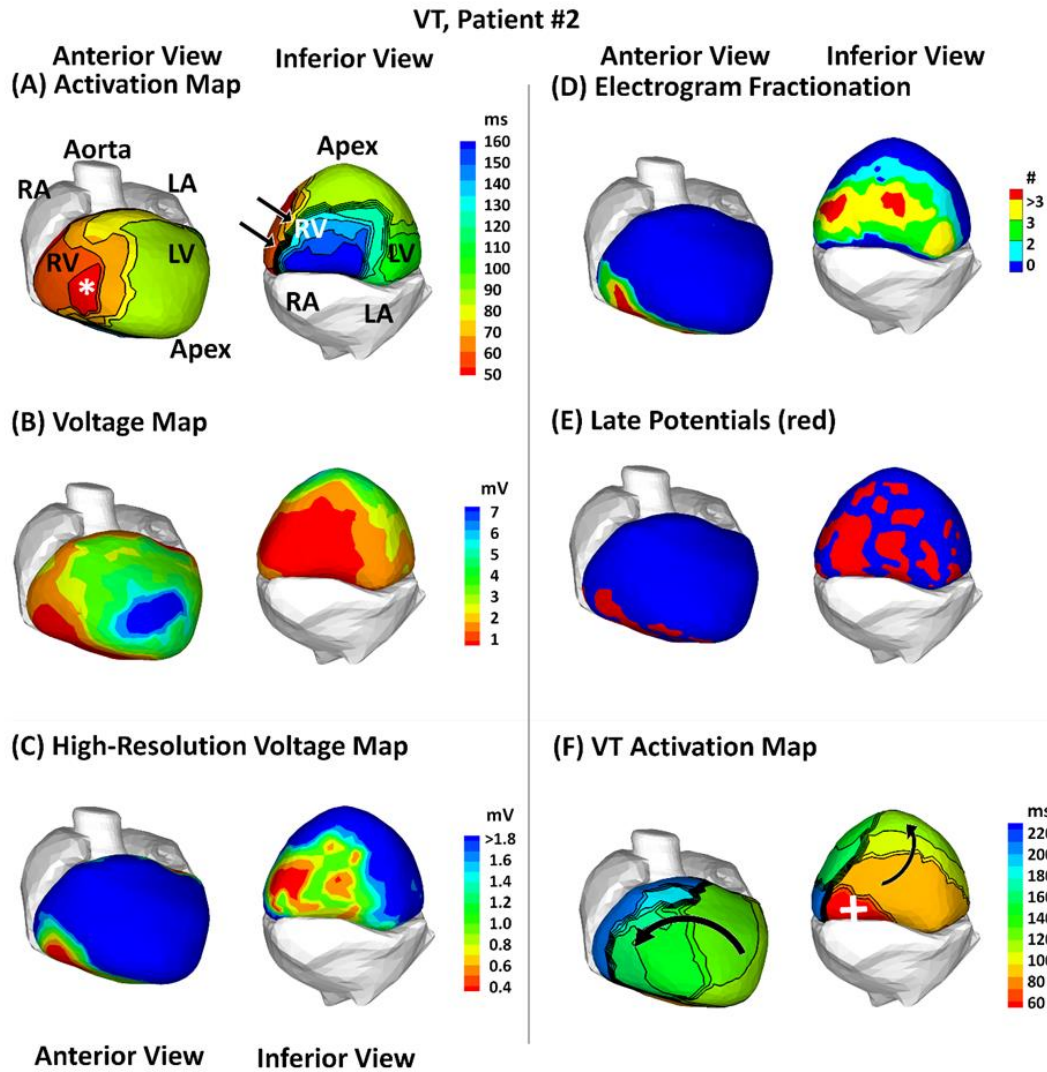


**Figure 2-8: Patient #2: VT patient; inferior myocardial infarction**

(A) Activation isochrone map. (B) Global voltage map; magnitude of unipolar electrograms. (C) High-resolution scar voltage map with adjusted threshold and color scale. (D) Electrogram fractionation; number of intrinsic deflections per electrogram. (E) Late potentials; regions with late potentials shown in red. (F) VT activation map. All panels display the heart in anterior view (left) and inferior view (right). In panel A, epicardial breakthrough is indicated by an asterisk “\*”, isochrones are depicted with thin black lines, and black arrows point to conduction block. In panel F, the VT site of origin is indicated by a plus sign “+”, curved arrows indicate propagation of the VT wavefront.

The VT site of origin was localized to the dense scar near the inferior base.

### VT, Patient #3

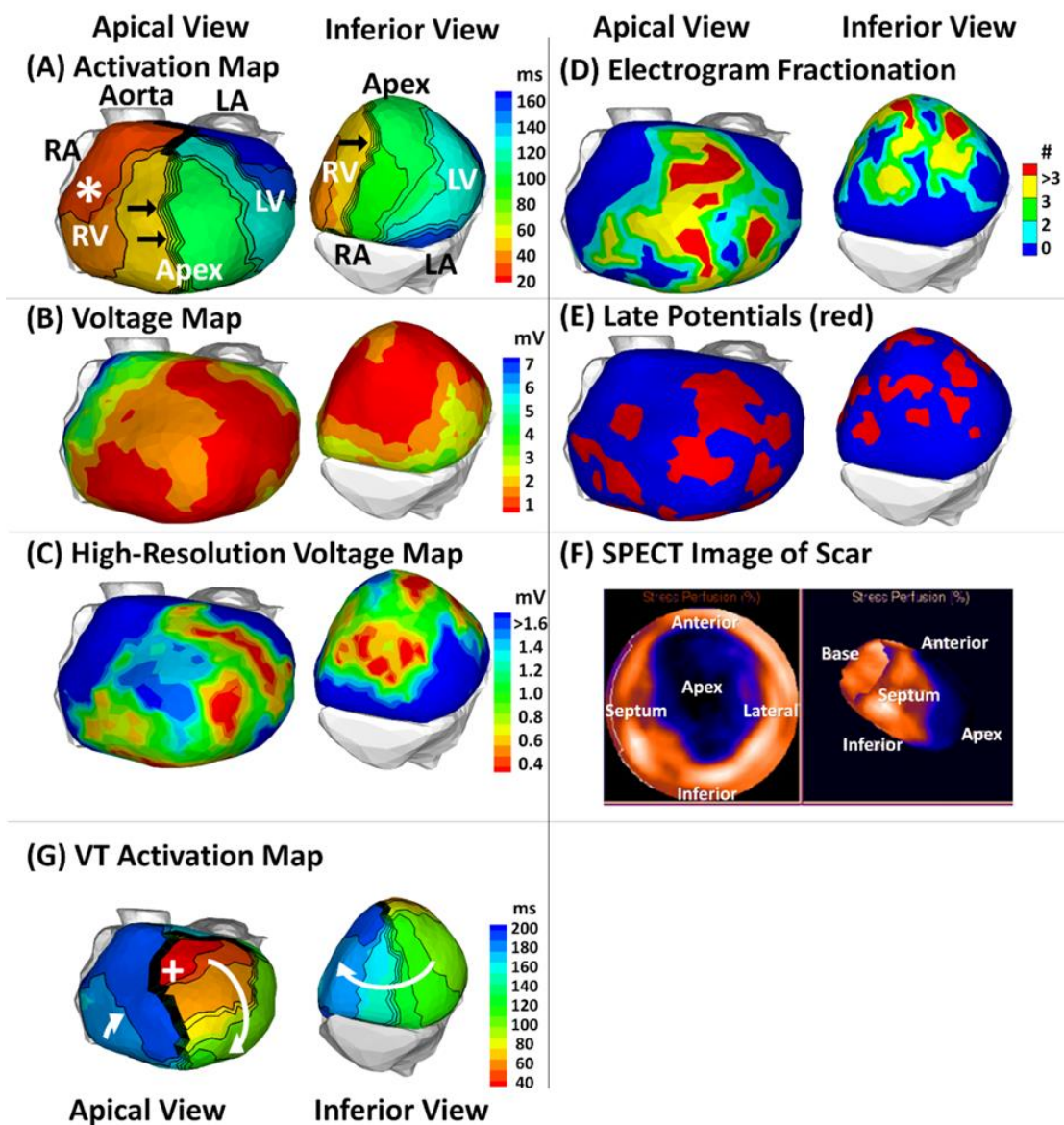


**Figure 2-9: Patient #3: VT patient; apical myocardial infarction**

(A) Activation isochrone map. (B) Global voltage map; magnitude of unipolar electrograms. (C) High-resolution scar voltage map with adjusted threshold and color scale. (D) Electrogram fractionation; number of intrinsic deflections per electrogram. (E) Late potentials; regions with late potentials shown in red. (F) Single-photon emission computed tomography (SPECT) anatomic scar in apical view (left) and long-axis view (right); (G) VT activation map. Panels A-E and G display the heart in apical view (left) and inferior view (right). In panel A, epicardial breakthrough is indicated by an asterisk “\*”, isochrones are depicted with thin black lines, and black arrows point to conduction block. In panel G, the VT site of origin is indicated by a plus sign “+”, curved arrows indicate propagation of the VT wavefront.

The VT site of origin was localized to the peripheral scar on the anterior wall near the apex.

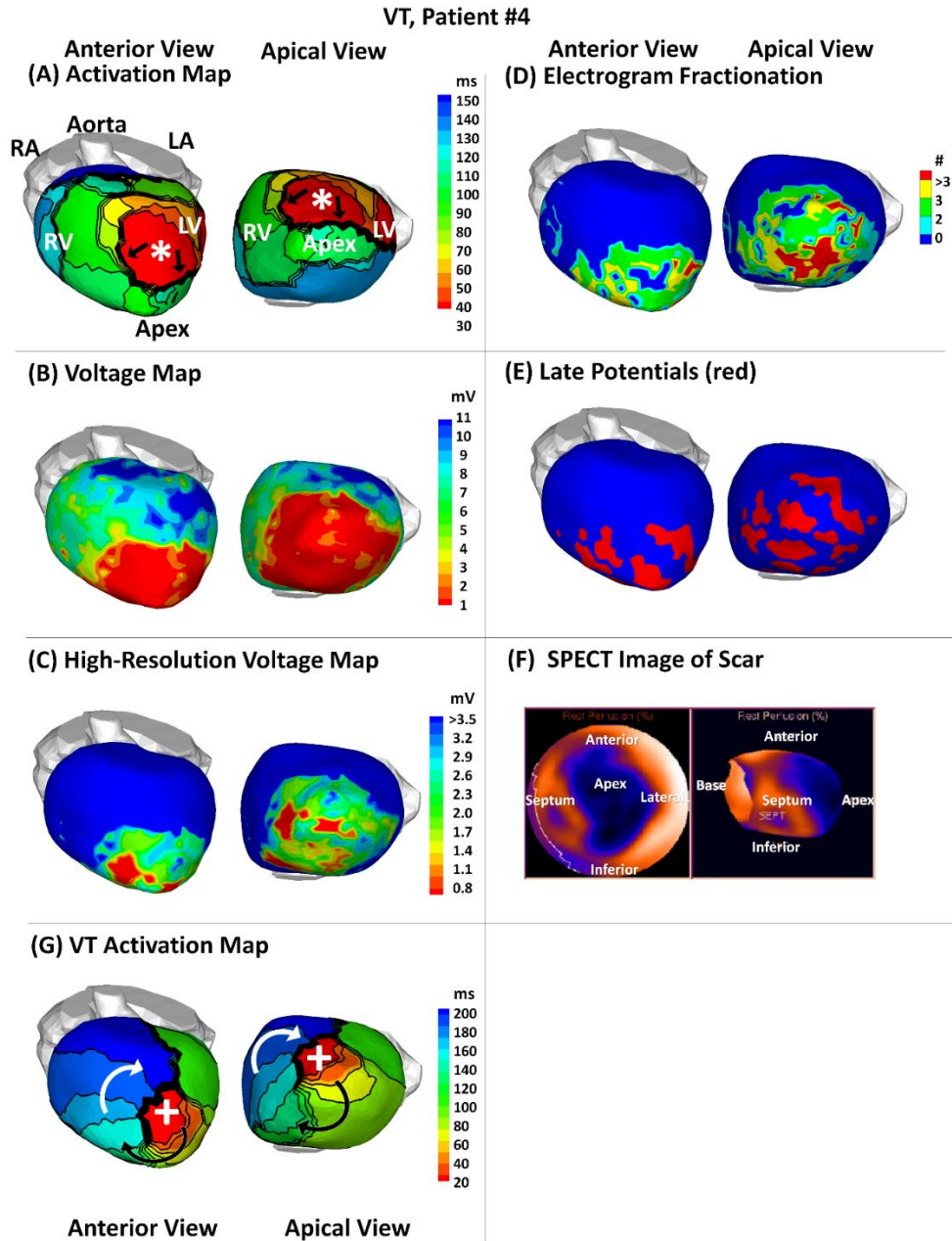


**Figure 2-10: Patient #4: VT patient; apical myocardial infarction**

(A) Activation isochrone map. (B) Global voltage map; magnitude of unipolar electrograms. (C) High-resolution scar voltage map with adjusted threshold and color scale. (D) Electrogram fractionation; number of intrinsic deflections per electrogram. (E) Late potentials; regions with late potentials shown in red. (F) Single-photon emission computed tomography (SPECT) anatomic scar in apical view (left) and long-axis view (right); (G) VT activation map. Panels A-E and G display the heart in anterior view (left) and apical view (right). In panel A, epicardial breakthrough is indicated by an asterisk “\*”, isochrones are depicted with thin black lines, and black arrows point to conduction block. In panel G, the VT site of origin is indicated by a plus sign “+”, curved arrows indicate propagation of the VT wavefront.

The VT site of origin was localized to the peripheral scar on the anterior wall near the apex.

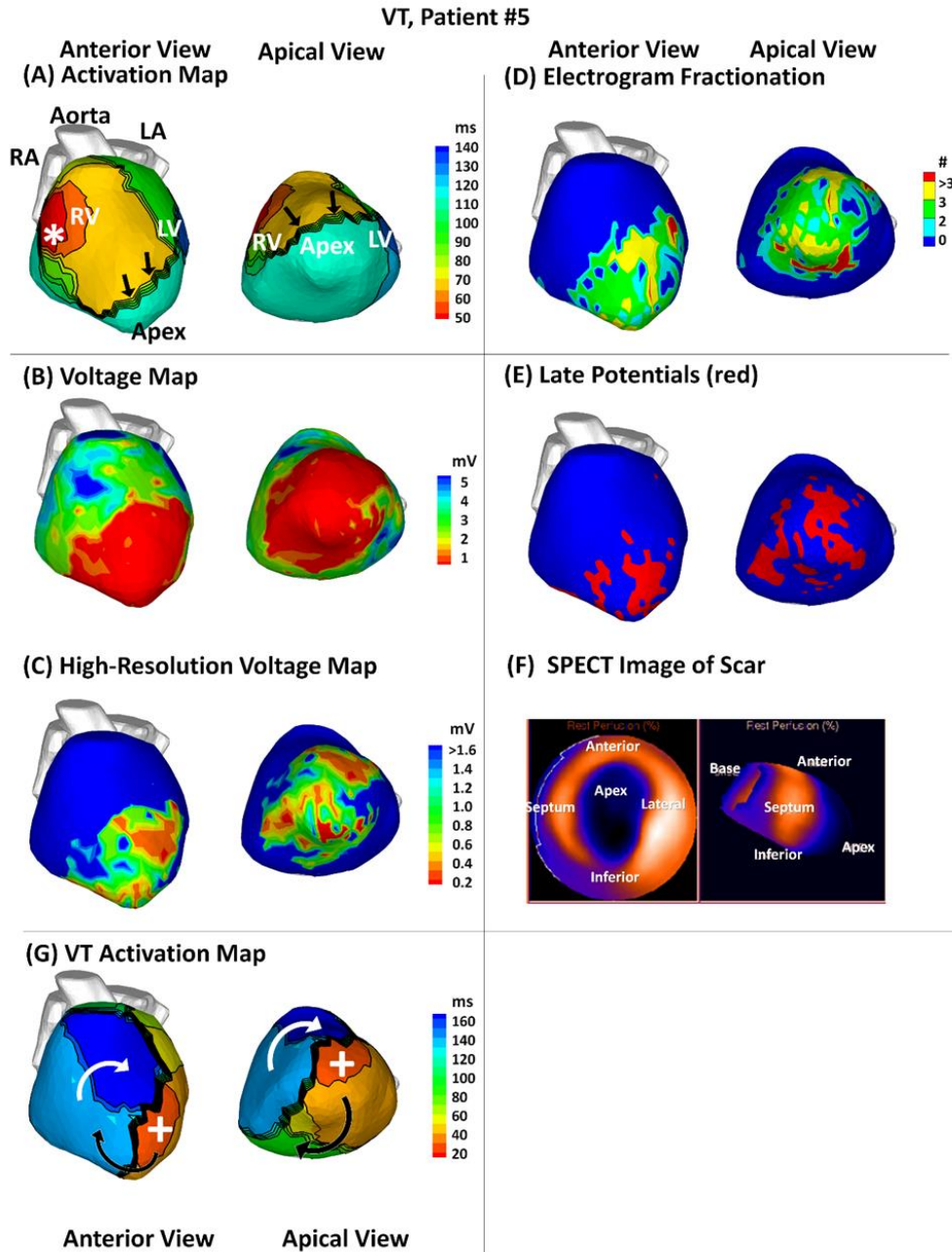


**Figure 2-11: Patient #5: VT patient; apical myocardial infarction**

(A) Activation isochrone map. (B) Global voltage map; magnitude of unipolar electrograms. (C) High-resolution scar voltage map with adjusted threshold and color scale. (D) Electrogram fractionation; number of intrinsic deflections per electrogram. (E) Late potentials; regions with late potentials shown in red. (F) Single-photon emission computed tomography (SPECT) anatomic scar in apical view (left) and long-axis view (right); (G) VT activation map. Panels A-E and G display the heart in anterior view (left) and apical view (right). In panel A, epicardial breakthrough is indicated by an asterisk “\*”, isochrones are depicted with thin black lines, and black arrows point to conduction block. In panel G, the VT site of origin is indicated by a plus sign “+”, curved arrows indicate propagation of the VT wavefront.

The VT site of origin was localized to the peripheral scar on the anterior wall near the apex.

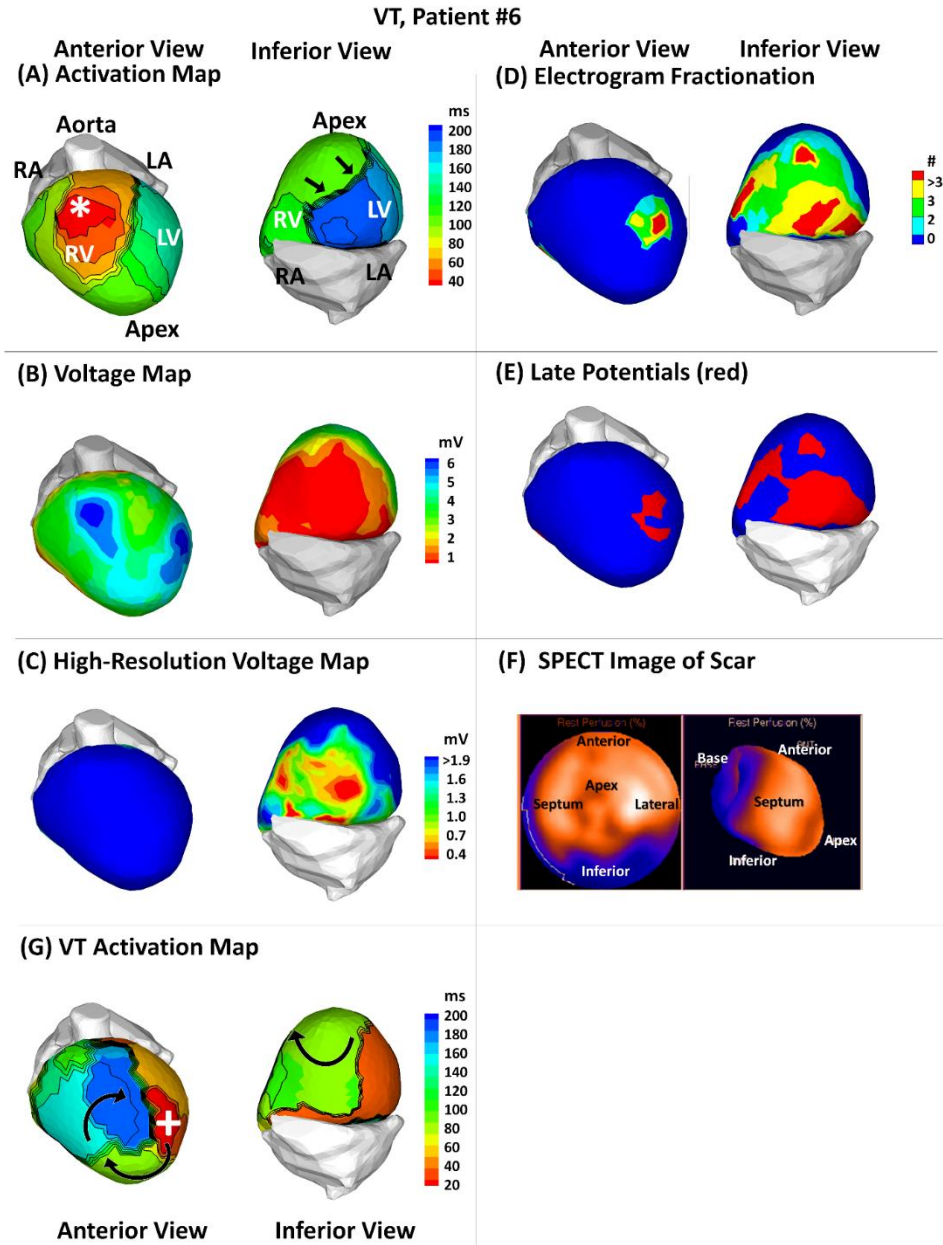


**Figure 2-12: Patient #6: VT patient; inferior myocardial infarction**

(A) Activation isochrone map. (B) Global voltage map; magnitude of unipolar electrograms. (C) High-resolution scar voltage map with adjusted threshold and color scale. (D) Electrogram fractionation; number of intrinsic deflections per electrogram. (E) Late potentials; regions with late potentials shown in red. (F) Single-photon emission computed tomography (SPECT) anatomic scar in apical view (left) and long-axis view (right); (G) VT activation map. Panels A-E and G display the heart in anterior view (left) and inferior view (right). In panel A, epicardial breakthrough is indicated by an asterisk “\*”, isochrones are depicted with thin black lines, and black arrows point to conduction block. In panel G, the VT site of origin is indicated by a plus sign “+”, curved arrows indicate propagation of the VT wavefront.

The VT site of origin was localized to the anterior wall near the apex. EGMs with normal voltage but fractionation and late potentials were found in this region.



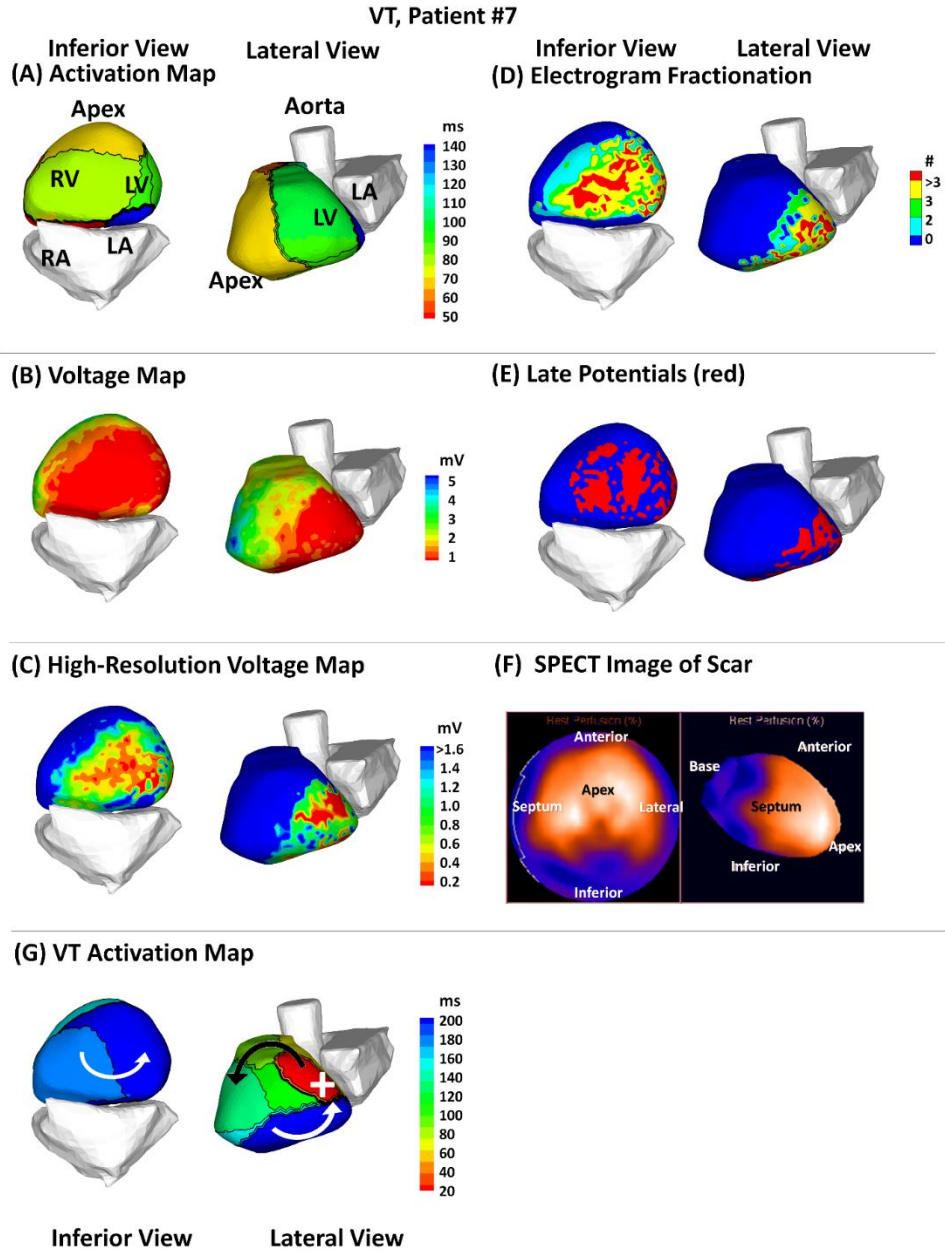


**Figure 2-13: Patient #7: VT patient; inferior and infero-lateral myocardial infarction**

(A) Activation isochrone map. (B) Global voltage map; magnitude of unipolar electrograms. (C) High-resolution scar voltage map with adjusted threshold and color scale. (D) Electrogram fractionation; number of intrinsic deflections per electrogram. (E) Late potentials; regions with late potentials shown in red. (F) Single-photon emission computed tomography (SPECT) anatomic scar in apical view (left) and long-axis view (right); (G) VT activation map. Panels A-E and G display the heart in inferior view (left) and lateral view (right). In panel A, epicardial breakthrough is indicated by an asterisk “\*”, isochrones are depicted with thin black lines, and black arrows point to conduction block. In panel G, the VT site of origin is indicated by a plus sign “+”, curved arrows indicate propagation of the VT wavefront.

The VT site of origin was localized to the dense scar near the lateral left ventricular base.

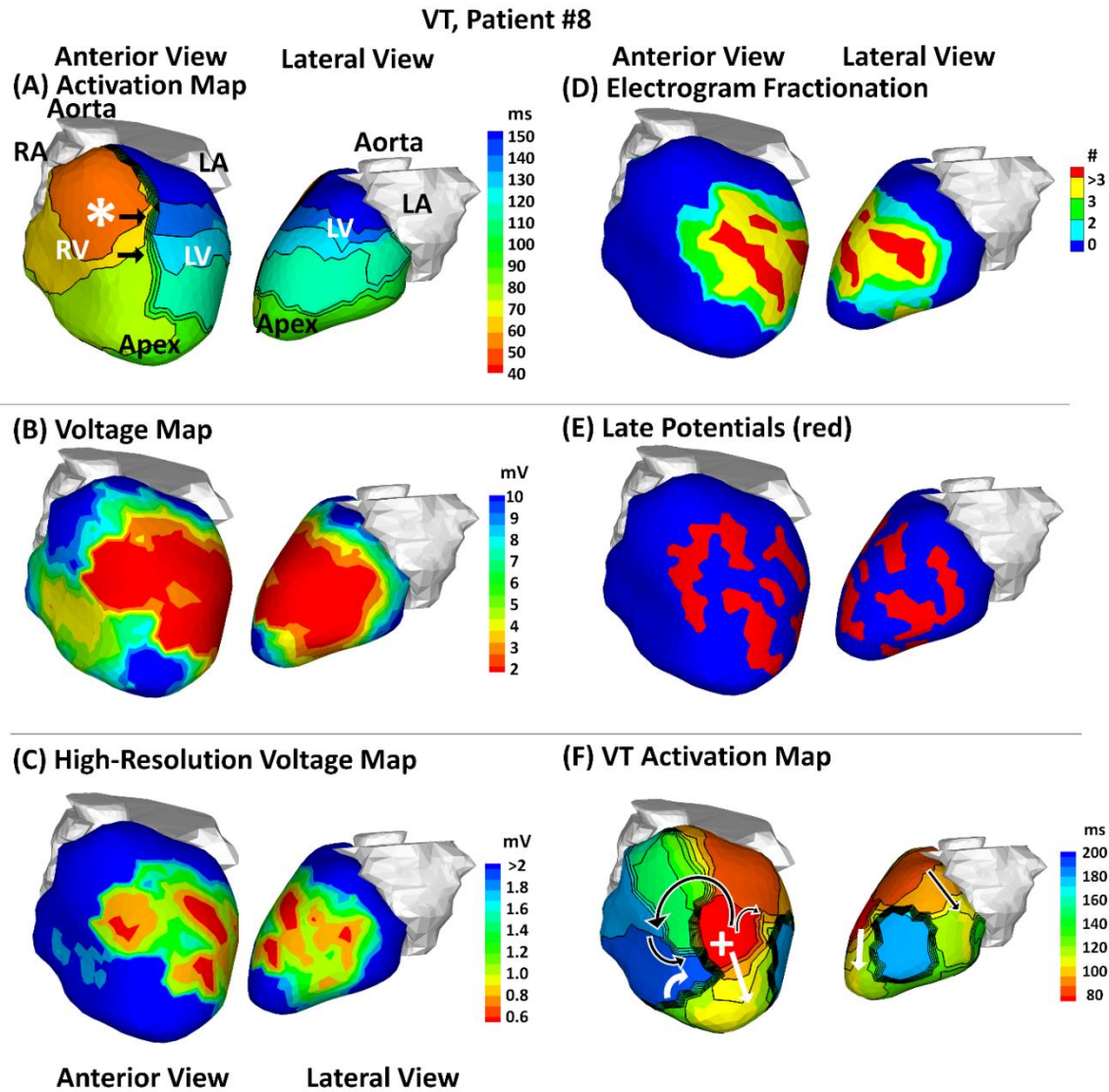


**Figure 2-14: Patient #8: VT patient; anterior myocardial infarction**

(A) Activation isochrone map. (B) Global voltage map; magnitude of unipolar electrograms. (C) High-resolution scar voltage map with adjusted threshold and color scale. (D) Electrogram fractionation; number of intrinsic deflections per electrogram. (E) Late potentials; regions with late potentials shown in red. (F) VT activation map. All panels display the heart in anterior view (left) and lateral view (right). In panel A, epicardial breakthrough is indicated by an asterisk “\*”, isochrones are depicted with thin black lines, and black arrows point to conduction block. In panel F, the VT site of origin is indicated by a plus sign “+”, curved arrows indicate propagation of the VT wavefront.

The VT site of origin was localized to the peripheral scar on the anterior wall near the apex.

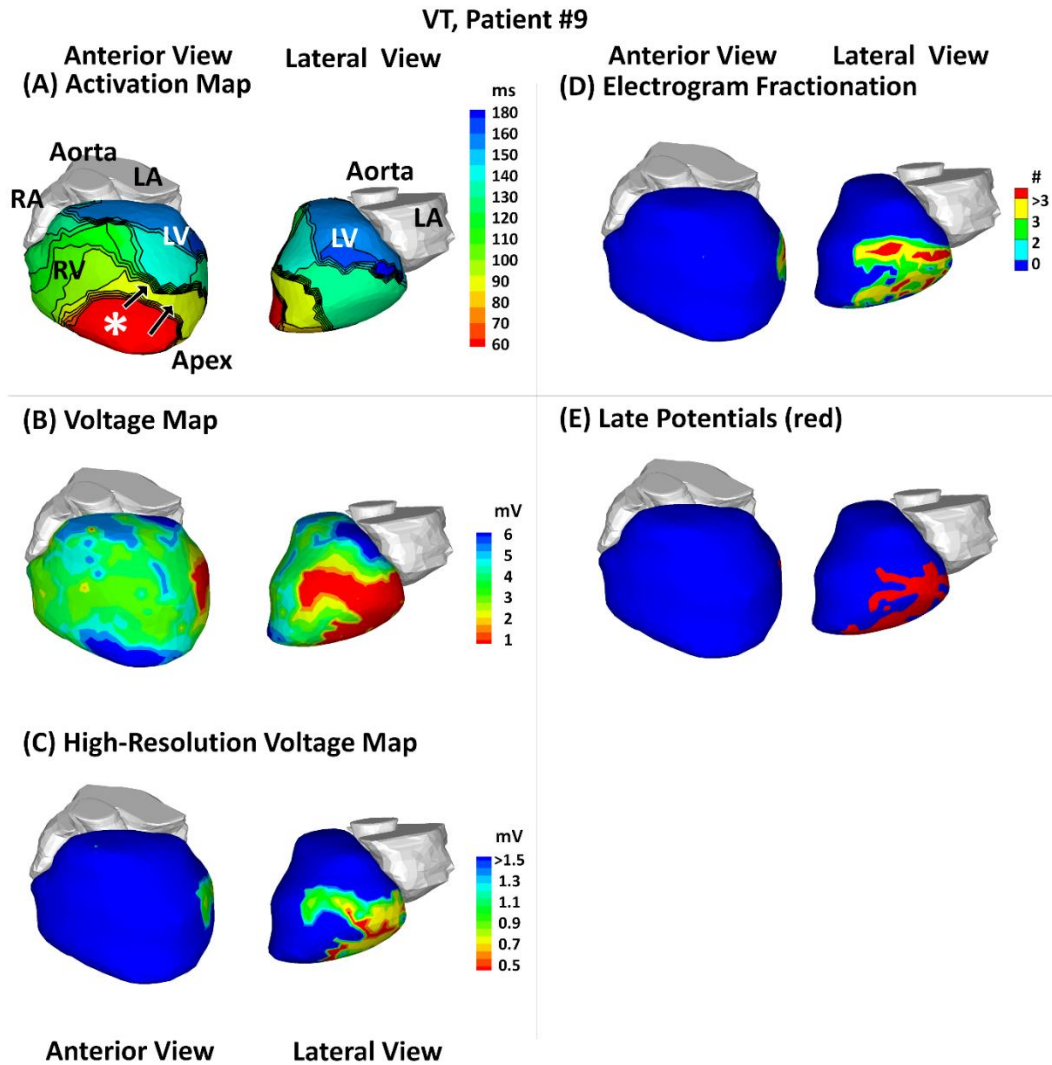


**Figure 2-15: Patient #9: VT patient; inferior and infero-lateral myocardial infarction**

(A) Activation isochrone map. (B) Global voltage map; magnitude of unipolar electrograms. (C) High-resolution scar voltage map with adjusted threshold and color scale. (D) Electrogram fractionation; number of intrinsic deflections per electrogram. (E) Late potentials; regions with late potentials shown in red. All panels display the heart in anterior view (left) and lateral view (right). In panel A, epicardial breakthrough is indicated by an asterisk “\*”, isochrones are depicted with thin black lines, and black arrows point to conduction block.

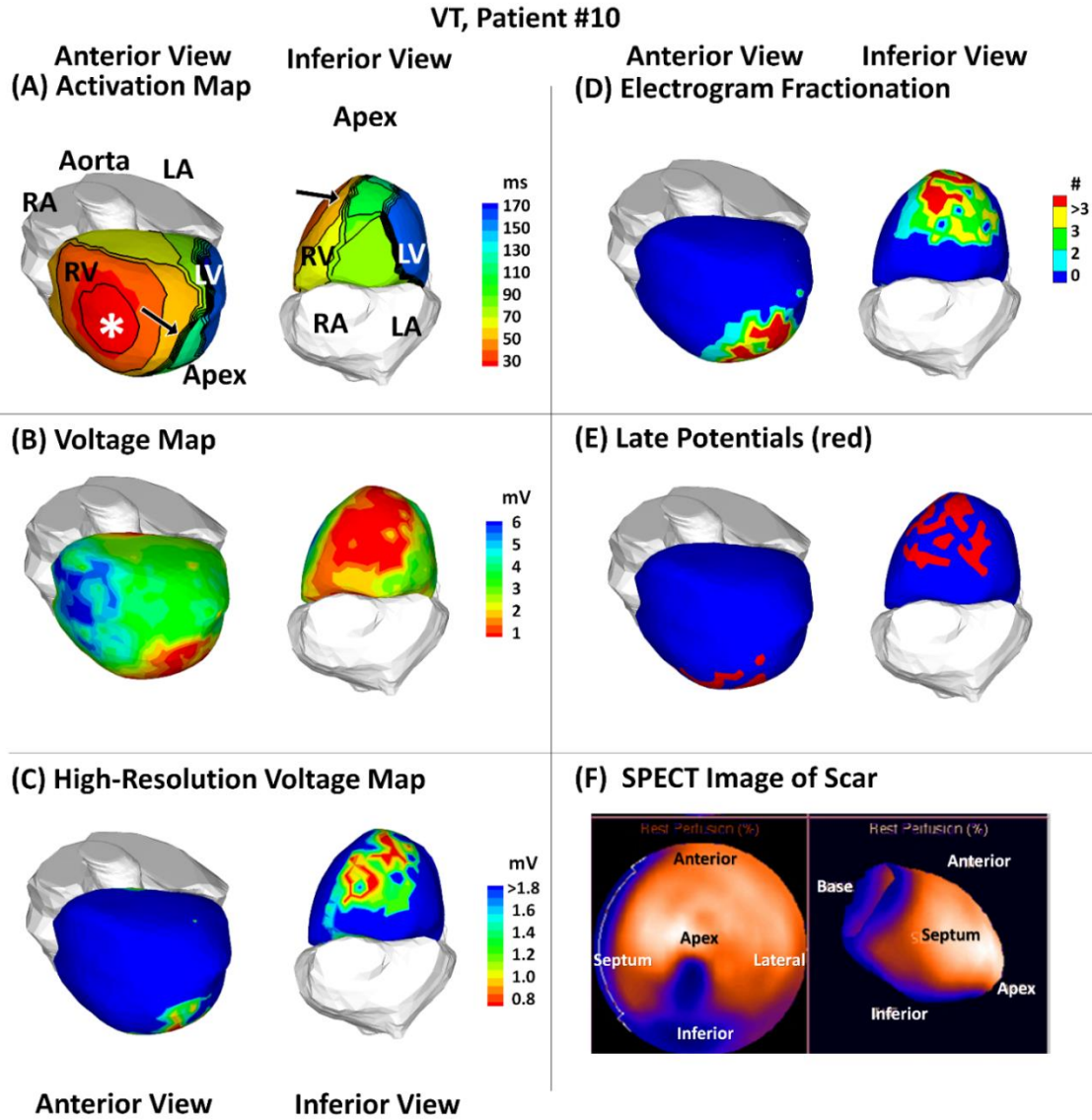


**Figure 2-16: Patient #10: VT patient; inferior and apical myocardial infarction**

(A) Activation isochrone map. (B) Global voltage map; magnitude of unipolar electrograms. (C) High-resolution scar voltage map with adjusted threshold and color scale. (D) Electrogram fractionation; number of intrinsic deflections per electrogram. (E) Late potentials; regions with late potentials shown in red. (F) Single-photon emission computed tomography (SPECT) anatomic scar in apical view (left) and long-axis view (right). Panels A-E display the heart in anterior view (left) and inferior view (right). In panel A, epicardial breakthrough is indicated by an asterisk “\*”, isochrones are depicted with thin black lines, and black arrows point to conduction block.

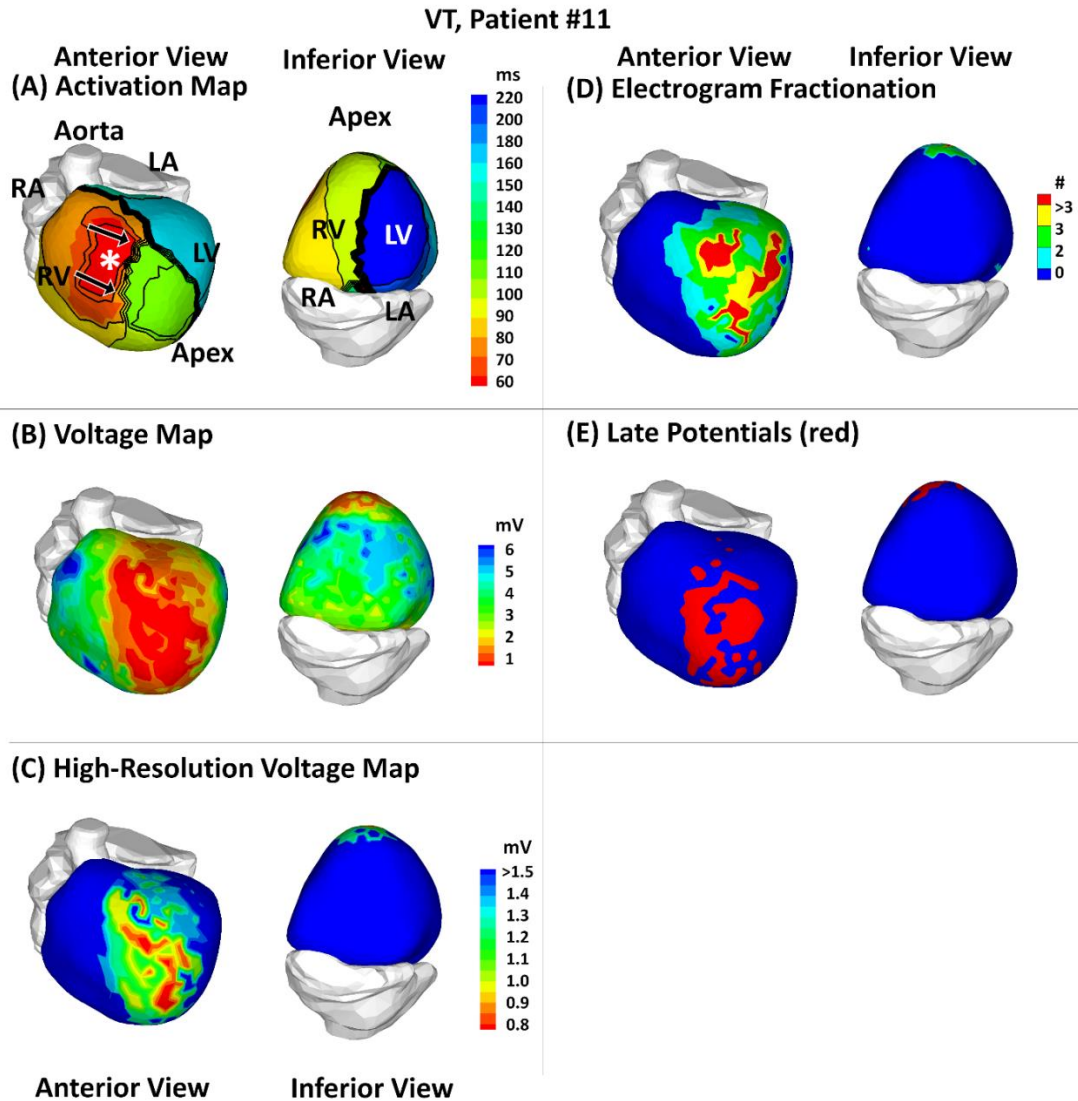


**Figure 2-17: Patient #11: VT patient; anterior and apical myocardial infarction**

(A) Activation isochrone map. (B) Global voltage map; magnitude of unipolar electrograms. (C) High-resolution scar voltage map with adjusted threshold and color scale. (D) Electrogram fractionation; number of intrinsic deflections per electrogram. (E) Late potentials; regions with late potentials shown in red. All panels display the heart in anterior view (left) and inferior view (right). In panel A, epicardial breakthrough is indicated by an asterisk “\*”, isochrones are depicted with thin black lines, and black arrows point to conduction block.

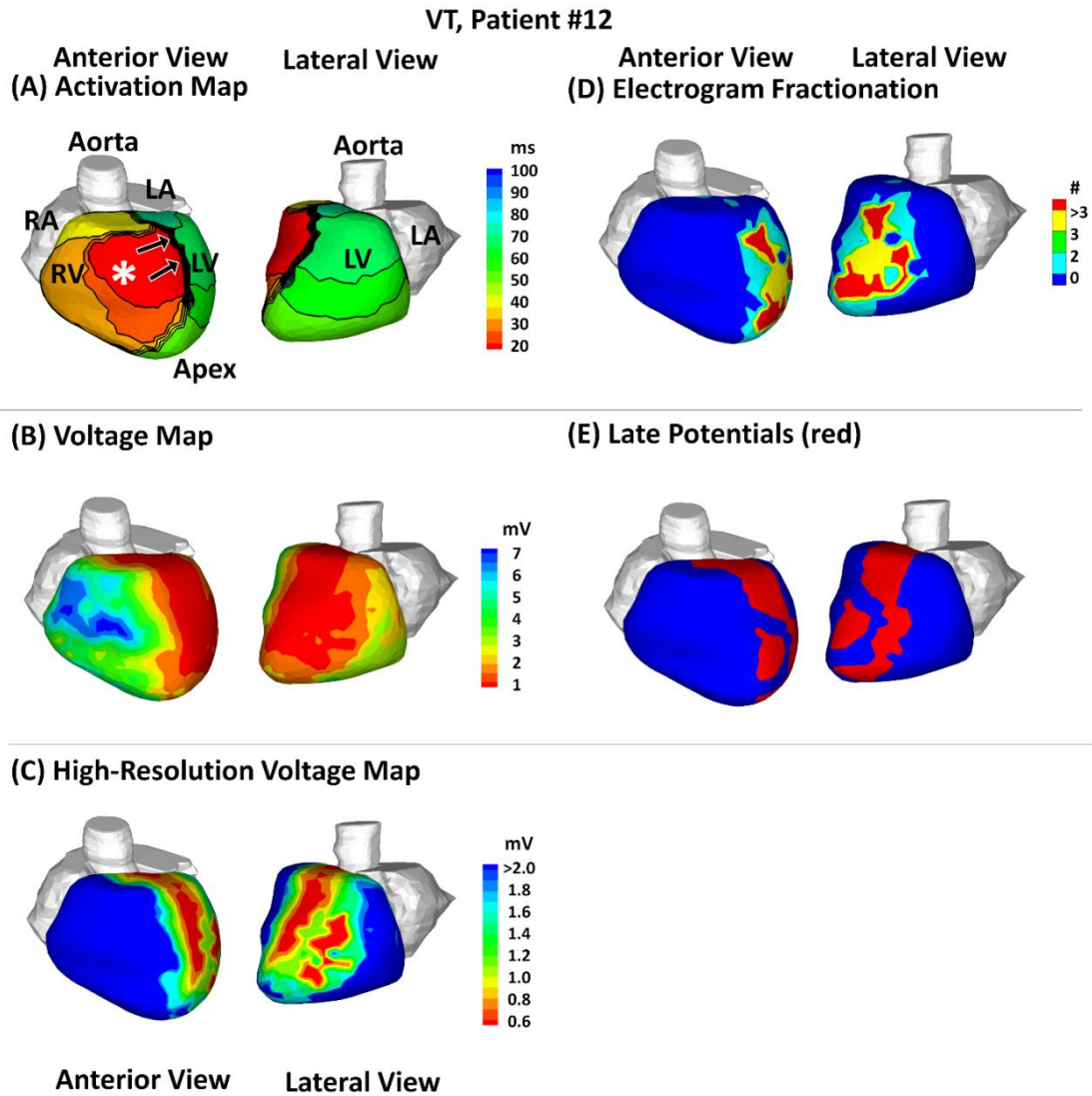


**Figure 2-18: Patient #12: VT patient; anterior and apical myocardial infarction**

(A) Activation isochrone map. (B) Global voltage map; magnitude of unipolar electrograms. (C) High-resolution scar voltage map with adjusted threshold and color scale. (D) Electrogram fractionation; number of intrinsic deflections per electrogram. (E) Late potentials; regions with late potentials shown in red. All panels display the heart in anterior view (left) and lateral view (right). In panel A, epicardial breakthrough is indicated by an asterisk “\*”, isochrones are depicted with thin black lines, and black arrows point to conduction block.

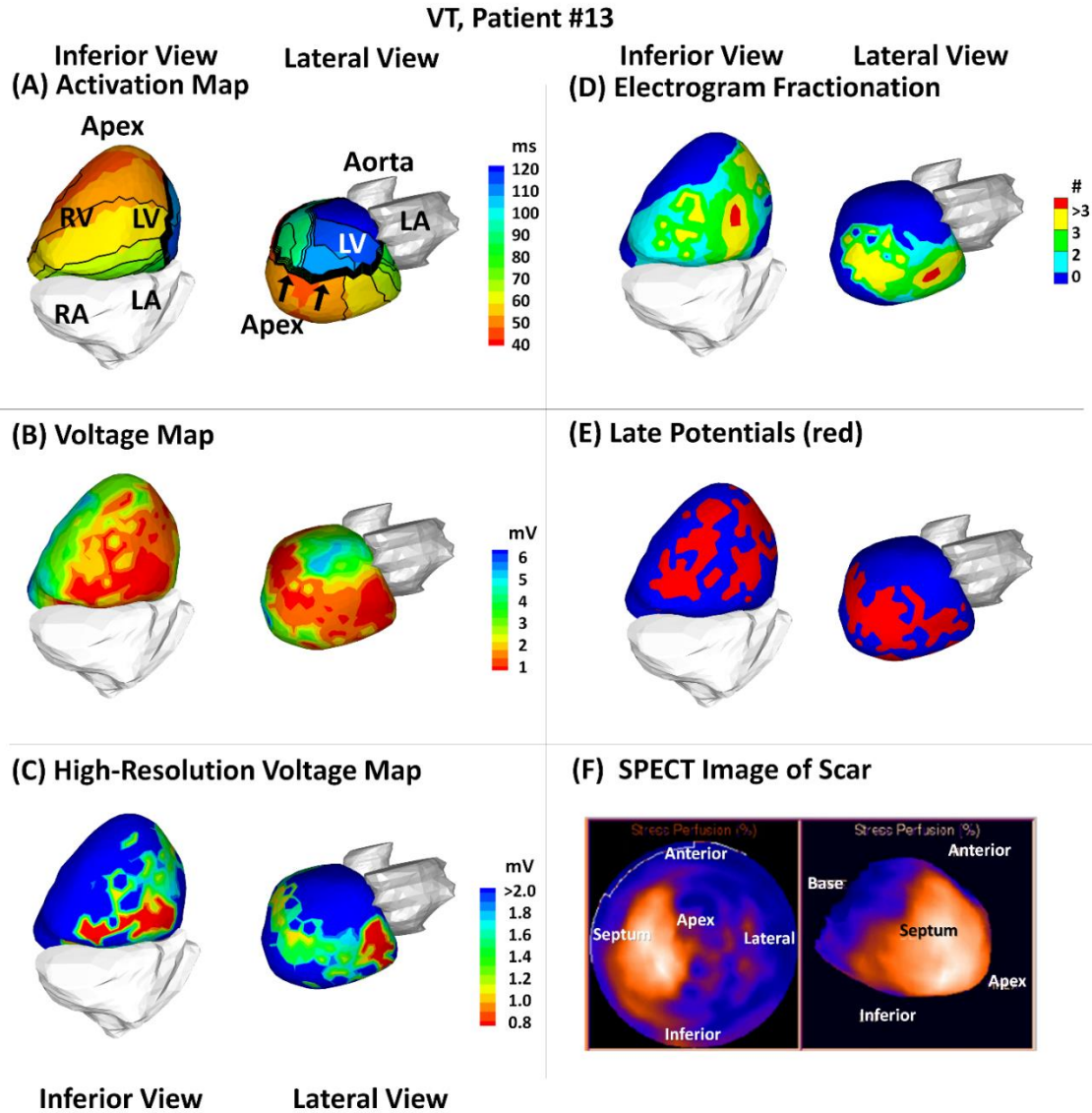


**Figure 2-19: Patient #13: VT patient; anterior, lateral and inferior myocardial infarction**

(A) Activation isochrone map. (B) Global voltage map; magnitude of unipolar electrograms. (C) High-resolution scar voltage map with adjusted threshold and color scale. (D) Electrogram fractionation; number of intrinsic deflections per electrogram. (E) Late potentials; regions with late potentials shown in red. (F) Single-photon emission computed tomography (SPECT) anatomic scar in apical view (left) and long-axis view (right). Panels A-E display the heart in inferior view (left) and lateral view (right). In panel A, isochrones are depicted with thin black lines, and black arrows point to conduction block.

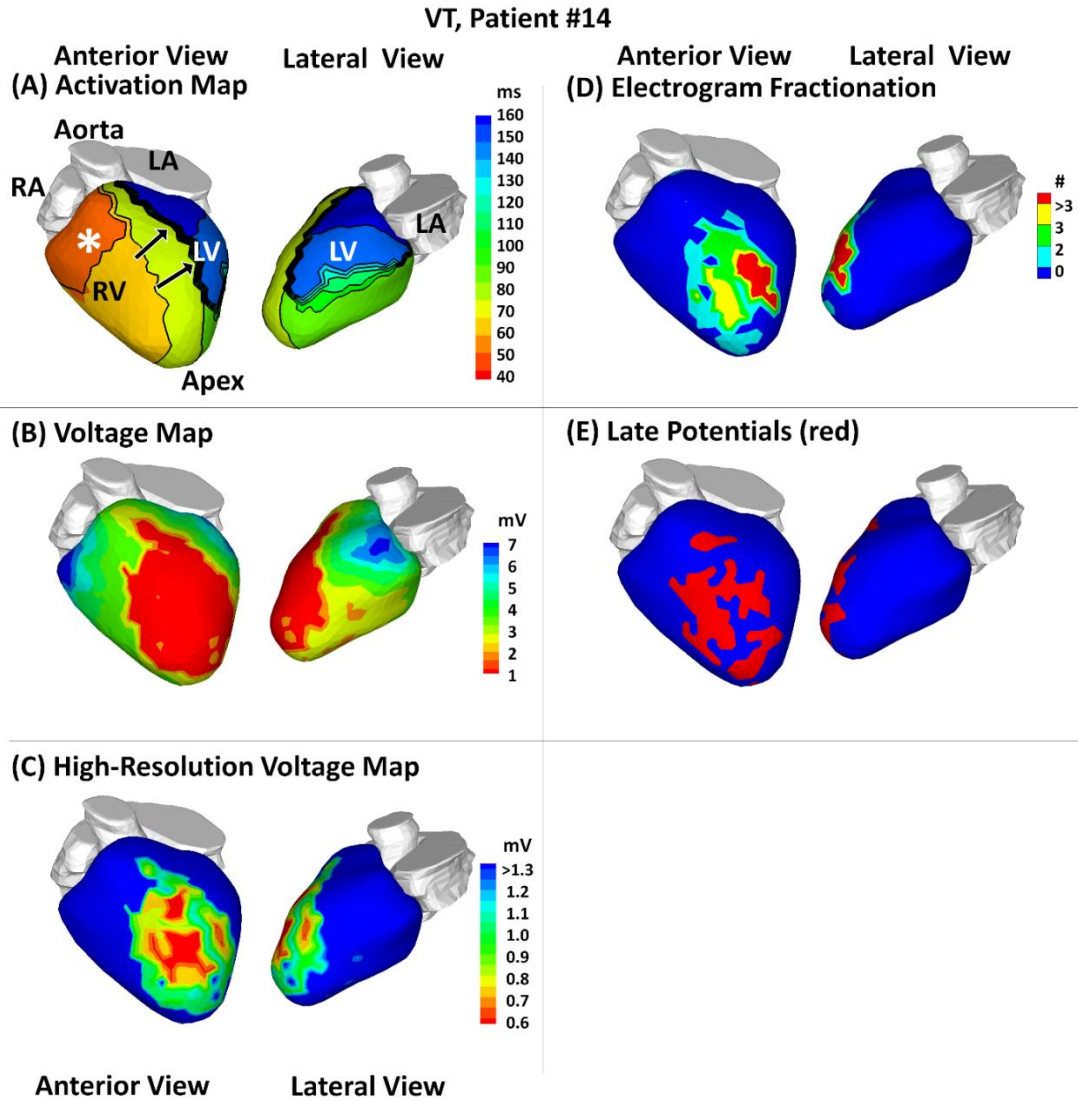


**Figure 2-20: Patient #14: VT patient; anterior myocardial infarction**

(A) Activation isochrone map. (B) Global voltage map; magnitude of unipolar electrograms. (C) High-resolution scar voltage map with adjusted threshold and color scale. (D) Electrogram fractionation; number of intrinsic deflections per electrogram. (E) Late potentials; regions with late potentials shown in red. All panels display the heart in anterior view (left) and lateral view (right). In panel A, epicardial breakthrough is indicated by an asterisk “\*”, isochrones are depicted with thin black lines, and black arrows point to conduction block.



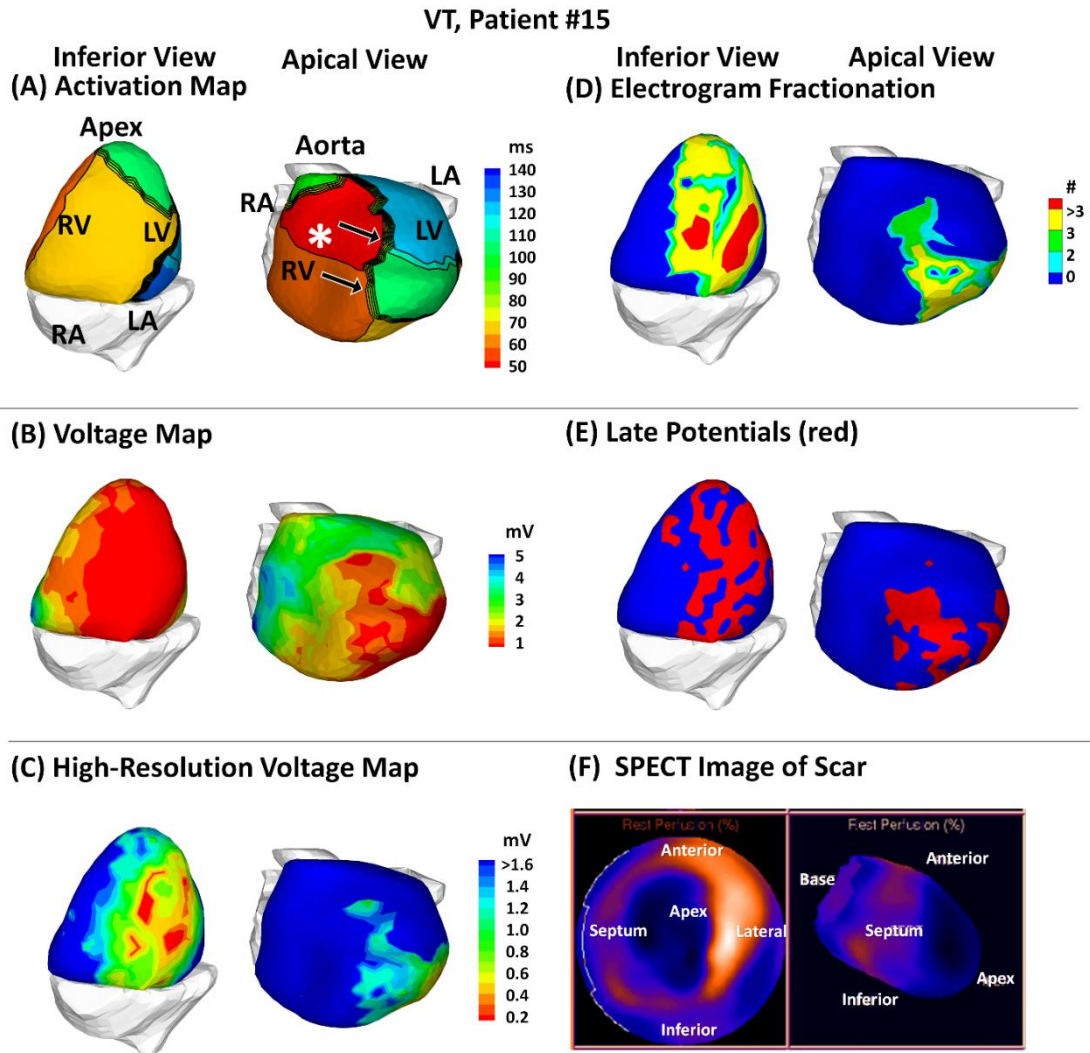


**Figure 2-21: Patient #15: VT patient; lateral, inferior and apical myocardial infarction**

(A) Activation isochrone map. (B) Global voltage map; magnitude of unipolar electrograms. (C) High-resolution scar voltage map with adjusted threshold and color scale. (D) Electrogram fractionation; number of intrinsic deflections per electrogram. (E) Late potentials; regions with late potentials shown in red. (F) Single-photon emission computed tomography (SPECT) anatomic scar in apical view (left) and long-axis view (right). Panels A-E display the heart in inferior view (left) and apical view (right). In panel A, epicardial breakthrough is indicated by an asterisk “\*”, isochrones are depicted with thin black lines, and black arrows point to conduction block.

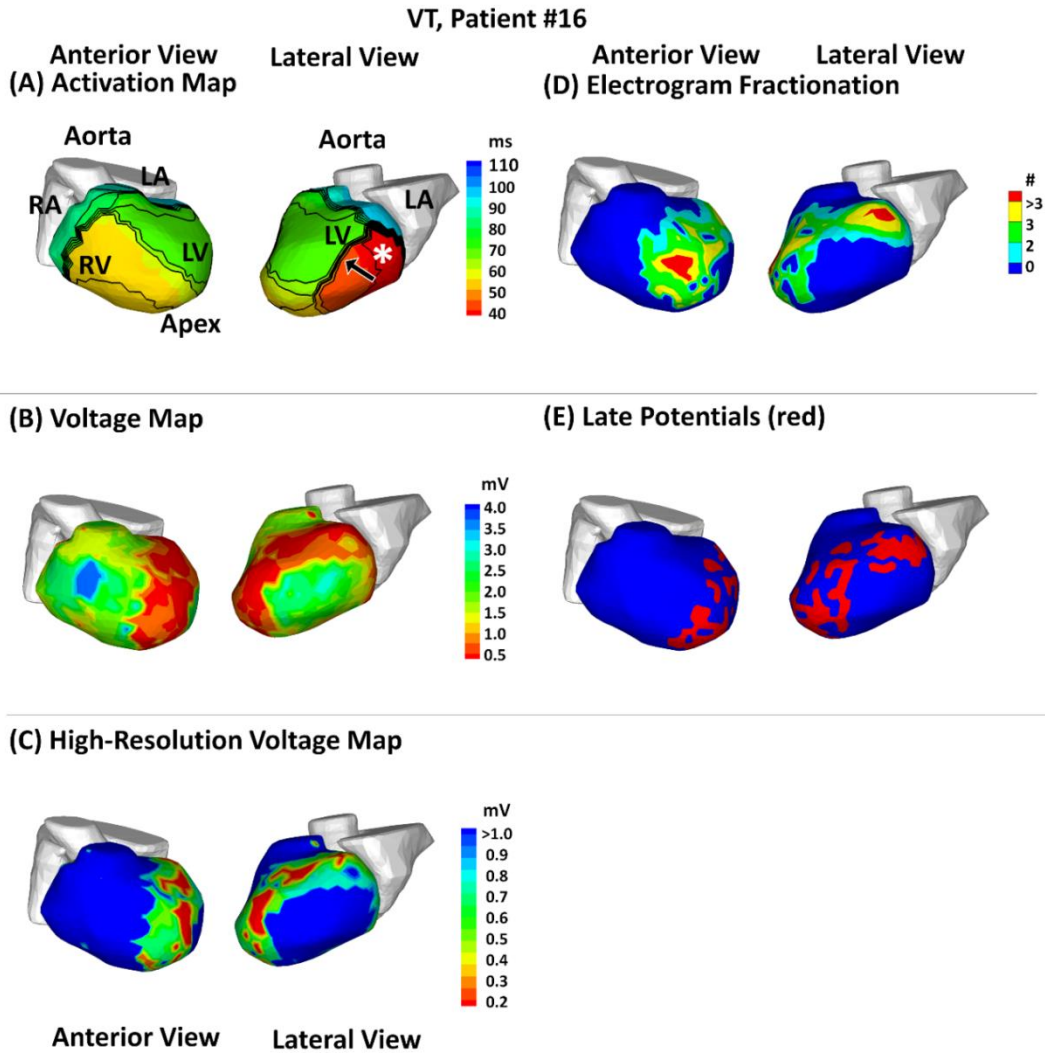


**Figure 2-22: Patient #16: VT patient; anterior and apical myocardial infarction**

(A) Activation isochrone map. (B) Global voltage map; magnitude of unipolar electrograms. (C) High-resolution scar voltage map with adjusted threshold and color scale. (D) Electrogram fractionation; number of intrinsic deflections per electrogram. (E) Late potentials; regions with late potentials shown in red. All panels display the heart in anterior view (left) and lateral view (right). In panel A, epicardial breakthrough is indicated by an asterisk “\*”, isochrones are depicted with thin black lines, and black arrows point to conduction block.

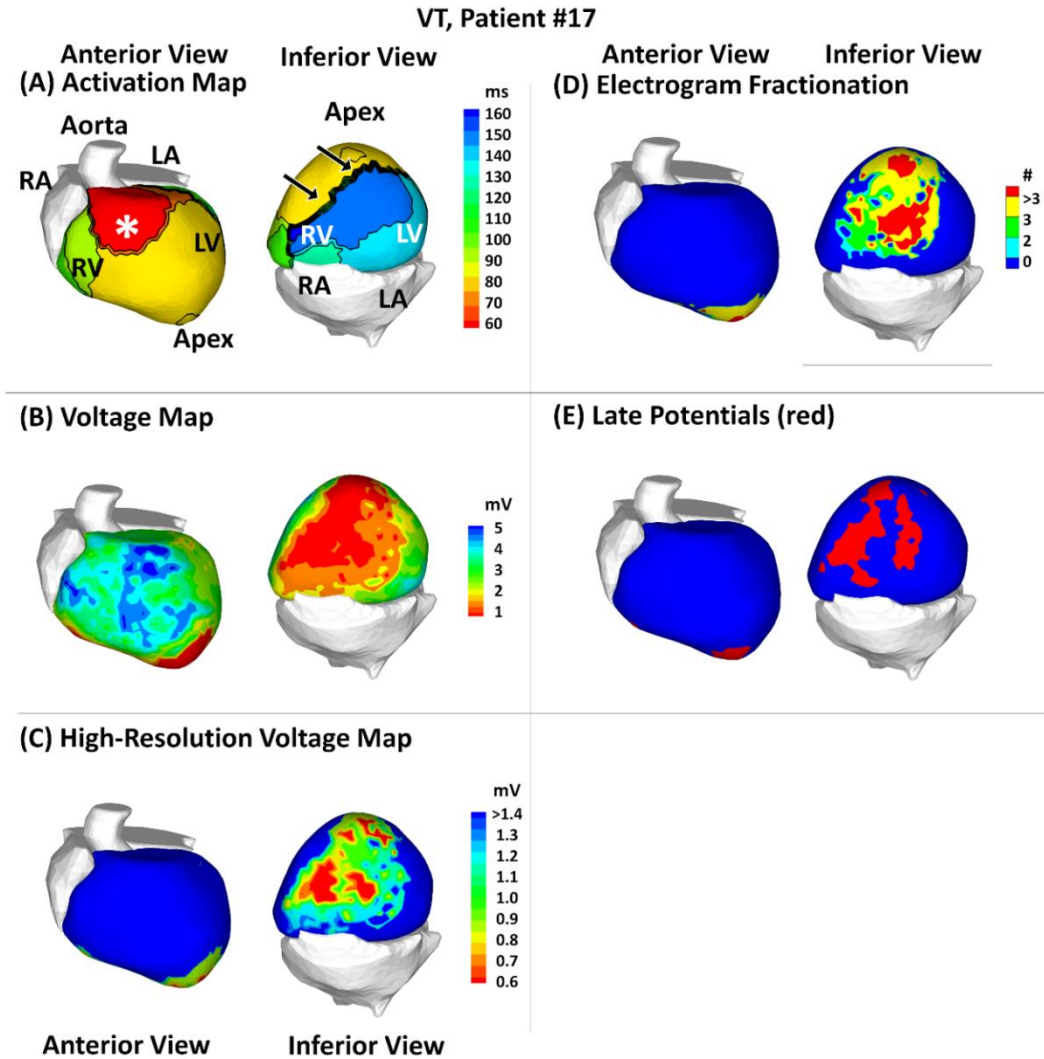


**Figure 2-23: Patient #17: VT patient; inferior and apical myocardial infarction**

(A) Activation isochrone map. (B) Global voltage map; magnitude of unipolar electrograms. (C) High-resolution scar voltage map with adjusted threshold and color scale. (D) Electrogram fractionation; number of intrinsic deflections per electrogram. (E) Late potentials; regions with late potentials shown in red. All panels display the heart in anterior view (left) and inferior view (right). In panel A, epicardial breakthrough is indicated by an asterisk “\*”, isochrones are depicted with thin black lines, and black arrows point to conduction block.

## 2.7.2 Maps of EP Substrate for Non-VT Patients

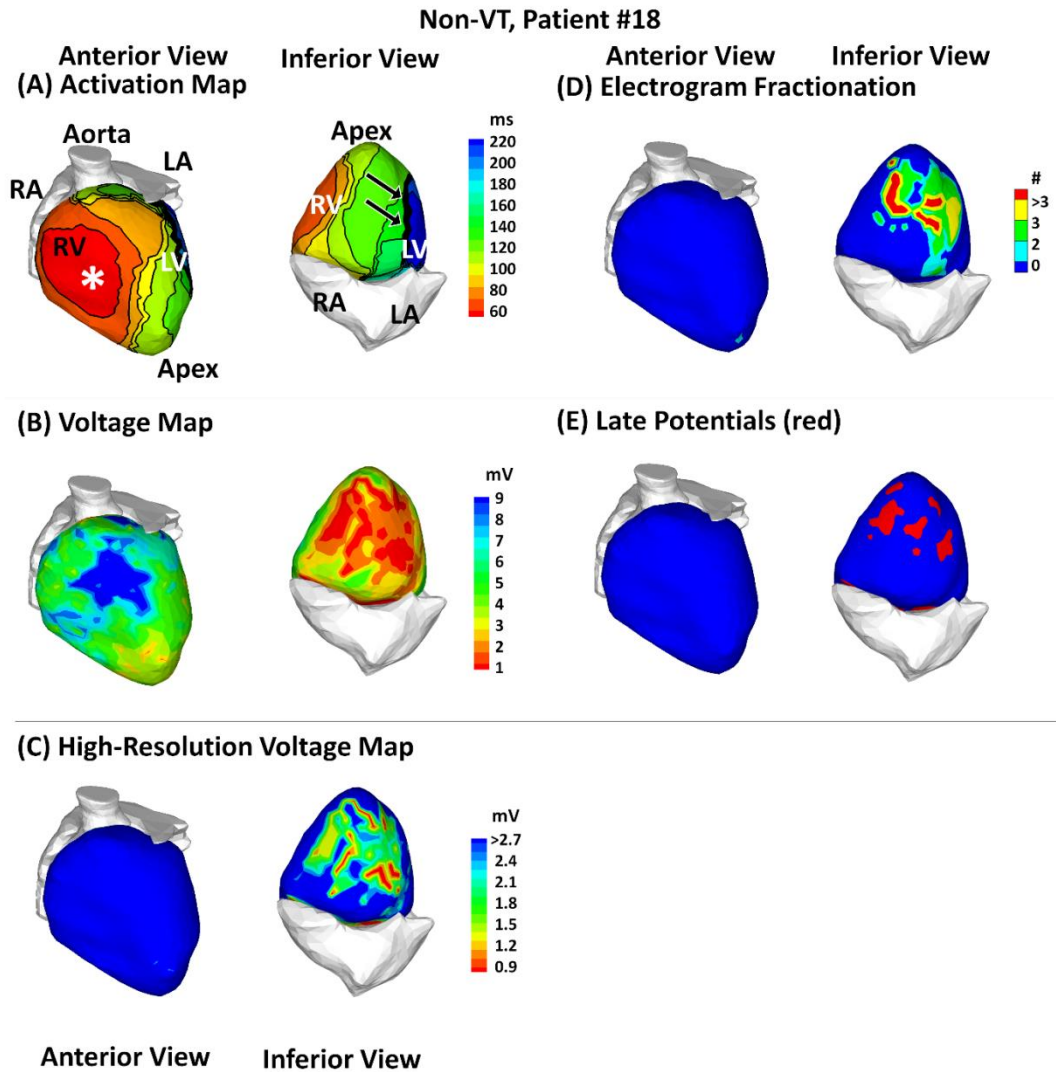


**Figure 2-24: Patient #18: Non-VT patient; inferior myocardial infarction**

(A) Activation isochrone map. (B) Global voltage map; magnitude of unipolar electrograms. (C) High-resolution scar voltage map with adjusted threshold and color scale. (D) Electrogram fractionation; number of intrinsic deflections per electrogram. (E) Late potentials; regions with late potentials shown in red. All panels display the heart in anterior view (left) and inferior view (right). In panel A, epicardial breakthrough is indicated by an asterisk “\*”, isochrones are depicted with thin black lines, and black arrows point to conduction block.

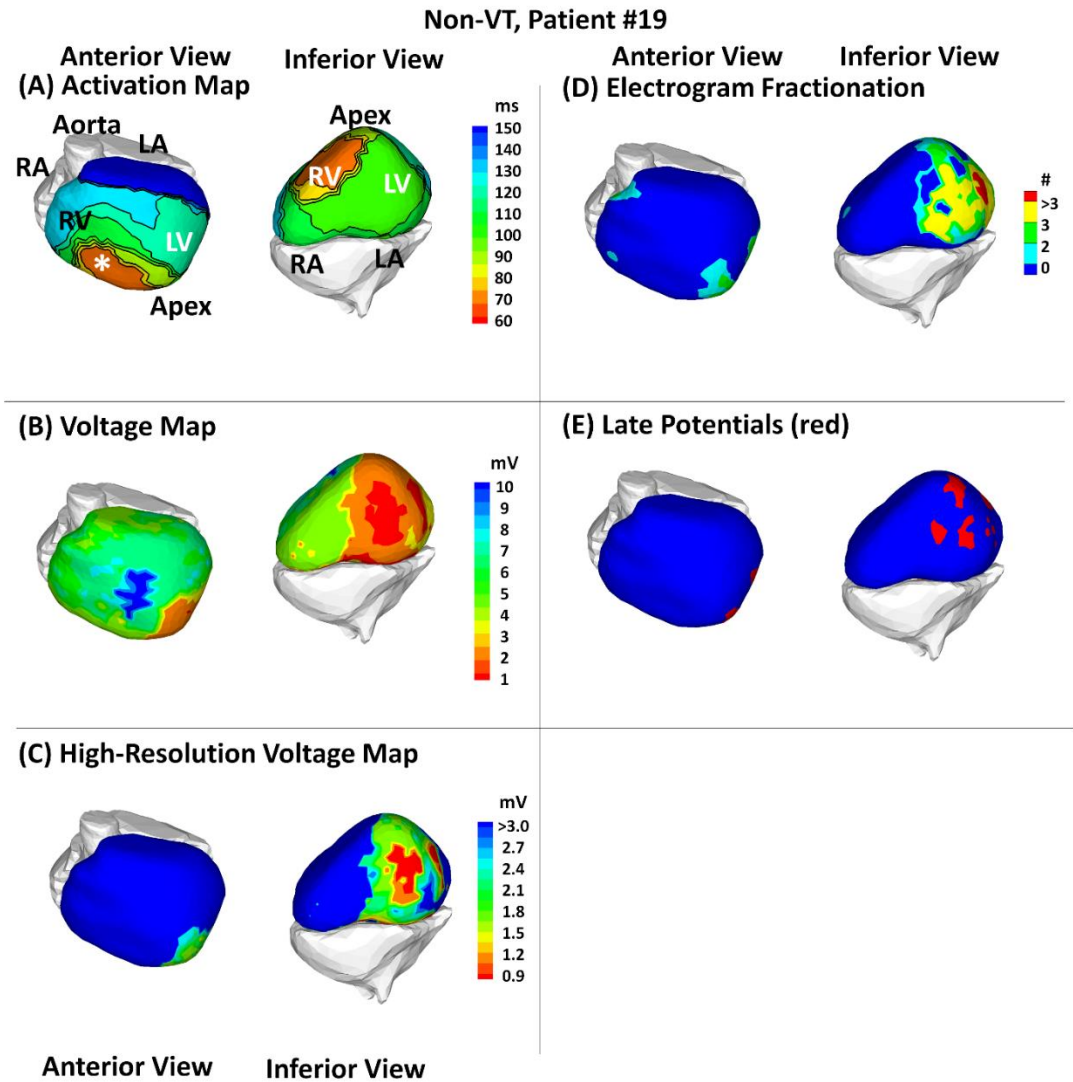


**Figure 2-25: Patient #19: Non-VT patient; apical, inferior and infero-lateral myocardial infarction**

(A) Activation isochrone map. (B) Global voltage map; magnitude of unipolar electrograms. (C) High-resolution scar voltage map with adjusted threshold and color scale. (D) Electrogram fractionation; number of intrinsic deflections per electrogram. (E) Late potentials; regions with late potentials shown in red. All panels display the heart in anterior view (left) and inferior view (right). In panel A, epicardial breakthrough is indicated by an asterisk “\*”, isochrones are depicted with thin black lines.

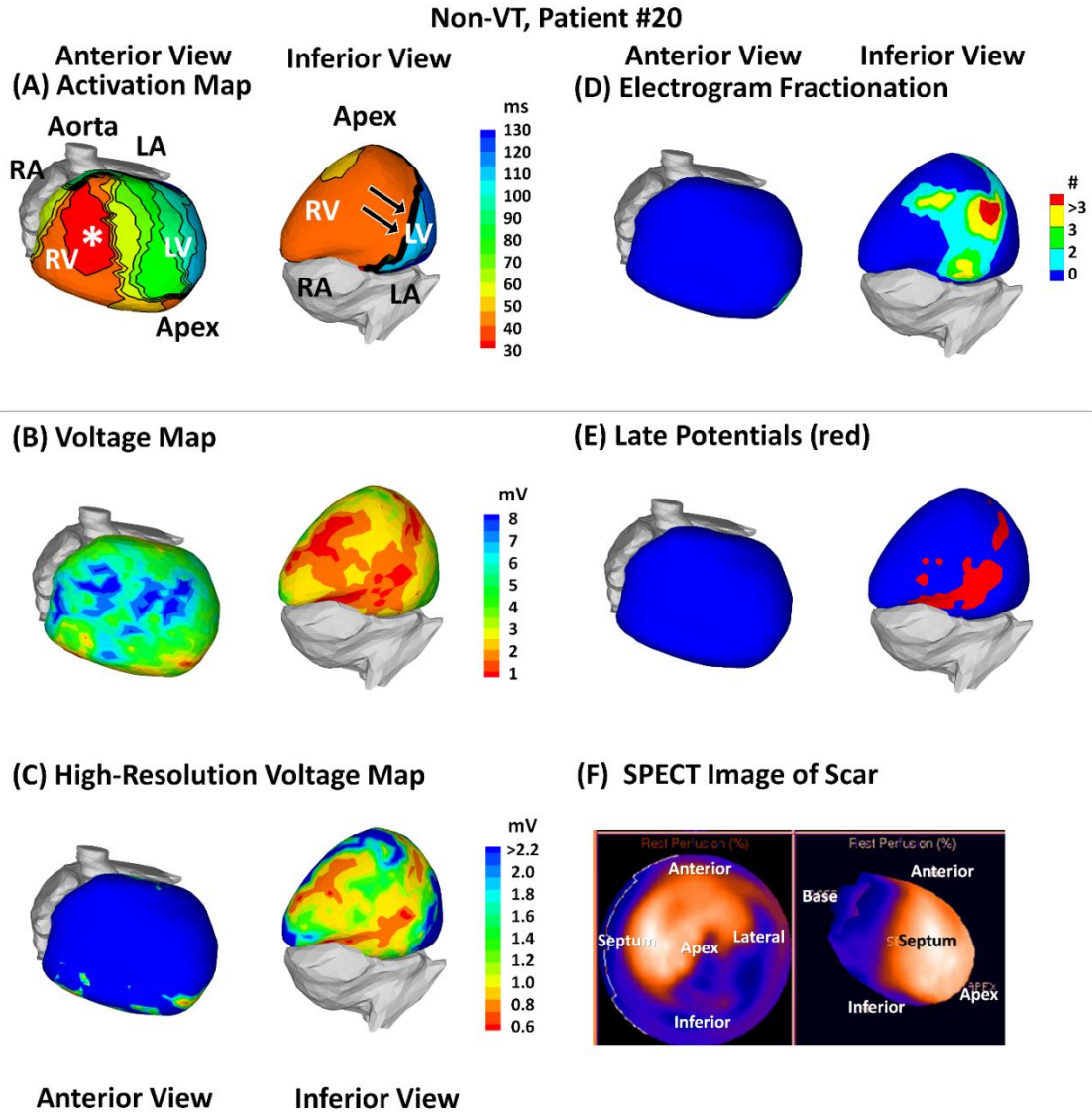


**Figure 2-26: Patient #20: Non-VT patient; apical and inferior myocardial infarction**

(A) Activation isochrone map. (B) Global voltage map; magnitude of unipolar electrograms. (C) High-resolution scar voltage map with adjusted threshold and color scale. (D) Electrogram fractionation; number of intrinsic deflections per electrogram. (E) Late potentials; regions with late potentials shown in red. (F) Single-photon emission computed tomography (SPECT) anatomic scar in apical view (left) and long-axis view (right). Panels A-E display the heart in anterior view (left) and inferior view (right). In panel A, epicardial breakthrough is indicated by an asterisk “\*”, isochrones are depicted with thin black lines, and black arrows point to conduction block.

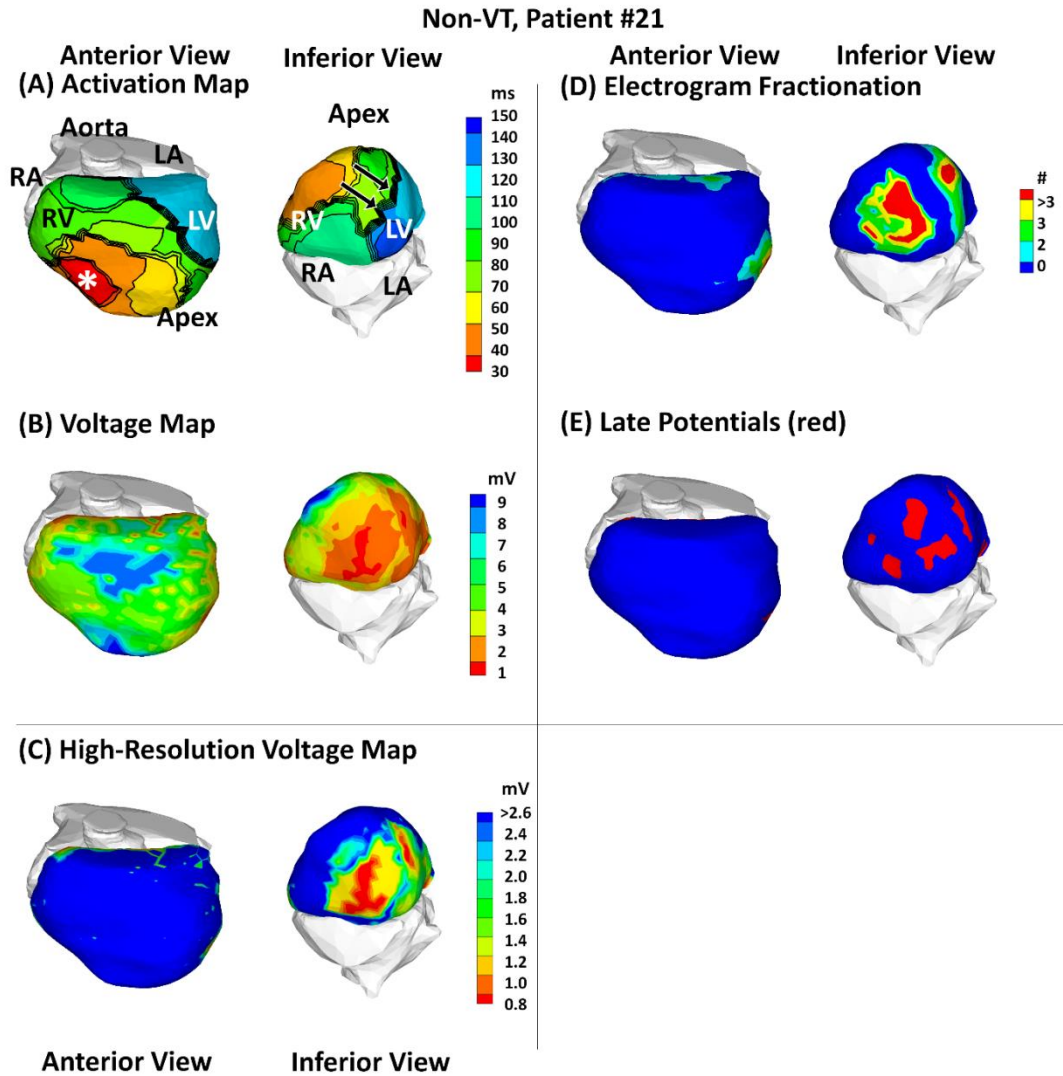


**Figure 2-27: Patient #21: Non-VT patient; inferior myocardial infarction**

(A) Activation isochrone map. (B) Global voltage map; magnitude of unipolar electrograms. (C) High-resolution scar voltage map with adjusted threshold and color scale. (D) Electrogram fractionation; number of intrinsic deflections per electrogram. (E) Late potentials; regions with late potentials shown in red. All panels display the heart in anterior view (left) and inferior view (right). In panel A, epicardial breakthrough is indicated by an asterisk “\*”, isochrones are depicted with thin black lines, and black arrows point to conduction block.

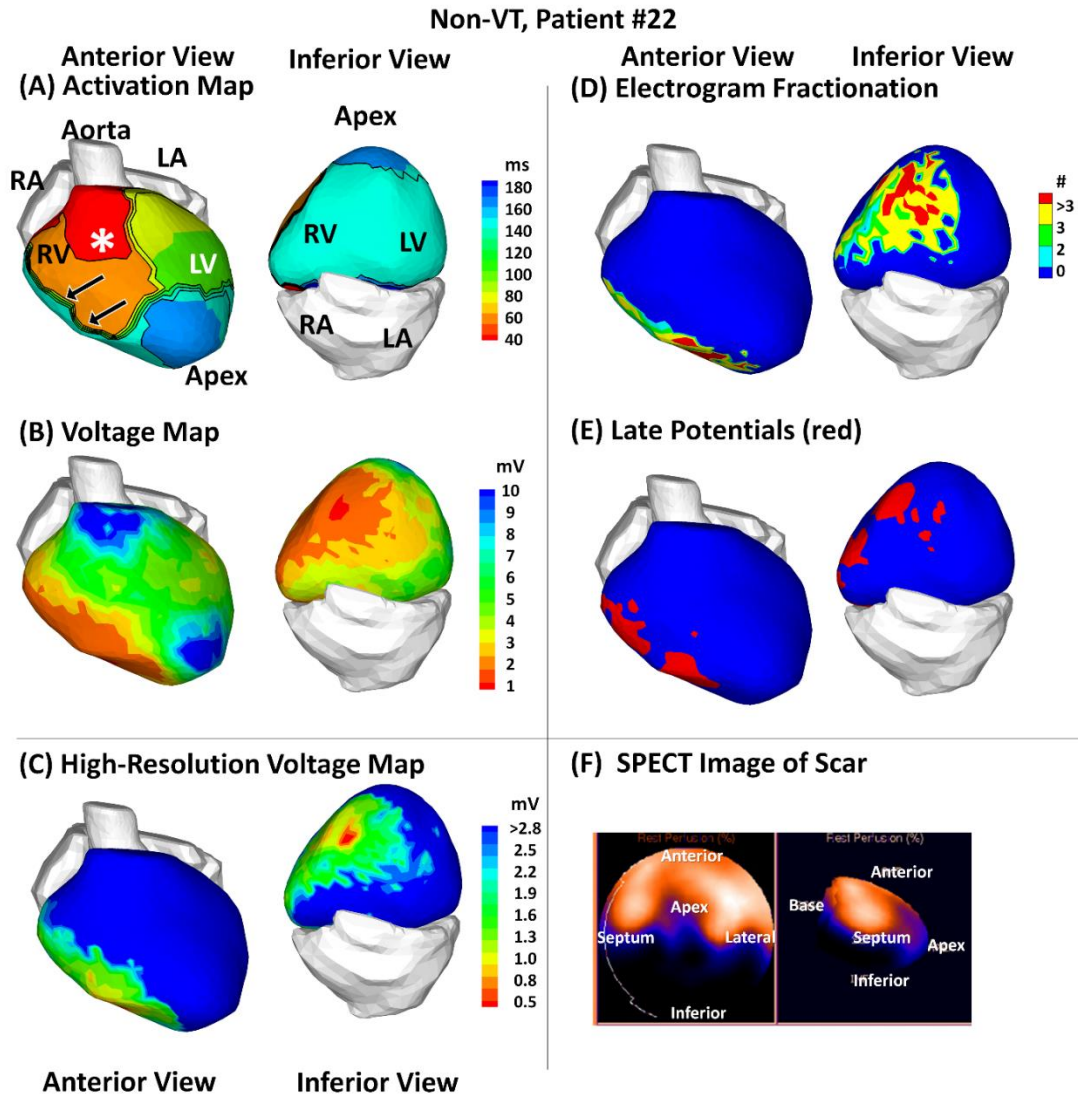


**Figure 2-28: Patient #22: Non-VT patient; inferior myocardial infarction**

(A) Activation isochrone map. (B) Global voltage map; magnitude of unipolar electrograms. (C) High-resolution scar voltage map with adjusted threshold and color scale. (D) Electrogram fractionation; number of intrinsic deflections per electrogram. (E) Late potentials; regions with late potentials shown in red. (F) Single-photon emission computed tomography (SPECT) anatomic scar in apical view (left) and long-axis view (right). Panels A-E display the heart in anterior view (left) and inferior view (right). In panel A, epicardial breakthrough is indicated by an asterisk “\*”, isochrones are depicted with thin black lines, and black arrows point to conduction block.



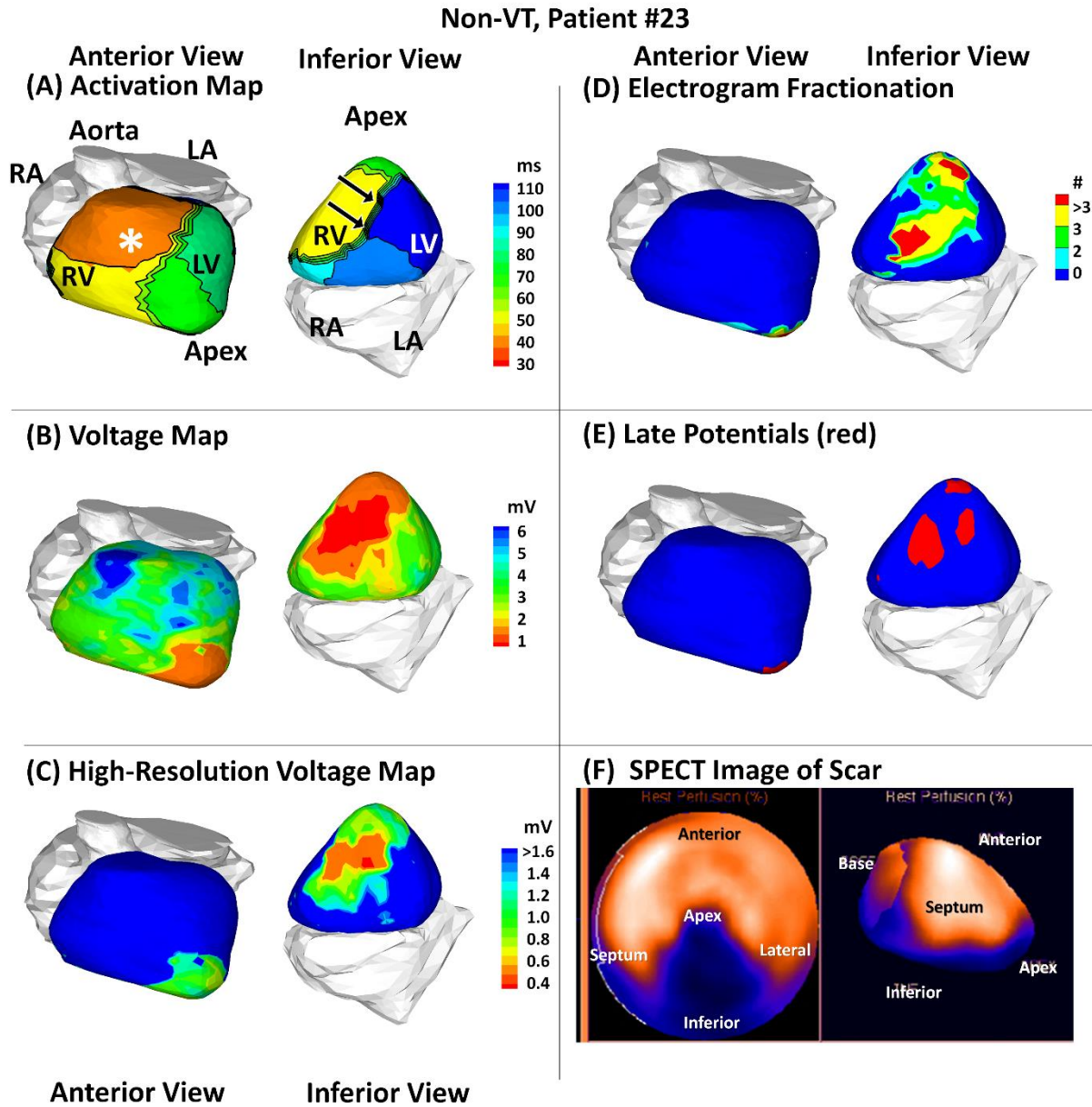


**Figure 2-29: Patient #23: Non-VT patient; apical and inferior myocardial infarction**

(A) Activation isochrone map. (B) Global voltage map; magnitude of unipolar electrograms. (C) High-resolution scar voltage map with adjusted threshold and color scale. (D) Electrogram fractionation; number of intrinsic deflections per electrogram. (E) Late potentials; regions with late potentials shown in red. (F) Single-photon emission computed tomography (SPECT) anatomic scar in apical view (left) and long-axis view (right). Panels A-E display the heart in anterior view (left) and inferior view (right). In panel A, epicardial breakthrough is indicated by an asterisk “\*”, isochrones are depicted with thin black lines, and black arrows point to conduction block.

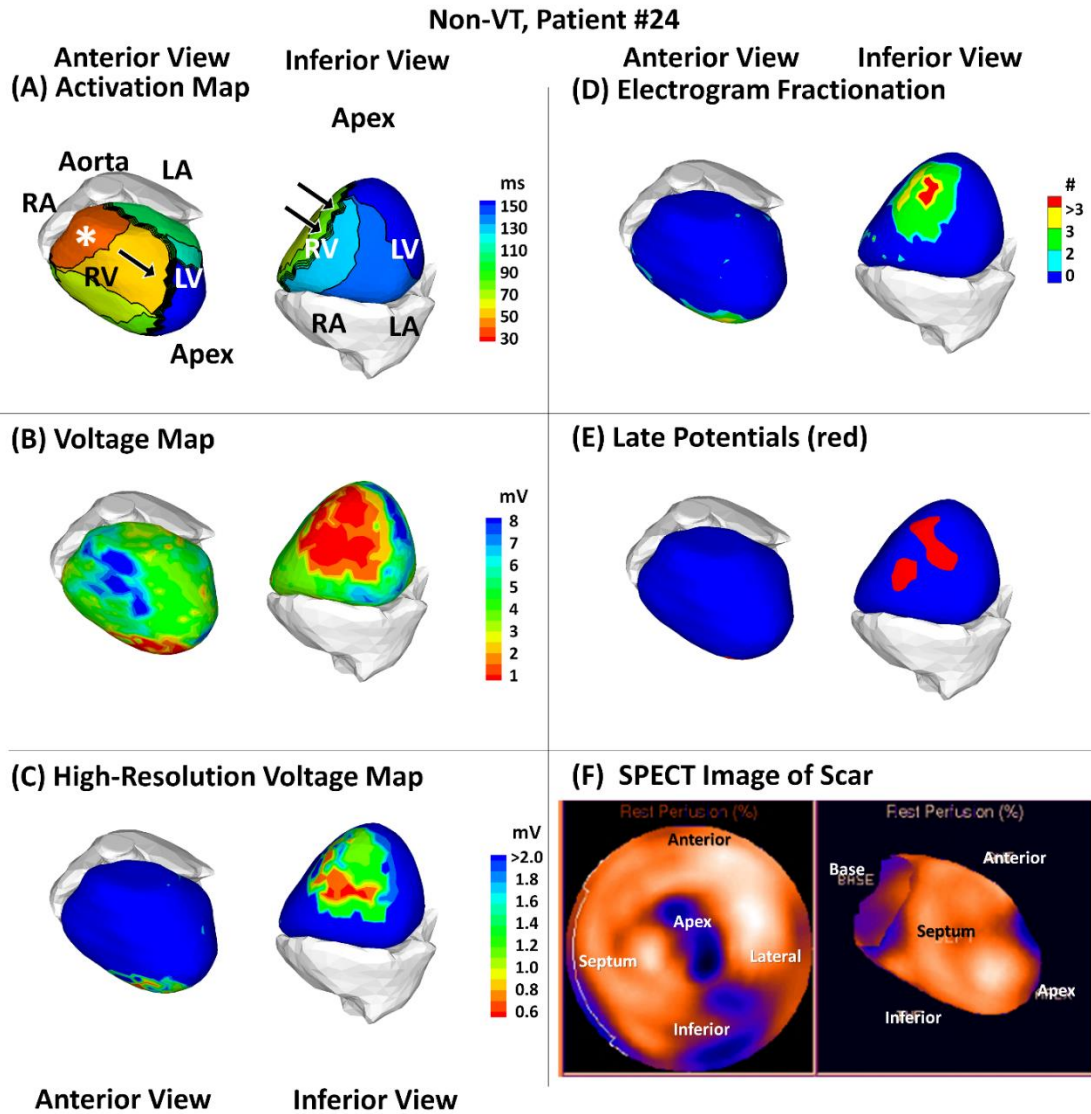


**Figure 2-30: Patient #24: Non-VT patient; apical and inferior myocardial infarction**

(A) Activation isochrone map. (B) Global voltage map; magnitude of unipolar electrograms. (C) High-resolution scar voltage map with adjusted threshold and color scale. (D) Electrogram fractionation; number of intrinsic deflections per electrogram. (E) Late potentials; regions with late potentials shown in red. (F) Single-photon emission computed tomography (SPECT) anatomic scar in apical view (left) and long-axis view (right). Panels A-E display the heart in anterior view (left) and inferior view (right). In panel A, epicardial breakthrough is indicated by an asterisk “\*”, isochrones are depicted with thin black lines, and black arrows point to conduction block.

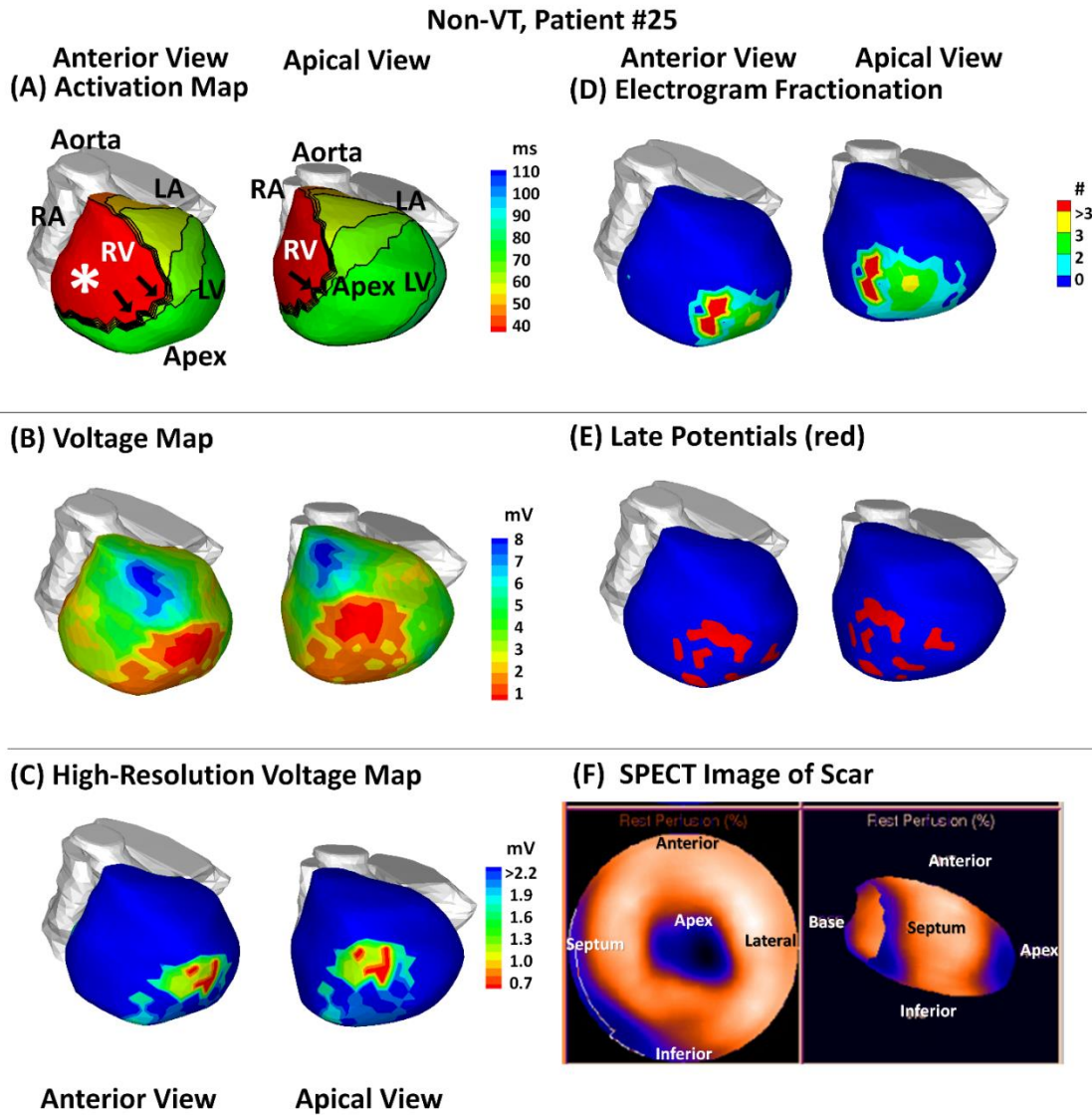


**Figure 2-31: Patient #25: Non-VT patient; apical myocardial infarction**

(A) Activation isochrone map. (B) Global voltage map; magnitude of unipolar electrograms. (C) High-resolution scar voltage map with adjusted threshold and color scale. (D) Electrogram fractionation; number of intrinsic deflections per electrogram. (E) Late potentials; regions with late potentials shown in red. (F) Single-photon emission computed tomography (SPECT) anatomic scar in apical view (left) and long-axis view (right). Panels A-E display the heart in anterior view (left) and apical view (right). In panel A, epicardial breakthrough is indicated by an asterisk “\*”, isochrones are depicted with thin black lines, and black arrows point to conduction block.

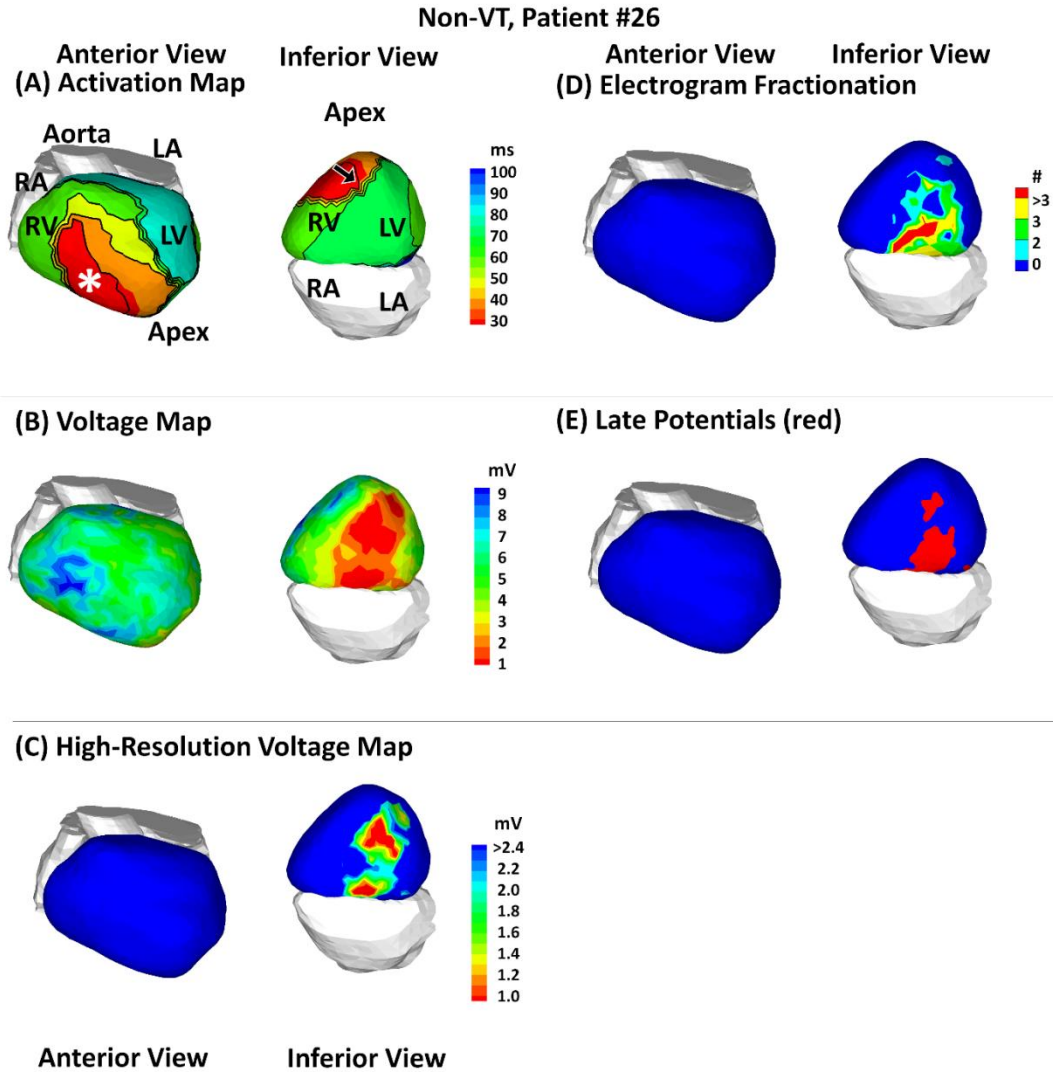


**Figure 2-32: Patient #26: Non-VT patient; inferior myocardial infarction**

(A) Activation isochrone map. (B) Global voltage map; magnitude of unipolar electrograms. (C) High-resolution scar voltage map with adjusted threshold and color scale. (D) Electrogram fractionation; number of intrinsic deflections per electrogram. (E) Late potentials; regions with late potentials shown in red. All panels display the heart in anterior view (left) and inferior view (right). In panel A, epicardial breakthrough is indicated by an asterisk “\*”, isochrones are depicted with thin black lines, and black arrows point to conduction block.

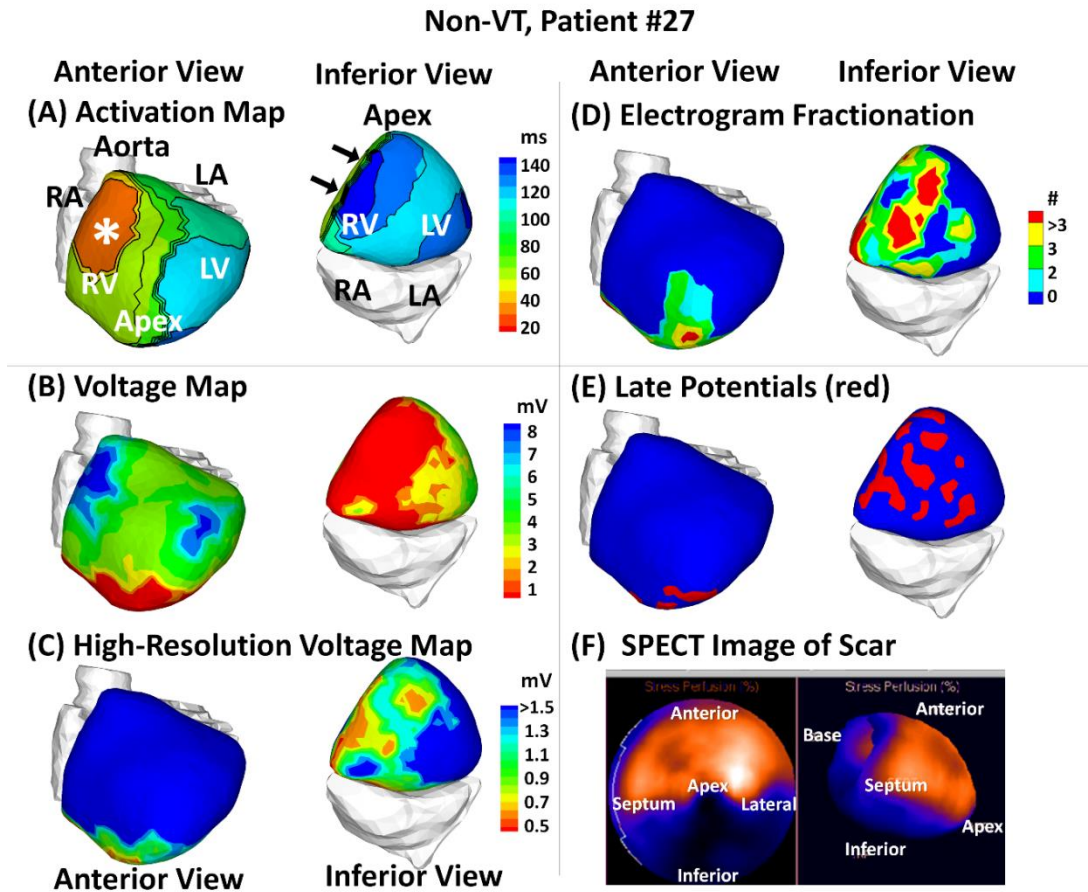


**Figure 2-33: Patient #27: Non-VT patient; inferior myocardial infarction**

(A) Activation isochrone map. (B) Global voltage map; magnitude of unipolar electrograms. (C) High-resolution scar voltage map with adjusted threshold and color scale. (D) Electrogram fractionation; number of intrinsic deflections per electrogram. (E) Late potentials; regions with late potentials shown in red. (F) Single-photon emission computed tomography (SPECT) anatomic scar in apical view (left) and long-axis view (right). Panels A-E display the heart in anterior view (left) and inferior view (right). In panel A, epicardial breakthrough is indicated by an asterisk “\*”, isochrones are depicted with thin black lines, and black arrows point to conduction block.

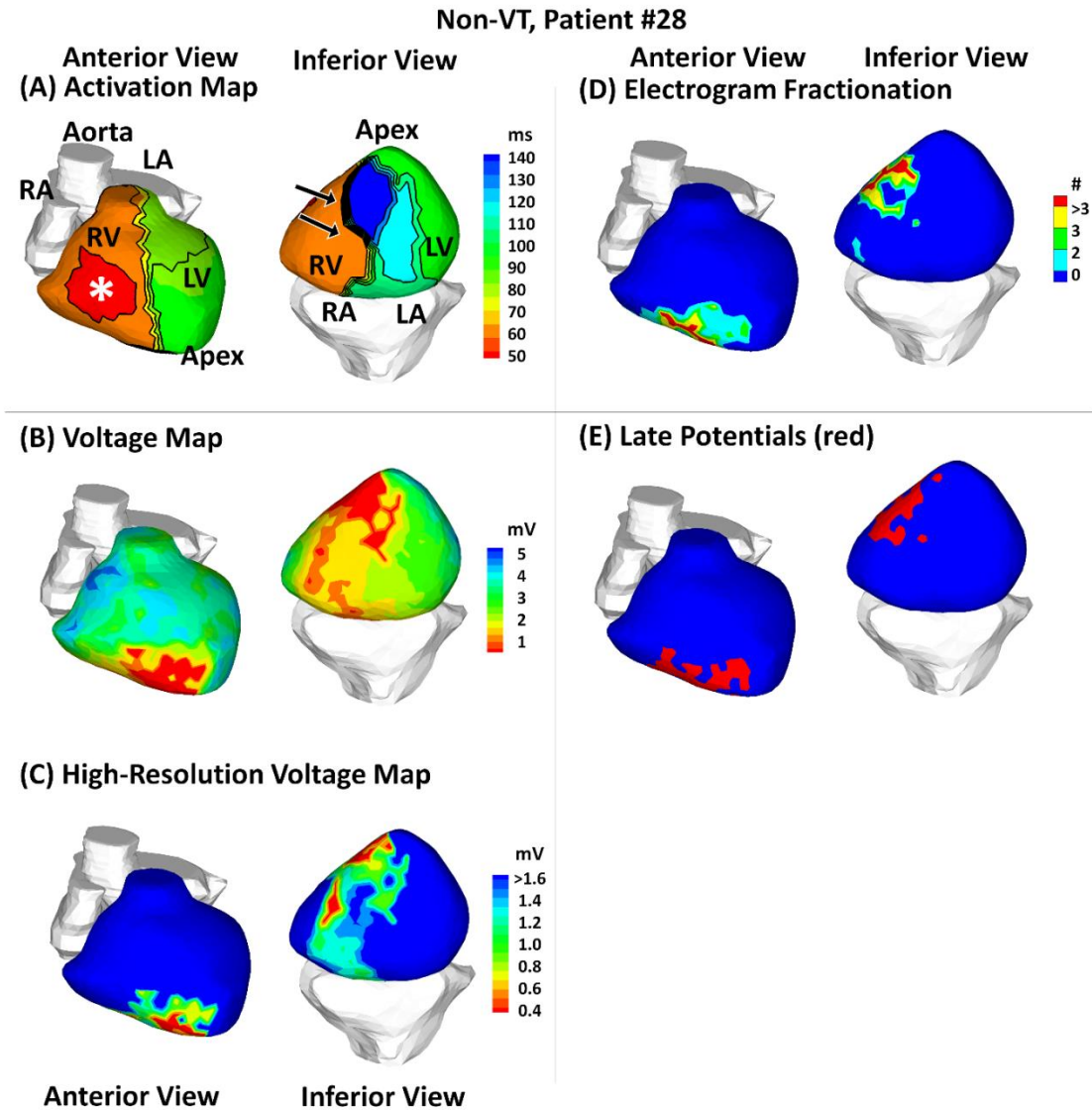


**Figure 2-34: Patient #28: Non-VT patient; apical myocardial infarction**

(A) Activation isochrone map. (B) Global voltage map; magnitude of unipolar electrograms. (C) High-resolution scar voltage map with adjusted threshold and color scale. (D) Electrogram fractionation; number of intrinsic deflections per electrogram. (E) Late potentials; regions with late potentials shown in red. All panels display the heart in anterior view (left) and inferior view (right). In panel A, epicardial breakthrough is indicated by an asterisk "\*", isochrones are depicted with thin black lines, and black arrows point to conduction block.

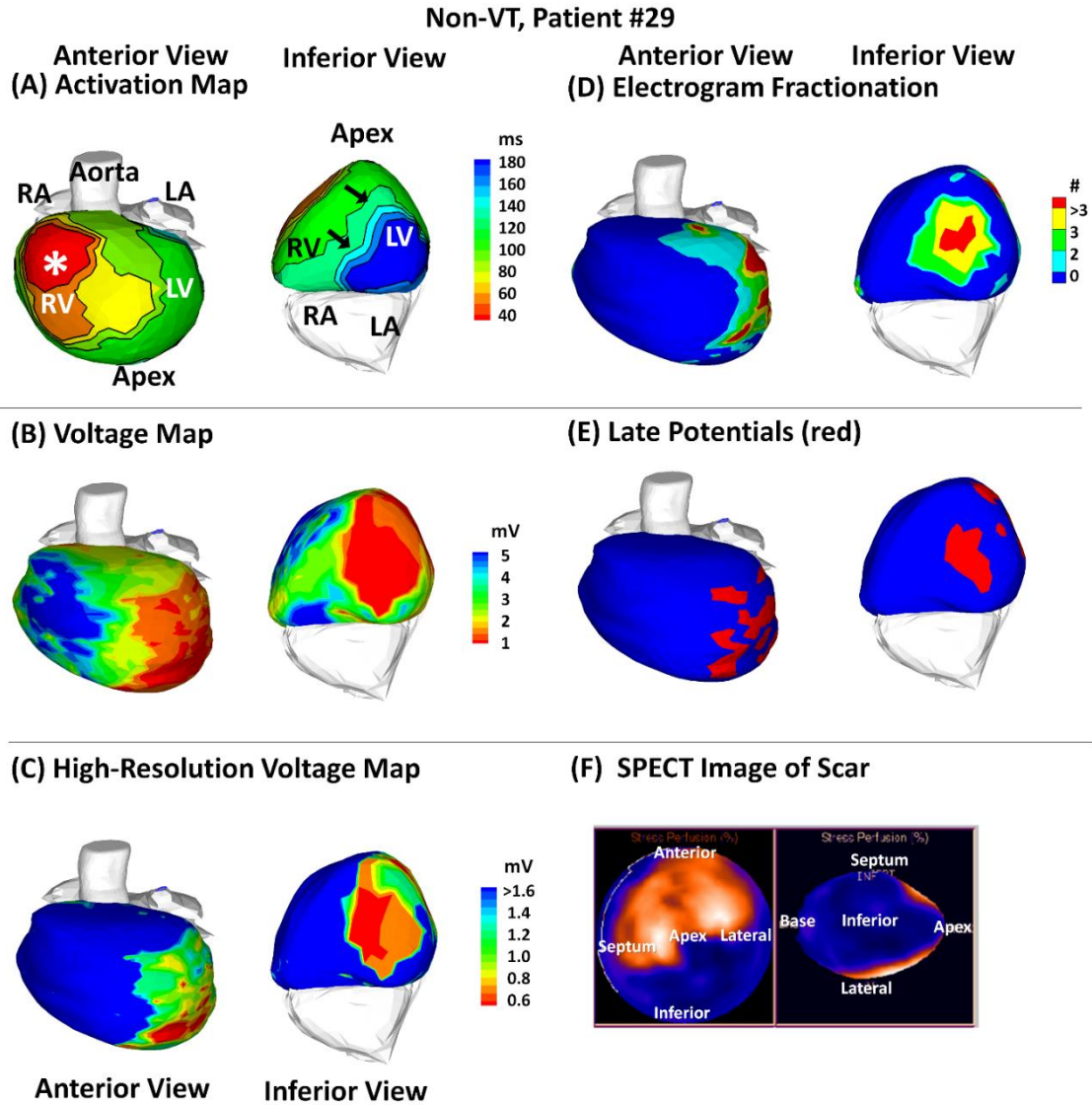


**Figure 2-35: Patient #29: Non-VT patient; inferior myocardial infarction**

(A) Activation isochrone map. (B) Global voltage map; magnitude of unipolar electrograms. (C) High-resolution scar voltage map with adjusted threshold and color scale. (D) Electrogram fractionation; number of intrinsic deflections per electrogram. (E) Late potentials; regions with late potentials shown in red. (F) Single-photon emission computed tomography (SPECT) anatomic scar in apical view (left) and inferior view (right). Panels A-E display the heart in anterior view (left) and inferior view (right). In panel A, epicardial breakthrough is indicated by an asterisk “\*”, isochrones are depicted with thin black lines, and black arrows point to conduction block.

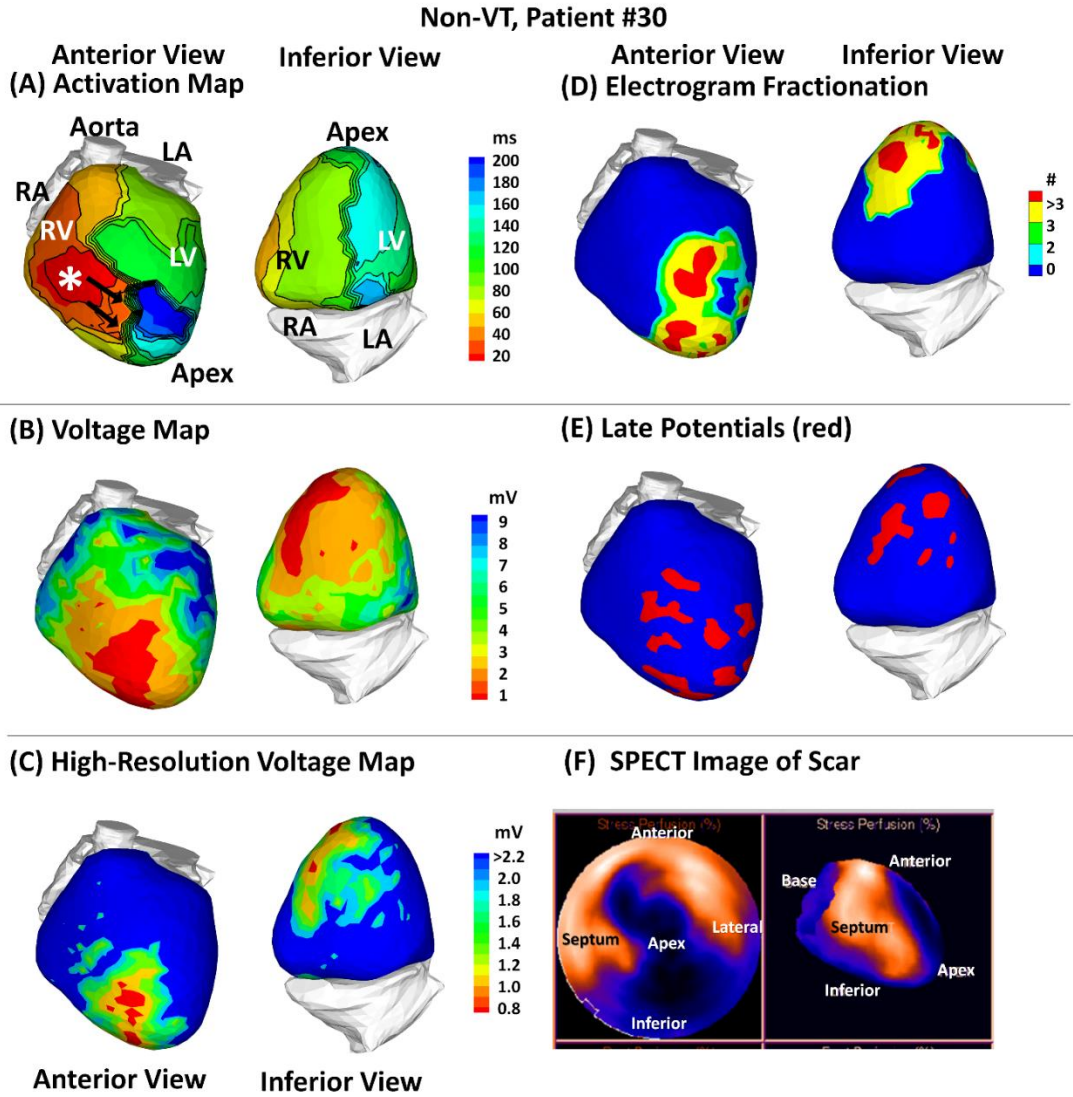


**Figure 2-36: Patient #30: Non-VT patient; anterior, apical and inferior myocardial infarction**

(A) Activation isochrone map. (B) Global voltage map; magnitude of unipolar electrograms. (C) High-resolution scar voltage map with adjusted threshold and color scale. (D) Electrogram fractionation; number of intrinsic deflections per electrogram. (E) Late potentials; regions with late potentials shown in red. (F) Single-photon emission computed tomography (SPECT) anatomic scar in apical view (left) and long-axis view (right). Panels A-E display the heart in anterior view (left) and inferior view (right). In panel A, epicardial breakthrough is indicated by an asterisk “\*”, isochrones are depicted with thin black lines, and black arrows point to conduction block.



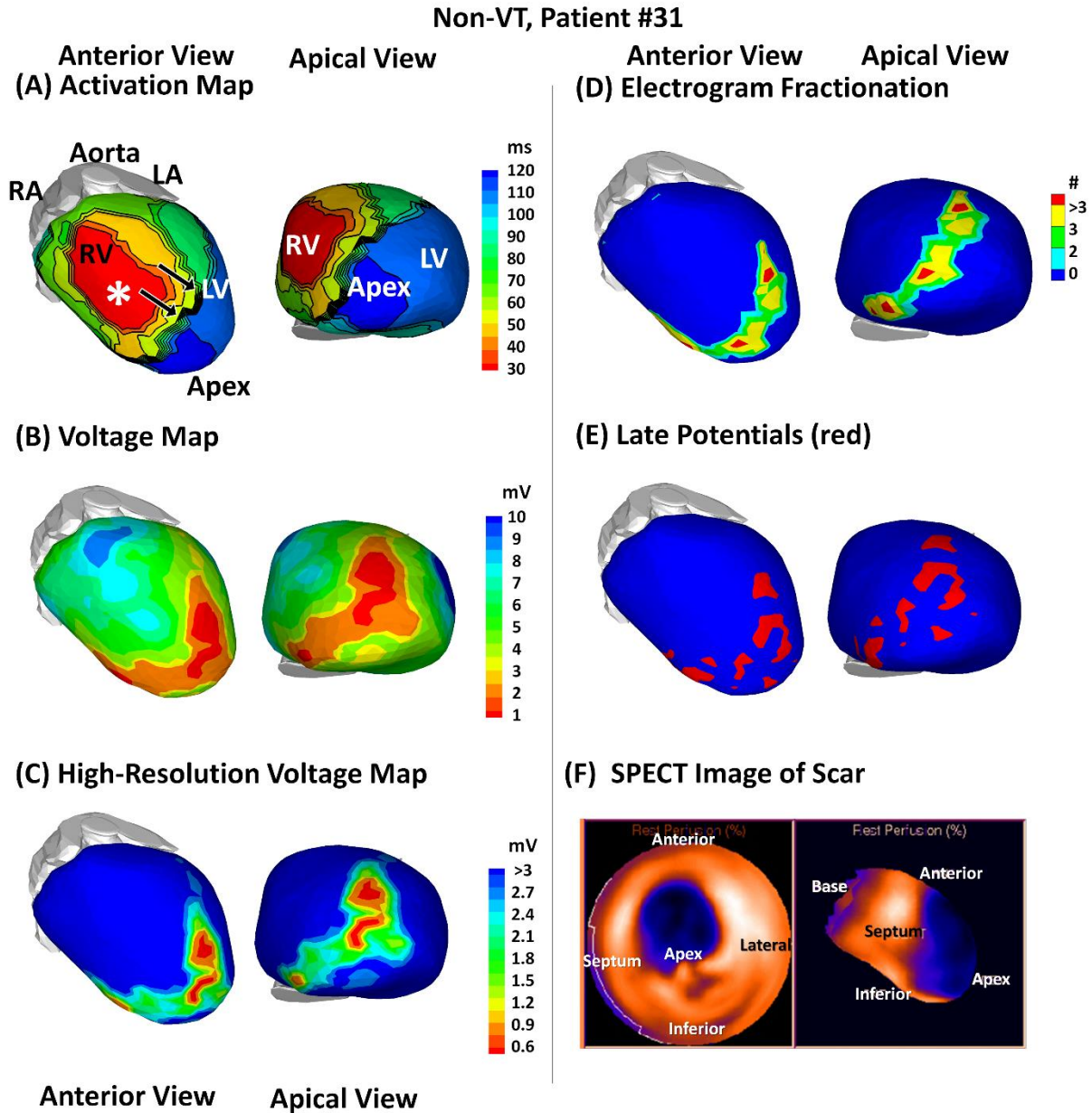


**Figure 2-37: Patient #31: Non-VT patient; anterior and apical myocardial infarction**

(A) Activation isochrone map. (B) Global voltage map; magnitude of unipolar electrograms. (C) High-resolution scar voltage map with adjusted threshold and color scale. (D) Electrogram fractionation; number of intrinsic deflections per electrogram. (E) Late potentials; regions with late potentials shown in red. (F) Single-photon emission computed tomography (SPECT) anatomic scar in apical view (left) and long-axis view (right). Panels A-E display the heart in anterior view (left) and apical view (right). In panel A, epicardial breakthrough is indicated by an asterisk “\*”, isochrones are depicted with thin black lines, and black arrows point to conduction block.

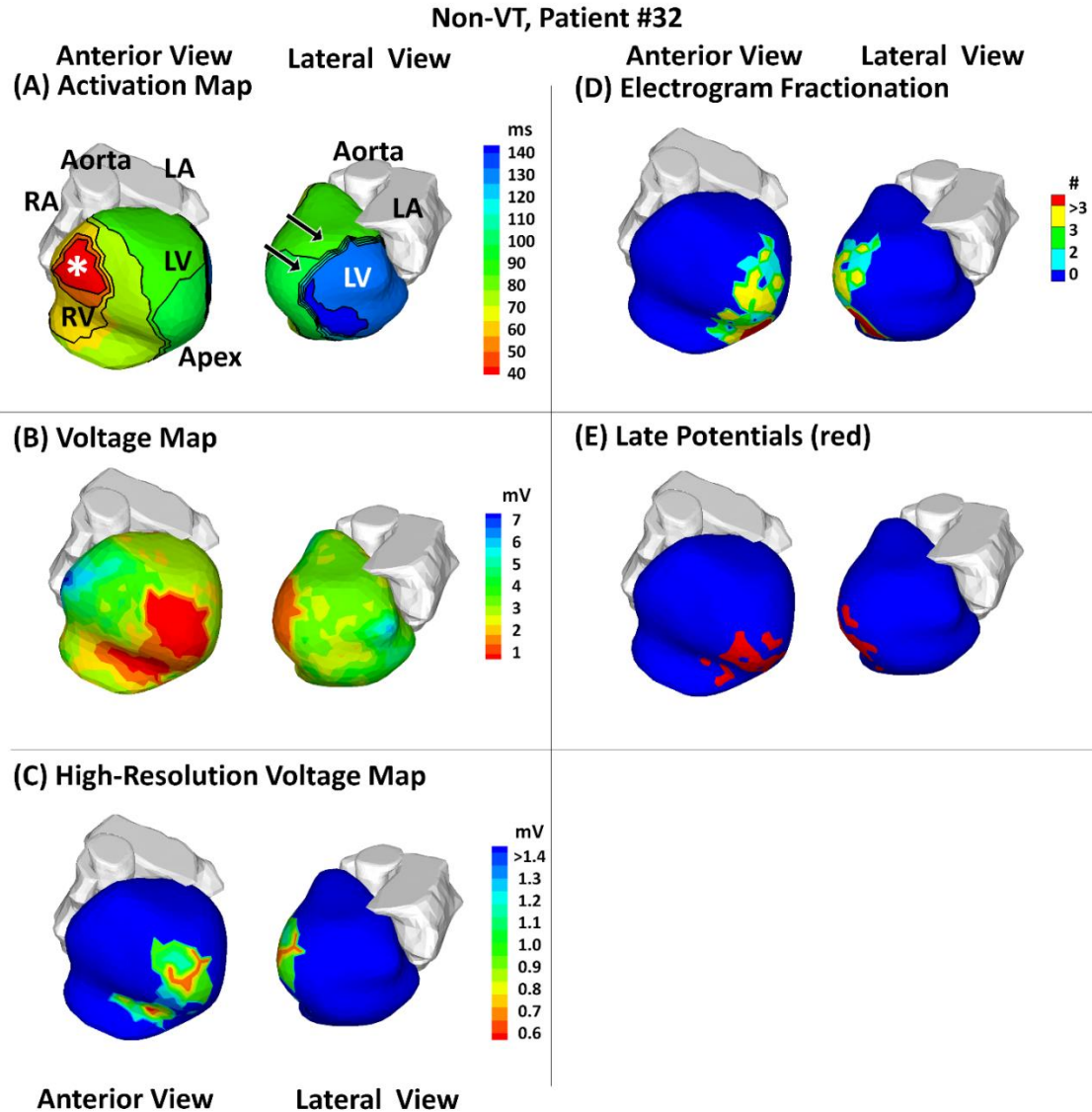


**Figure 2-38: Patient #32: Non-VT patient; anterior and apical myocardial infarction**

(A) Activation isochrone map. (B) Global voltage map; magnitude of unipolar electrograms. (C) High-resolution scar voltage map with adjusted threshold and color scale. (D) Electrogram fractionation; number of intrinsic deflections per electrogram. (E) Late potentials; regions with late potentials shown in red. All panels display the heart in anterior view (left) and lateral view (right). In panel A, epicardial breakthrough is indicated by an asterisk “\*”, isochrones are depicted with thin black lines, and black arrows point to conduction block.

### **2.7.3 Video Files (available in the attached CD): ECGI Activation Movies**

Movie 2-1: The activation sequence during VT for patient #3.

Movie 2-2: The activation sequence during VT for patient #8.

## **Chapter 3: The Electrophysiological Substrate of Early Repolarization Syndrome: Noninvasive Mapping in Patients**

### **3.1 Abstract**

The early repolarization (ER) pattern is a common ECG finding. Recent studies established a definitive clinical association between ER and fatal ventricular arrhythmias. Although the underlying mechanisms have been studied at the cellular level, the arrhythmogenic substrate in the intact human heart remains poorly understood.

Using noninvasive Electrocardiographic Imaging (ECGI), we studied 29 ER syndrome patients to characterize the electrophysiological (EP) substrate. Seven normal subjects provided control data. The abnormal EP substrate in ER syndrome patients has the following properties: (1) Abnormal epicardial EGMs characterized by presence of J-waves; (2) Absence of conduction abnormalities, including delayed activation, conduction block, or low-voltage and fractionated electrograms; (3) Marked abbreviation of ventricular repolarization in areas with epicardial J-waves. The action potential duration (APD) was significantly shorter than normal ( $196 \pm 19$  vs.  $235 \pm 21$  ms,  $p < 0.05$ ). Shortening of APD occurred heterogeneously, leading to steep repolarization gradients compared to normal control ( $45 \pm 17$  vs.  $7 \pm 5$  ms/cm,  $p < 0.05$ ). Premature ventricular contractions (PVCs) were recorded in 2 patients. The PVC sites of origin were closely associated with the abnormal EP substrate with J-waves and steep repolarization gradients.

ECGI identifies regions with steep repolarization gradients caused by localized shortening of APD in ER syndrome patients. It also correlates the PVC initiation site with the abnormal EP substrate.

## 3.2 Introduction

The early repolarization (ER) pattern on the ECG is characterized by a J-wave  $\geq 0.1$  mV in inferior and/or lateral leads.<sup>48-50</sup> It resolves during exercise and fast pacing, but accentuates during bradycardia. The prevalence of ER pattern in the general population is estimated to range between 1% and 13%.<sup>48-49, 51</sup> It is thought to be more common in males, young athletes and people of African descent.

Early descriptions of the ER pattern came from cases of hypothermia and hypercalcemia. For decades, the ER pattern was recognized as a benign ECG manifestation.<sup>52</sup> Since the 1980s, this view has been challenged by animal experiments<sup>50, 53</sup>, case reports<sup>54-57</sup> and review articles<sup>58-59</sup> that linked the ER pattern with ventricular arrhythmia. In a recent study with a large cohort of patients, the prevalence of ER pattern was significantly higher in patients with idiopathic ventricular fibrillation (VF) compared to control subjects.<sup>60</sup> This was the first study that provided clinical evidence supporting a definitive association between the ER pattern and an increased risk of ventricular arrhythmia. Following this study, additional population-based studies provided corroborating evidences.<sup>49, 61-65</sup> The critical role of the ER pattern in initiating ventricular fibrillation has been supported by observations of a consistent and marked J-wave accentuation preceding the onset of arrhythmia<sup>60, 66</sup> and by electrophysiology (EP) mapping data that showed a consistency between the origin of ectopy that initiated VF and the localization of repolarization abnormalities.<sup>60</sup>

ER has been extensively studied at the molecular and cellular levels.<sup>50, 67</sup> Based on the prevailing theory, the notch at phase-1 of the epicardial action potential (AP) is more prominent than that of the endocardial AP. The transmural voltage gradients give rise to the J-wave on the ECG. Further outward shift of the currents can cause loss of the AP plateau. Spatially

heterogeneous loss of the AP plateau can lead to reentry (termed “phase-2 reentry”).<sup>68</sup> However, limitations apply to this model. Extrapolation from cellular processes to tissue and organ behavior is difficult, because information at the molecular level is not sufficient to predict and understand the complex integrated behavior at higher levels of the physiological system. In particular, information on the electrophysiology and arrhythmic behaviors of the intact human heart in vivo, where arrhythmias occur, is missing.

Studies in patients with ER syndrome (ERS) have been so far confined to investigation of the ECG characteristics and extrapolating possible mechanisms. However, ECG characteristics have been shown to be inadequate measures of underlying repolarization properties.<sup>7</sup> Reports of EP mapping in patients with ERS provide limited information about the abnormal EP substrate.<sup>60, 69-70</sup> Understanding the mechanism of ER and how it may predispose patients to an increased risk of arrhythmias requires detailed mapping of the EP substrate in the intact heart of ERS patients. Recent developments in noninvasive Electrocardiographic Imaging<sup>1, 6-7, 10, 13, 16-17</sup> (ECGI; also known as ECG mapping, ECM) have demonstrated its ability to obtain high-resolution panoramic EP data of epicardial activation, repolarization and their alteration by disease and interventions in humans. In the current study, we characterize the epicardial EP substrate in ERS patients based on high-resolution ECGI data obtained during sinus rhythm (SR), in an effort to provide insights into the mechanism of ER and related arrhythmogenesis.

### **3.3 Methods**

#### **3.3.1 Patient Population**

ERS patients from one center in the United States (Washington University) and one center in France (Bordeaux University Hospital) were enrolled. The clinical diagnosis is ER pattern on the ECG, defined as an elevation of the J-point (J-wave) in at least two leads. The J-wave is

manifested either as QRS slurring (a smooth transition from the QRS complex to the ST segment) or QRS notching (a positive deflection inscribed on the S wave) in the inferior lead, lateral lead, or both. The patients should have at least one of the following: idiopathic ventricular tachycardia (VT) or VF, unexplained syncope and familial incidence of unexplained sudden cardiac death. Patients with ischemic heart disease and other conditions including long QT syndrome, short QT syndrome, Brugada syndrome (BrS) and arrhythmogenic right ventricular cardiomyopathy were excluded. All patients had structurally normal hearts and normal ventricular function. Data from seven normal subjects provided normal control.<sup>13</sup> Protocols were approved by the Institutional Review Boards at both centers; written informed consent was obtained from all patients.

### **3.3.2 Noninvasive Mapping**

Details of ECGI methodology were described previously.<sup>1, 6-7, 10, 13, 16-17</sup> Body surface potentials were acquired simultaneously using 256 electrodes and a multichannel mapping system. Next, the patient underwent thoracic computer tomography with ECG-gating to obtain the epicardial geometry and torso electrode positions. The body surface potentials and the patient-specific heart-torso geometry were processed with ECGI algorithms to reconstruct epicardial potentials, unipolar electrograms (EGMs), and maps of epicardial activation and repolarization. ECGI has been validated extensively in canine experiments and humans studies. It provides high accuracy and high-resolution (2 to 6 mm) panoramic data for noninvasive evaluation of EP properties.<sup>12</sup>

### **3.3.3 Data Analysis**

Characteristics of the abnormal EP substrate in ERS patients were analyzed by using data recorded during sinus rhythm. The EP mapping data were analyzed for EGM morphology,

conduction and repolarization. The ER pattern on epicardial EGMs was defined as J-point elevation at the end of QRS. The size of the epicardium with J-waves in the EGMs was measured as well (as a percentage of total epicardial surface area). Conduction was evaluated by activation time (AT), activation duration (AD), EGM fractionation and voltage. AT was determined by the maximal negative slope of the EGM during QRS inscription. All ATs were referenced to the beginning of QRS in ECG lead II. Epicardial activation isochrone maps were created from ATs. AD was defined as the interval between the earliest and latest AT, considering all epicardial EGMs. EGMs with low voltage and fractionation indicate slow, discontinuous and non-uniform conduction. EGM magnitude was measured peak-to-peak during the EGM QRS. Fractionation was expressed as the number of intrinsic, sharp deflections per EGM. Repolarization was assessed by recovery time (RT) and activation-recovery interval (ARI). Local RT was determined from the maximal positive slope of the EGM T-wave, which reflects the sum of local AT and local action potential duration (APD). Steep RT dispersion has been shown to provide substrate for unidirectional block and reentry. ARI was defined as the difference between RT and AT. ARI is independent of AT and a surrogate for local APD.<sup>71</sup> From the RT map and ARI map, epicardial dispersion of repolarization was measured as the maximal difference  $\Delta RT$  and  $\Delta ARI$  between two adjacent EGM sites on the epicardium. Epicardial RT and ARI gradients ( $\Delta RT/\Delta x$  and  $\Delta ARI/\Delta x$ ) were computed through division by the distance  $\Delta x$  between the two adjacent sites.

### **3.3.4 Statistical Analysis:**

All continuous data are presented as mean $\pm$ SD. Continuous variables were analyzed by unpaired t-test. The Satterthwaite modified t-test was used for variables with unequal variances. The Mann-Whitney U test was used for variables with non-normal distribution. All tests with



P<0.05 were considered statistically significant. Statistical analysis was performed by using SPSS

v19.

Patient ID	Age	Gender	Previously Aborted SCD/ Documented VT or VF	Syncope	Family History of SCD/ ERS	ICD Implant	ECG Leads with ER	
							Inferior Leads	Lateral Leads
ER-1	27	M	+	-	+	+	II, III, aVF	V4, V5, V6
ER-2	60	F	-	+	+	-	II, III	
ER-3	64	M	+	-	-	+	II	I, V5, V6
ER-4	24	M	+	+	-	+		I, V4, V5, V6
ER-5	49	M	+	-	-	-	II	I
ER-6	23	M	-	+	-	-	II, III, aVF	V4, V5, V6
ER-7	59	M	+	-	-	+	II, aVF	V4, V5, V6
ER-8	24	M	-	-	+	-	II, III, aVF	V5, V6
ER-9	48	F	+	+	+	+		V5, V6
ER-10	25	M	-	+	-	-	II	V5, V6
ER-11	31	M	-	-	+	-		V4, V5, V6
ER-12	28	M	+	+	+	+	II, III, aVF	
ER-13	25	M	+	-	+	-	II, aVF	V5, V6
ER-14	37	M	+	-	-	-	II, III, aVF	I, V4, V5, V6
ER-15	35	M	-	+	-	-	II, III, aVF	V4, V5, V6
ER-16	34	M	+	+	-	-	II	I, V5, V6
ER-17	65	M	-	-	+	-	II, III, aVF	V4, V5
ER-18	41	M	+	-	-	-		V4, V5
ER-19	48	M	-	+	-	-		V5, V6
ER-20	27	M	-	+	-	-	II, III	
ER-21	24	M	-	+	-	-	II	V5, V6
ER-22	58	M	+	-	-	+		V4, V5

<b>ER-23</b>	49	M	+	+	-	+	II, III, aVF	V4, V5, V6
<b>ER-24</b>	21	M	+	-	-	-	II, III, aVF	I, V4, V5, V6
<b>ER-25</b>	40	M	+	+	-	-	II, III	I, V4, V5, V6
<b>ER-26</b>	26	F	-	+	-	-	II, III, aVF	V4, V5, V6
<b>ER-27</b>	31	M	-	-	+	-	II, III, aVF	V5, V6
<b>ER-28</b>	23	M	+	-	+	+	II, III, aVF	
<b>ER-29</b>	22	M	+	-	-	+		V4, V5, V6

**Table 3-1: Clinical Characteristics of the ERS Patients**

### **3.4 Results:**

Twenty-nine ERS patients (26 men, 3 women) were enrolled in this study. Seventeen (59%) had previous aborted SCD or arrhythmic events (idiopathic VT/VF), 10 of which received implantable cardioverter-defibrillator (ICD). Fourteen (48%) experienced unexplained syncope. Ten (34%) had a family history of SCD or ERS. Detailed characteristics for individual patient are provided in Table 3-1.

#### **3.4.1 EGM Characterization and Localization**

Figure 3-1 shows epicardial EGM characteristics and localization for representative examples in 3 ERS patients. Patient ER-11 was an asymptomatic patient with a family history of sudden death. He had ER pattern in lateral leads. Patient ER-14 experienced previously aborted sudden death, and had ER pattern in inferior leads and lateral leads. Patient ER-20 did not have clinical arrhythmic events, but experienced unexplained syncope. His ER pattern was found in inferior leads. Data from a normal subject is provided for reference. Epicardial J-wave was observed in EGMs from all 25 ERS patients ( $0.68 \pm 0.25$  mV vs. 0 mV in control,  $p < 0.05$ ); 6 in the

anterior wall, 19 in the lateral wall and 23 in the inferior wall (most patients had epicardial J-wave in multiple locations). The proportion of epicardium that presented J-wave ranges from 23% to 57%, with a mean value of  $39\% \pm 9\%$ . EGMs with abnormal low-voltage and fractionation were not found in any ERS patient.

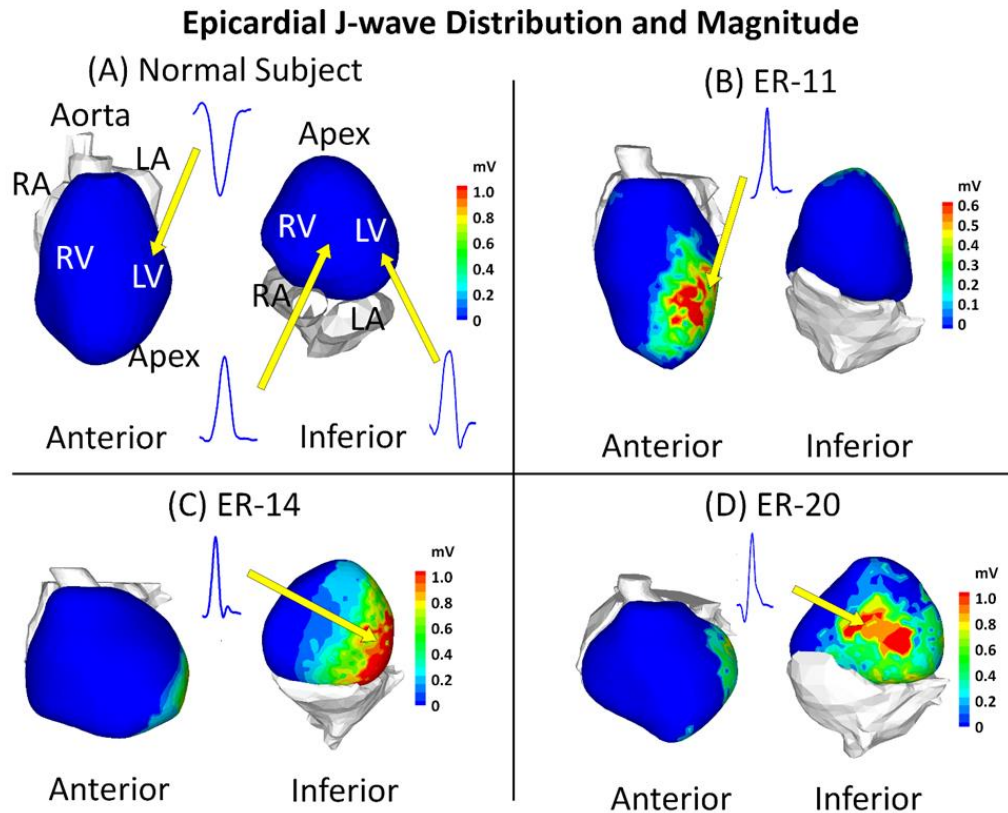


**Figure 3-1: Epicardial J-wave Distribution and Magnitude**

Abnormal epicardial EGMs with a J-wave that resemble the ER pattern (terminal-QRS notch or slurring) on the surface ECG are observed in ERS patients, but not seen in normal subjects. Example maps of epicardial J-wave magnitude in 3 ERS patients are shown. The maps are shown in anterior view and inferior view for each subject. The locations of epicardial J-waves are ER-11: lateral and apical left ventricle (LV); ER-14: lateral and inferior LV; ER-20: lateral and inferior LV. Inset: representative EGMs with a J-wave (QRS only) in ERS patients (Panels B, C, D) and EGMs from corresponding locations in the normal control subject (Panel A). LA = left atrium; LV = left ventricle; RA = right atrium; RV = right ventricle.

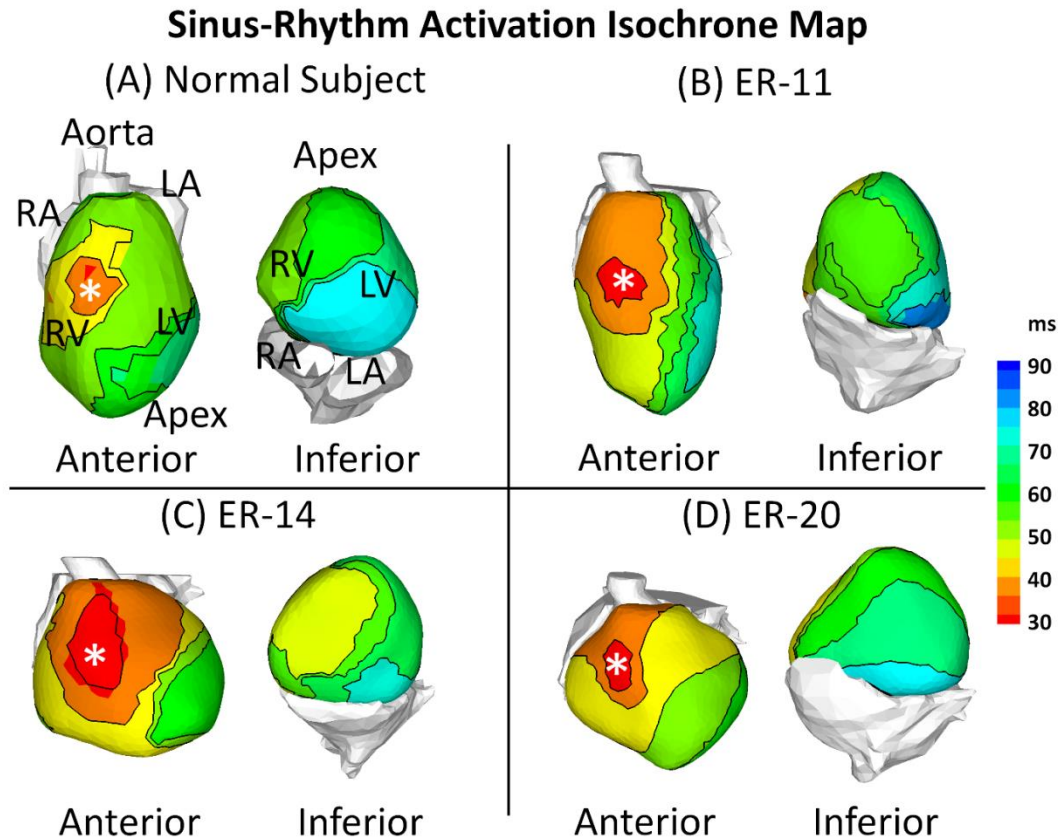


**Figure 3-2: Activation Isochrone Maps**

Examples of activation during sinus rhythm (SR) are shown for a normal control subject and 3 ERS patients. The maps are shown in anterior view and inferior view for each subject. ERS patients and the normal subject have similar activation patterns. After breakthrough in the anterior right ventricle (asterisk), the wavefront propagates uniformly to activate both ventricles. The LV base is the latest region to activate. Conduction block and slow conduction were not observed in the ERS patients.

### 3.4.2 Epicardial Activation

Figure 3-2 shows ECGI epicardial activation isochrone maps for a control subject and 3 ERS patients (same patients as in Figure 3-1). The epicardial activation pattern during SR in ERS patients was characterized by a normal epicardial breakthrough (white asterisks) in the right ventricle (RV). The excitation wavefront spread uniformly and rapidly to activate both ventricles. The left ventricular (LV) base was the latest region to activate. The activation pattern was not affected by the presence of the J-wave: regions of slow conduction (isochrone crowding) or

conduction block (adjacent activation times differ by more than 50 ms) were not found in ERS patients. A similar activation sequence was observed in the normal control subjects, as well as in the isolated human heart from individuals with no history of cardiac disease.<sup>72</sup> AD, the time needed for activation of both ventricles, was  $54 \pm 7$  ms for ERS patients, comparable with  $47 \pm 9$  ms for normal control.

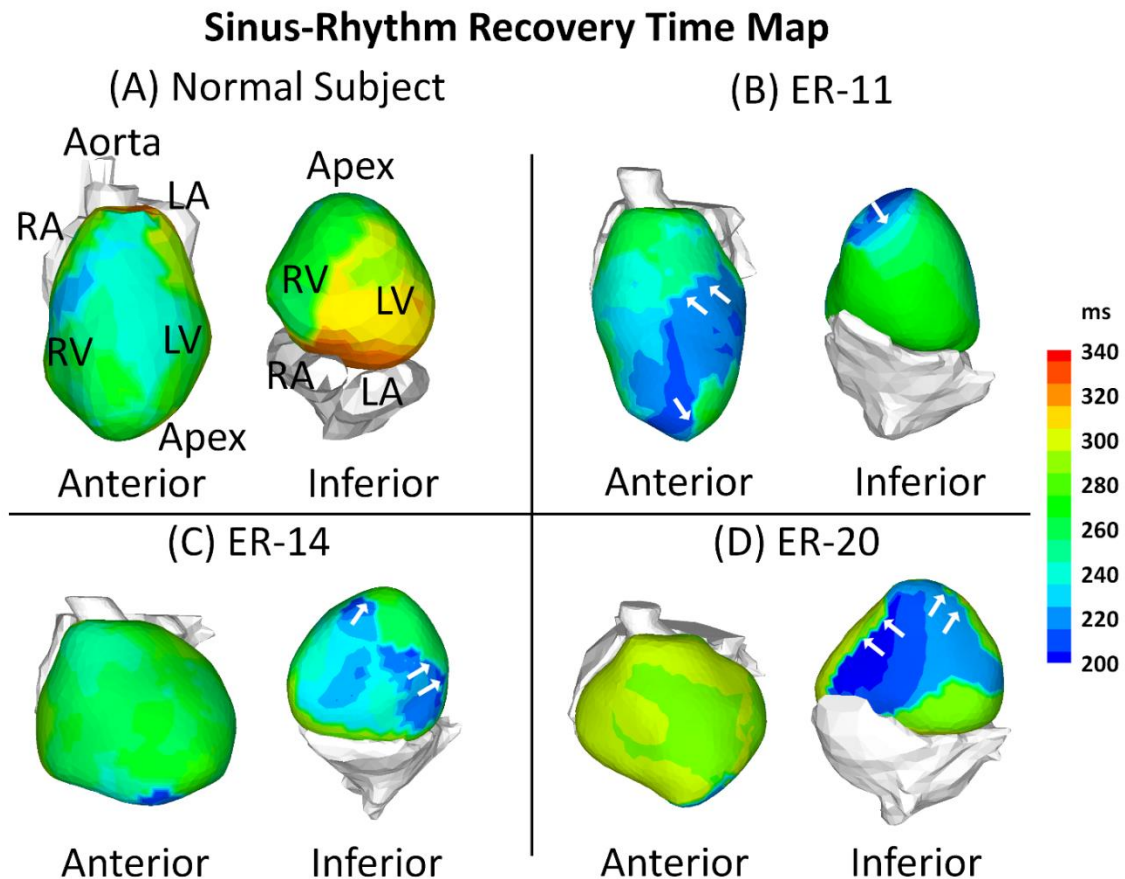


**Figure 3-3: Recovery Time (RT) Maps**

Examples of epicardial RT during SR are shown for a normal control subject and 3 ERS patients. Maps are shown in anterior view and inferior view for each subject. ERS patients have regions with abnormally short RT (dark blue). White arrows in Panels B-C point to regions with steep RT gradients.

## Sinus-Rhythm Activation-Recovery Interval Map

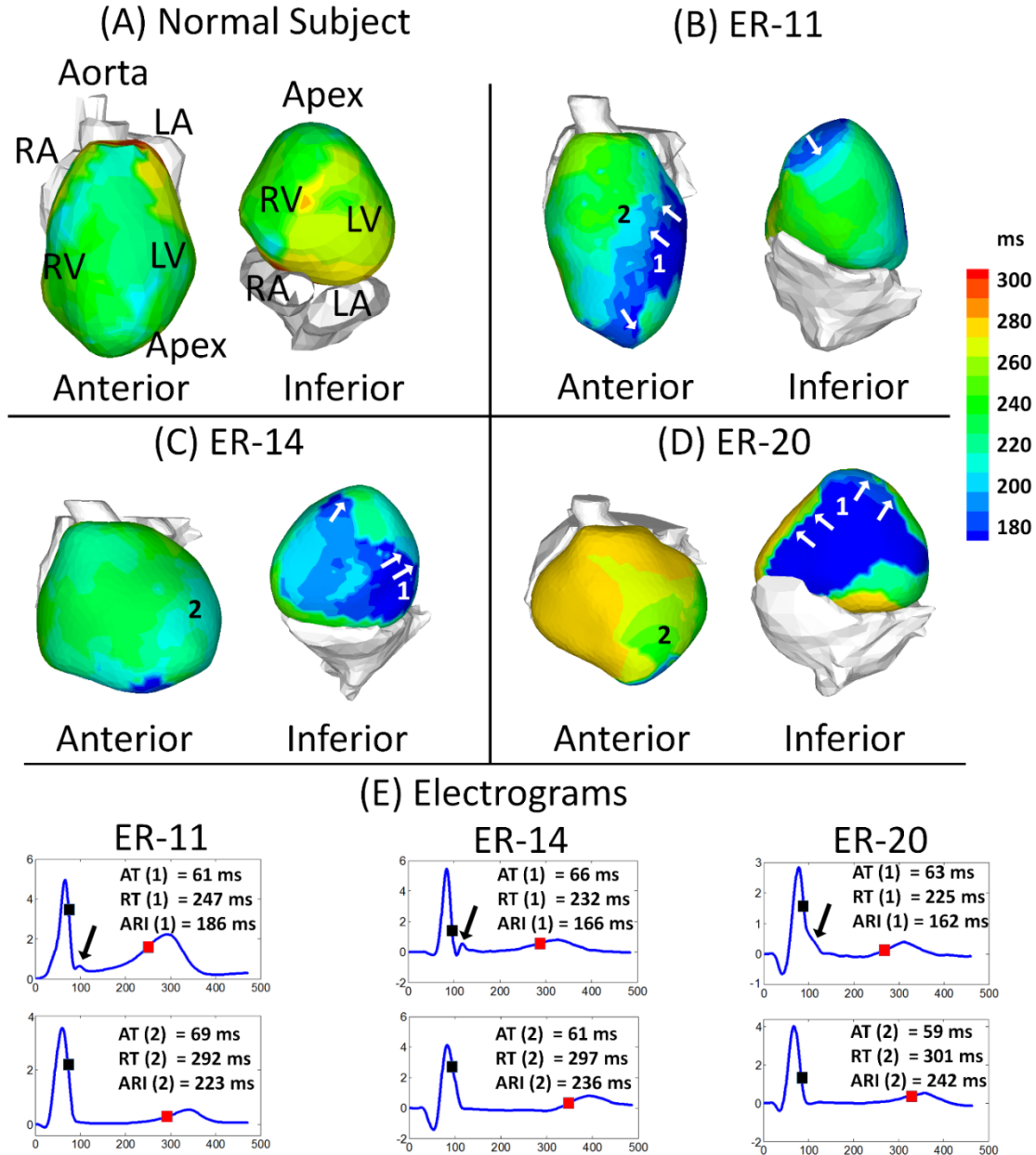


**Figure 3-4: Activation-recovery Interval (ARI) Maps**

Panels A to D: ARI maps for a normal control subject and 3 ERS patients. Maps are shown in anterior view and inferior view for each subject. ERS patients have regions with abnormally short ARI (dark blue). White arrows in Panels B-C point to regions with steep ARI gradients. Panel E shows the ECGI reconstructed electrograms (EGMs) from two adjacent locations for each ERS patient. Location 1: prominent J-wave and short ARI; location 2: absence of J-wave and normal ARI. There is a steep gradient of repolarization across these two locations. The time instances of activation (AT; black square), recovery (RT; red square) and corresponding ARIs are indicated.

### 3.4.3 Epicardial Repolarization

Representative maps of RT (Figure 3-3) and ARI (Figure 3-4) from a normal subject and 3 ERS patients (same patients as in Figure 3-1) demonstrate marked local changes in repolarization in ERS patients compared with normal control. Abnormal repolarization was observed primarily in regions with a prominent J-wave. Steep epicardial RT gradients and ARI gradients occurred mostly at the border of regions where J-wave were present (Figure 3-3, Panel B-D, white arrows). Figure 3-4E shows EGMs with prominent J-wave (location 1) and EGMs without J-wave from an adjacent location (location 2) for 3 ER patients. Take patient ER-11 for example, ATs at location 1 and 2 were similar (AT(1) =66 ms, AT(2) =61 ms), but repolarization dispersion was observed between the two locations:  $\Delta RT$  was 65 ms (RT(1) =232 ms, RT(2) =297 ms) and  $\Delta ARI$  was 70 ms (ARI(1) =166 ms, ARI(2) =236 ms). This resulted in steep gradients of RT and ARI ( $\Delta RT/\Delta x$  =43 ms/cm;  $\Delta ARI/\Delta x$  =46 ms/cm), much steeper than those of control (typically 5~8 ms/cm and 4~10 ms/cm, respectively, in the same region). Patients ER-14 and ER-20 also had shortened RT and ARI, as well as increased gradients of RT and ARI, but the location of abnormal repolarization varied.

Table 3-2 summarizes the ECGI-derived parameters. Compared with normal control, ERS patients had shortened RT ( $223 \pm 28$  vs.  $265 \pm 30$  ms,  $p < 0.05$ ) and ARI ( $196 \pm 19$  vs.  $235 \pm 21$  ms,  $p < 0.05$ ), increased repolarization dispersion  $\Delta RT$  ( $52 \pm 15$  vs.  $18 \pm 14$  ms,  $p < 0.05$ ) and  $\Delta ARI$  ( $53 \pm 15$  vs.  $16 \pm 10$  ms,  $p < 0.05$ ) and increased repolarization gradients  $\Delta RT/\Delta x$  ( $48 \pm 18$  vs.  $8 \pm 6$  ms/cm,  $p < 0.05$ ) and  $\Delta ARI/\Delta x$  ( $45 \pm 17$  vs.  $7 \pm 5$  ms/cm,  $p < 0.05$ ).

Parameters	Normal Control (N=7)	ERS Patients (N=29)	P value
<b>J-wave Magnitude (mV)</b>	0	0.68±0.25	P<0.05
<b>AD (ms)</b>	47±9	54±7	NS
<b>Mean RT (ms)</b>	265±30	223±28	P<0.05
<b>ΔRT (ms)</b>	18±14	52±15	P<0.05
<b>ΔRT/Δx (ms/cm)</b>	8±6	48±18	P<0.05
<b>Mean ARI (ms)</b>	235±21	196±19	P<0.05
<b>ΔARI (ms)</b>	16±10	53±15	P<0.05
<b>ΔARI/Δx (ms/cm)</b>	7±5	45±17	P<0.05

**Table 3-2: Comparison of ECGI Parameters between ERS Patients and Normal Subjects**

Data are presented as mean ±SD. AD = activation duration; ARI = activation-recovery interval; RT = recovery time; NS = not significant.

### 3.4.4 Ventricular Arrhythmias

Premature ventricular contractions (PVCs) were recorded in two patients, ER-1 and ER-11. Figure 3-5 shows substrate maps (J-wave and ARI) and PVC activation maps for patients ER-1 and ER-11. Panel A shows that in patient ER-1, a large portion of epicardium (54%) was affected by abnormal EGMs with J-waves, including anterior RV, anterior LV, lateral LV, apical LV and inferior LV (not shown). In patient ER-11, about 32% of the epicardium had J-waves in the EGMs, located in the antero-lateral and apical LV. Panel B shows that in patient ER-1, the anterior RV had the shortest ARI (about 140 ms), and the majority of LV had ARI less than 180 ms, significantly below the normal range. Patient ER-11 had shortened ARI (about 160 ms) in the antero-lateral and apical LV. Panel C shows the PVC activation patterns. In patient ER-1, the PVC originated from the apical LV region, then propagated towards the basal RV. In patient ER-11, the



PVC initiation site was located in mid anterior LV near the septum. The inferior LV was the latest region to activate during a PVC. In both cases, locations of the EP substrate with abnormal EGMs, shortened ARIs and steep ARI gradients correlated with the PVC sites of origin.

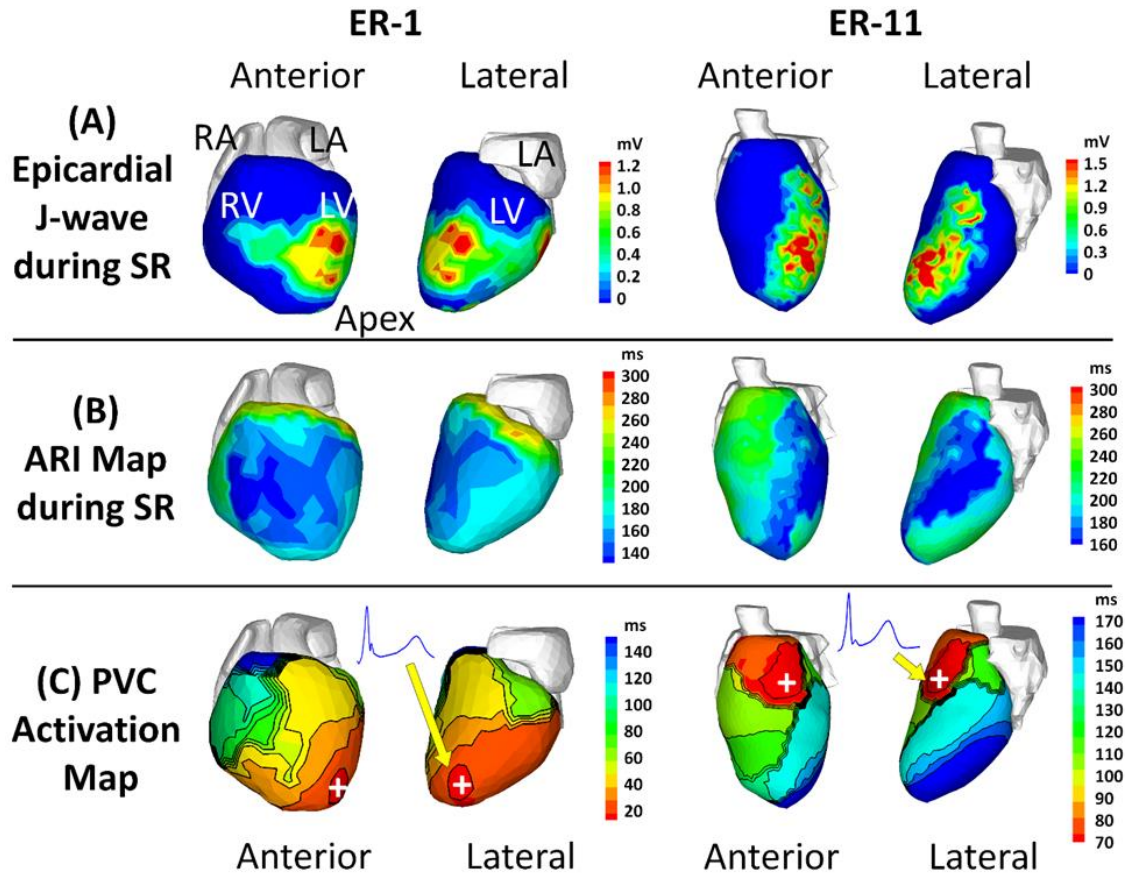


**Figure 3-5: The electrophysiological substrate in relation to premature ventricular contractions (PVCs)**

Panel A: Epicardial J-wave magnitude and Panel B: Activation-recovery interval (ARI) maps during SR. Panel C: PVC activation map. Each panel shows the maps for 2 patients, ER-1 (left) and ER-11 (right). The hearts are displayed in anterior view and lateral view. Inset: abnormal electrograms (EGMs) with J-waves during SR from the PVC sites of origin. The PVC initiation sites are indicated by plus signs “+”. Note that an EP substrate with abnormal EGMs, shortened ARIs and steep ARI gradients correlated with the PVC site of origin in both cases.

### 3.5 Discussion:

This is the first noninvasive mapping study in ERS patients that identifies key epicardial EP properties that may account for the arrhythmogenicity in this syndrome. High-resolution panoramic mapping was essential for characterizing the properties of the EP substrate; it was made possible by noninvasive ECGI. The results indicate that ERS patients present with regions of abnormal EP substrate with the following properties: (1) Abnormal epicardial EGMs characterized by the presence of a J-wave, which is consistent with the ECG-based clinical phenotype; (2) Absence of conduction abnormalities, such as delayed activation, EGMs with low voltage and fractionation; (3) Marked abbreviation of ventricular repolarization in areas with epicardial J-waves, leading to steep repolarization gradients.

The cellular mechanisms underlying the ER pattern and arrhythmogenesis have been studied using canine ventricular wedge preparation.<sup>67-68</sup> Because the expression of transient outward current ( $I_{to}$ ) is highest in the epicardium and diminishes transmurally towards the endocardium, a phase-1 notch is present in epicardial AP, but not in endocardial AP. The transmural voltage gradient during an early phase of ventricular repolarization registers as J-wave on the ECG. Under pathological conditions, in the presence of an intense  $I_{to}$  or with a greater outward shift of currents active at the end of phase 1 of the AP (increase in  $I_{K-ATP}$ ,  $I_{K-ACh}$  or decrease in  $I_{Ca-L}$  or late  $I_{Na}$ ), the membrane is repolarized prematurely, losing the epicardial AP plateau, which leads to marked abbreviation of the AP. The loss of the AP plateau in epicardium but not endocardium creates transmural voltage gradients during phase 2 and 3 of the AP that manifest as a prominent ST-segment elevation.<sup>50</sup> Spatially heterogeneous loss of the AP plateau can generate substrate with steep repolarization gradients that may facilitate the development of phase 2 reentry and polymorphic VT/VF.<sup>68</sup> A recent study in a canine LV wedge preparation showed that

accentuation of the AP notch in the LV epicardium gave rise to the ER pattern.<sup>73</sup> This repolarization abnormality was accentuated by increased vagal tone, and normalized by administration of isoproterenol and quinidine. The levels of  $I_{to}$  was higher in the inferior LV wall, which may account for the greater sensitivity to development of VT/VF in this region.

Since the link between the ER pattern on the ECG and fatal cardiac arrhythmias has been confirmed,<sup>60</sup> numerous studies have been conducted in an effort to stratify risks of ventricular arrhythmias in the ER population. Risk stratification has profound clinical importance, given the prevalence of the ER pattern in the general population. Importantly, young otherwise healthy individuals with ER may be more vulnerable to idiopathic VF.<sup>74-75</sup> Currently, surface ECG is the only tool available and the identification of ERS patients at risk remains extremely challenging. Surface ECG markers, including the amplitude and distribution of the J-wave, morphology of the ST segment and the presence of ventricular ectopy have been demonstrated to predict arrhythmic risks. A higher J-wave amplitude is associated with increased risk of sudden death.<sup>49, 65</sup> A lateral distribution of ER does not portend risk, whereas an inferior and global distribution of ER predicts an increased risk of arrhythmic death.<sup>49, 60, 63</sup> A horizontal or descending ST segment also portends a higher risk of sudden death.<sup>65, 76-77</sup> Of note, although these ECG markers are associated with an increased relative risk of arrhythmia in the ER population, they have very limited utility in predicting the absolute risk in the general population, due to the extraordinarily low incidence of idiopathic VF.<sup>78</sup> A recent study investigated the role of EP studies in risk stratification in ERS patients.<sup>79</sup> Results indicate that VF inducibility does not have a role in risk stratification in ERS patients; it neither predicts arrhythmic risks, nor correlates with the ECG markers discussed earlier. Better understanding of the clinical entity is the key for development of diagnostic and risk stratification tools.

The fact that a significant number of individuals with ERS had a family history of sudden cardiac death suggests a genetic basis for this syndrome. ERS has been associated with mutations in 7 genes, including mutations in KCNJ8 and ABCC9 that encode the  $I_{K-ATP}$  channel,<sup>80-82</sup> mutations in CACNA1C, CACNB2 and CACNA2D1 associated with the  $I_{Ca-L}$  channel,<sup>83</sup> and a mutation in SCN5A that affects  $I_{Na}$ .<sup>84</sup> Interestingly, the  $I_{K-ATP}$  channel is inactive in non-ischemic ventricular myocardium; it activates and becomes increasingly outward with decreasing levels of ATP.<sup>85</sup>  $I_{K-ATP}$  is expressed in myocytes at very high levels, similar to that of  $I_{Na}$ .<sup>86-87</sup> Experimental and simulation studies consistently showed that opening of a small percentage of  $I_{K-ATP}$  channels (0.7% -1.2%) may shorten the APD by 50%.<sup>86, 88</sup> Mutations can cause  $I_{K-ATP}$  channels to open at normal ATP levels, thereby causing early AP repolarization. As discussed above, heterogeneous APD abbreviation can provide both the substrate and trigger that precipitate VF.

The current study investigated whether the electrocardiographic manifestation of ER reflects abnormal repolarization or late potentials associated with delayed conduction in certain regions of the heart. Conduction delay is a common cause for notching of the terminal QRS complex, especially in patients with a history of myocardial infarction. Asynchronous activation can also create voltage gradients, causing ST-segment elevation. The canine ventricular wedge model did not represent abnormal conduction in the myocardium; it investigated the mechanism of ER pattern in the setting of abnormal repolarization alone. The role of conduction abnormalities in the ER pattern and arrhythmogenesis was not explored in that model.

As the results show, all ERS patients had a normal activation pattern during SR. The mean ventricular AD (Table 3-2) was comparable with normal control. In addition to AT and activation pattern, the morphology of EGMs was also examined in detail. Experimental and clinical studies have shown that low-amplitude and fractionated EGMs reflect slow, non-uniform and

discontinuous conduction through a substrate with structural heterogeneity.<sup>38</sup> ECGI is able to reconstruct such EGMs with high accuracy and has been used to study the EP substrate associated with structural abnormalities including post-MI and BrS patients.<sup>5, 8, 16, 20</sup> EGMs with abnormal low-amplitude and fractionation were not found in ERS patients. Catheter mapping in ERS patients did not show abnormalities during ventricular depolarization that registered with the terminal QRS notch or slurring, confirming that the ECG J-wave was related to repolarization.<sup>69</sup> Taken together, these findings indicate that ventricular conduction is normal in ERS patients, and that the J-wave on the ECG is not likely to be caused by abnormal conduction.

Figure 3-3 and Figure 3-4 demonstrate that there is significant regional abbreviation of the AP (based on reconstructed ARIs) on the ventricular epicardium of ERS patients compared with normal control. As shown in Figure 3-4E, in regions with abnormal EGMs, the epicardial J-wave is followed by shortening of RT. These regions were located in close proximity to regions with relatively longer RT. The regional differences in RT gave rise to steep RT gradients. Given the fast and uniform conduction, the difference in ATs between two adjacent locations is too small to account for the difference in RTs. Thus, RT and RT dispersion are primarily determined by ARI and ARI dispersion, independent of conduction. With ARI being the surrogate for local APD, shortened ARI suggests abbreviated AP. The formation of regions with steep gradient of repolarization is caused by spatially heterogeneous abbreviation of the AP over short distances. In contrast, the apex-to-base ARI dispersion (about 42 ms) and inter-ventricular ARI dispersion (about 32 ms) result in much shallower gradients in normal subjects.<sup>13</sup> Results from this study are consistent with a previous case report that presented preliminary data from 2 ERS patients mapped by ECGI.<sup>15</sup>

Although ECG markers are currently the only noninvasive tool to identify high-risk ERS patients, it lacks sensitivity and specificity. Each ECG electrode on the body surface records an electric signal that reflects integrated activity over the entire heart. Therefore, spatial relationships in the heart are lost in the body-surface ECG. It has been shown that body-surface measures do not adequately reflect myocardial dispersion of repolarization.<sup>7</sup> This limitation is overcome by ECGI: it provides physiologically relevant information about myocardial repolarization by reconstructing the actual spatial properties and dispersion on the surface of the heart.

ER and BrS are often collectively referred to as “J-wave syndromes”, because the two conditions share similar ECG characteristics and a number of clinical features. Both are associated with vulnerability to fatal VT/VF in young adults without apparent structural heart disease, and have dominance in males.<sup>89</sup> The J-wave and associated ST-segment elevation are accentuated before the arrhythmic event, and VF is often initiated during bradycardia. Their responses to quinidine and isoproterenol are ameliorative (normalization of the J-wave and inhibition of VT/VF).<sup>68</sup> Nevertheless, there are several key characteristics that distinguish ERS from BrS, suggesting different underlying mechanisms for the ECG phenotype and arrhythmogenesis. Moderate structural abnormalities (RV interstitial derangement), though undetectable by noninvasive clinical imaging, have been found in endomyocardial biopsies of BrS patients, as well as in the explanted heart of a BrS patient.<sup>90-91</sup> In a recent study, ECGI was performed in 25 BrS patients.<sup>20</sup> Altered or delayed epicardial activation in the RVOT was found in 20 patients. EGMs with abnormally low voltage and fractionation were found in all patients. Prolonged repolarization and steep repolarization gradients were also observed. These findings demonstrate the coexistence of conduction and repolarization abnormalities in BrS. The abnormal EP substrate was confined to the RVOT. In contrast, the wide-spread distribution of J-waves in ERS patients indicates that

the EP substrate may not be localized to a specific region of the heart. The current study identifies additional differences between ERS and BrS. Conduction delays and EGMs indicative of slow discontinuous conduction were not found in ERS patients. The location and size of the abnormal EP substrate varied among ERS patients. Instead of ARI prolongation in BrS patients, shortened ARIs were observed in ERS patients during baseline SR.

There is a paucity of EP mapping data of ERS-related arrhythmias, given the small number of ERS patients who have experienced aborted sudden cardiac death. Catheter mapping was performed in 8 ERS patients with a history of idiopathic VF.<sup>60</sup> In 6 patients with ER pattern only in the inferior ECG leads, all ectopies were mapped to the inferior ventricular wall. In 2 patients with ER pattern in both inferior and lateral leads, ectopy originated from multiple locations. In the current study, PVCs were recorded in 2 patients. The PVC sites of origin were located in an epicardial region with marked J-waves and short ARIs. A recent study using ECGI in an ERS patient during VF identified VF rotors in the inferior-lateral LV wall.<sup>92</sup> These data suggest that the EP substrate in the inferior and lateral LV plays an important role in the development of arrhythmias. If a triggering ectopy interacts with a susceptible substrate of steep repolarization dispersion at the right time, direction and orientation, unidirectional block and reentrant arrhythmia could be initiated.

### **Limitations:**

The control data were not obtained at the time of this study; they were recorded previously with the same ECGI methodology.

Being the first ECGI study of ERS patients, its generalizability is limited by the relatively small number of patients. It does not differentiate between subgroups (e.g. symptoms and

genotype) within the population. Future large-scale ECGI studies should be conducted to establish the potential of the approach for noninvasive arrhythmic risk stratification in ER patients.

Changes in heart rate are known to affect the ER pattern on the ECG, but this protocol was not adopted in this study. Future studies will explore how the patterns of repolarization dispersion respond to heart rate changes.

Several drugs (including quinidine, isoproterenol, milrinone, and cilostazol) have been shown to have ameliorative effects on the ER pattern. Future studies should characterize drug effects on activation and repolarization patterns. The changes in activation and repolarization could provide additional information on the EP substrate and arrhythmia mechanisms associated with ERS.

### **3.6 Conclusions:**

Noninvasive ECGI revealed the presence of abnormal EP substrate in ERS patients, characterized by a regional distribution of epicardial J-waves and shortening of APD. Heterogeneous APD shortening leads to steep repolarization gradients. This defines a substrate susceptible to reentrant arrhythmias, not detectable by the surface ECG. Conduction abnormalities were not present. PVC sites of origin correlated with regions of J-wave presence and steep repolarization gradients, the abnormal EP substrate mapped during SR.



# **Chapter 4: The Cardiac Electrophysiologic Substrate Underlying the ECG Phenotype and Electrogram Abnormalities in Brugada Syndrome Patients**

## **4.1 Abstract**

Brugada syndrome (BrS) is a highly arrhythmogenic cardiac disorder, associated with an increased incidence of sudden death. Its arrhythmogenic substrate in the intact human heart remains ill-defined.

Using noninvasive ECG imaging (ECGI), we studied 25 BrS patients to characterize the electrophysiologic substrate, and 6 patients with right bundle branch block (RBBB) for comparison. Seven normal subjects provided control data. Abnormal substrate was observed exclusively in the right ventricular outflow tract (RVOT) with the following properties (compared to normal controls;  $p < 0.005$ ): (1) ST-segment elevation (STE) and inverted T-wave of unipolar electrograms (EGMs) ( $2.21 \pm 0.67$  vs.  $0$  mV); (2) delayed RVOT activation ( $82 \pm 18$  vs.  $37 \pm 11$  ms); (3) low amplitude ( $0.47 \pm 0.16$  vs.  $3.74 \pm 1.60$  mV) and fractionated EGMs, suggesting slow discontinuous conduction; (4) prolonged recovery time (RT;  $381 \pm 30$  vs.  $311 \pm 34$  ms) and activation-recovery intervals (ARIs;  $318 \pm 32$  vs.  $241 \pm 27$  ms), indicating delayed repolarization; (5) steep repolarization gradients ( $\Delta RT/\Delta x = 96 \pm 28$  vs.  $7 \pm 6$  ms/cm,  $\Delta ARI/\Delta x = 105 \pm 24$  vs.  $7 \pm 5$  ms/cm) at RVOT borders. With increased heart rate in 6 BrS patients, reduced STE and increased fractionation were observed. Unlike BrS, RBBB had delayed activation in the entire RV, without STE, fractionation, or repolarization abnormalities on EGMs.

The results indicate that both, slow discontinuous conduction and steep dispersion of repolarization are present in the RVOT of BrS patients. ECGI could differentiate between BrS and RBBB.

## 4.2 Introduction

Brugada syndrome (BrS) is an inherited disorder, affecting predominantly males in their 40s<sup>93</sup> and associated with an increased incidence of sudden cardiac death (SCD). It presents with ECG expression of atypical right bundle branch block (RBBB) pattern and ST-segment elevation (STE) in leads V1-V3.<sup>93-94</sup> It is estimated that BrS causes approximately 20% of SCD in cardiac patients with structurally normal hearts.<sup>93</sup> Understanding its pathophysiological mechanisms is essential for improving risk stratification, diagnosis and treatment to prevent SCD.

BrS is considered a primary electrical cardiac disease, since no structural anomalies are detected by conventional imaging. Up to 30% of patients test positive for mutations in the SCN5A gene,<sup>93</sup> which causes a loss-of-function of the cardiac sodium channel ( $I_{Na}$ ). A Brugada ECG pattern can be provoked, in some affected patients with a normal baseline ECG pattern, by administration of  $I_{Na}$  blockers.

There are two leading hypotheses for mechanisms underlying BrS phenotype and arrhythmias. (1) *The abnormal repolarization hypothesis (based on the canine wedge preparation):*<sup>95-97</sup> Phase-1 notch is present in epicardial action potentials (AP) due to a high density of transient outward current ( $I_{to}$ ), but absent in endocardial APs (low  $I_{to}$  density). A reduced  $I_{Na}$  in BrS exaggerates the phase-1 notch preferentially in right ventricular outflow tract (RVOT) epicardium, where  $I_{to}$  is expressed with maximal density. The resulting voltage gradients give rise to STE on the ECG. Further outward shift of the balance between  $I_{Na}$  and  $I_{to}$  can repolarize the

membrane during phase-1 below the voltage range for L-type calcium channels ( $I_{Ca-L}$ ) activation. When  $I_{Ca-L}$  fails to activate, the AP loses its plateau (dome). Spatially heterogeneous loss of the AP plateau in the RVOT can lead to reentry (termed “phase-2 reentry” by Antzelevitch and colleagues). (2) *The abnormal conduction hypothesis (based on whole-heart studies in BrS patients)*:<sup>90, 98-99</sup> Impaired  $I_{Na}$  in structurally deranged tissue causes slow discontinuous AP propagation. Asynchronous activation can promote reentrant arrhythmias and create voltage gradients, causing STE and fractionation on the ECG. Data from catheter mapping<sup>98</sup> showed that delayed conduction and abnormal electrograms (EGMs) with low voltage and fractionated late potentials (reflecting slow discontinuous conduction) were exclusively localized in the anterior aspect of the RVOT epicardium. Catheter ablation in this area normalized the Brugada ECG and prevented ventricular tachycardia (VT). The pathophysiological mechanisms of the abnormal ECG and arrhythmia in BrS are still a subject of debate.

While much is known at the molecular and cellular scales, understanding the cause of the BrS ECG pattern and associated arrhythmias requires detailed characterization of the electrophysiologic (EP) substrate in the intact hearts of BrS patients. This requires high resolution, panoramic EP mapping of the ventricles and cannot be achieved with invasive catheter mapping. The recent development of noninvasive mapping with Electrocardiographic Imaging (ECGI) allowed us to obtain the first high resolution panoramic EP data from BrS patients, including up to 1500 unipolar epicardial EGMs and epicardial maps of activation and repolarization.<sup>5-6, 10, 13, 16, 19, 100</sup> Based on these data recorded during sinus rhythm (SR), we characterized the EP substrate in BrS patients in an effort to provide insight into the mechanistic origin of the BrS phenotype. The results show that both, repolarization and structurally-based conduction abnormalities coexist in hearts of BrS patients. We also compared the BrS EP substrate to non-BrS RBBB (generally

considered benign) to determine whether the substrate is specific to BrS, and whether ECGI can differentiate between these two pathologies with similar ECGs.

## **4.3 Methods**

### **4.3.1 Patient Population**

Twenty-five BrS patients from two centers in the United States and one in France were enrolled. The BrS diagnosis was based on the consensus criteria<sup>93</sup> and was the basis for patient recruitment. Beyond the consensus criteria, pregnant women and children were excluded. Patient demographic data are provided in Table 4-1. Six RBBB patients with a prolonged QRS>120ms were studied for comparison. All BrS and RBBB patients had no evidence of structural heart disease on echocardiography or MRI. Data from seven normal subjects<sup>13</sup> provided normal control. Cumulative subject characteristics are provided in Table 4-2. Protocols were approved by the Institutional Review Boards at the three centers; written informed consent was obtained from all patients.

### **4.3.2 Noninvasive Mapping**

ECGI methodology was described previously<sup>5-6, 10, 13, 16, 100</sup> (Figure 4-1). Briefly, torso surface ECG potentials, recorded simultaneously from 250 electrodes, were combined mathematically with patient-specific heart-torso geometry from ECG-gated computed tomography (CT) to construct epicardial potentials, unipolar EGMs, and maps of epicardial activation and repolarization. Bipolar EGMs were constructed for fractionation analysis. The method was validated extensively for reconstruction of EGMs,<sup>5-6</sup> activation<sup>10, 13</sup> and repolarization.<sup>6, 13</sup>

Patient ID	Age	Gender	SCN5A Mutation	Previously Aborted SCD	Syncope	Family History of SCD/ Brugada ECG	ICD Implanted	ICD Therapy	ECG Leads with STE
BrS-1	34	M	-	+	-	-	+	+	V1, V2, V3
BrS-2	53	M	+	+	-	+	+	-	V1, V2
BrS-3	54	M	+	-	+	+	-	-	V1
BrS-4	48	M	+	-	+	+	-	-	V1, V2
BrS-5	52	M	+	-	+	+	-	-	V1, V2
BrS-6	62	F	+	-	-	+	-	-	V1
BrS-7	43	M	-	-	-	-	-	-	V1, V2
BrS-8	41	M	+	-	+	-	-	-	V1, V2, V3
BrS-9	66	M	-	-	-	-	-	-	V2
BrS-10	29	M	-	+	-	+	+	-	V1, V2, V3
BrS-11	44	M	+	-	-	+	-	-	V1, V2
BrS-12	45	M	-	-	-	-	-	-	V1, V2
BrS-13	78	M	N/A	+	-	-	-	-	V1
BrS-14	60	M	-	+	-	-	+	+	V2
BrS-15	31	M	+	-	-	-	-	-	V1, V2
BrS-16	30	M	N/A	-	-	+	-	-	V1, V2, V3
BrS-17	54	F	-	-	+	+	-	-	V1, V2
BrS-18	63	M	+	+	-	+	+	-	V2, V3
BrS-19	61	M	N/A	-	+	-	+	-	V1
BrS-20	45	M	N/A	+	-	-	+	+	V1, V2, V3
BrS-21	39	M	N/A	+	-	-	+	+	V1, V2
BrS-22	48	M	+	+	-	-	+	-	V1, V2
BrS-23	19	M	+	+	-	-	+	-	V1
BrS-24	45	M	N/A	-	+	+	-	-	V1
BrS-25	49	M	N/A	-	-	+	+	-	V1, V2

**Table 4-1: BrS Patient Demographics**

ICD = Implantable Cardioverter Defibrillator; SCD = Sudden Cardiac Death; STE = ST Segment Elevation.

	BrS (n=25)	RBBB (n=6)	Control (n=7)
Age (Year)	48±13	41±12	28±7
Male	23 (92%)	6 (100%)	4 (57%)
SCN5A Mutation	11 (44%)	N/A	N/A
Previously Aborted SCD	10 (40%)	0 (0%)	0 (0%)
Syncope	7 (28%)	0 (0%)	0 (0%)
Family History of SCD or Brugada ECG	12 (48%)	0 (0%)	0 (0%)
ICD Implant	11 (44%)	0 (0%)	0 (0%)
ICD Therapy	4 (16%)	0 (0%)	0 (0%)

**Table 4-2: Cumulative Subject Characteristics**

Data are presented as mean±SD or number (percentage) of patients. ICD = Implantable Cardioverter Defibrillator; SCD = Sudden Cardiac Death.

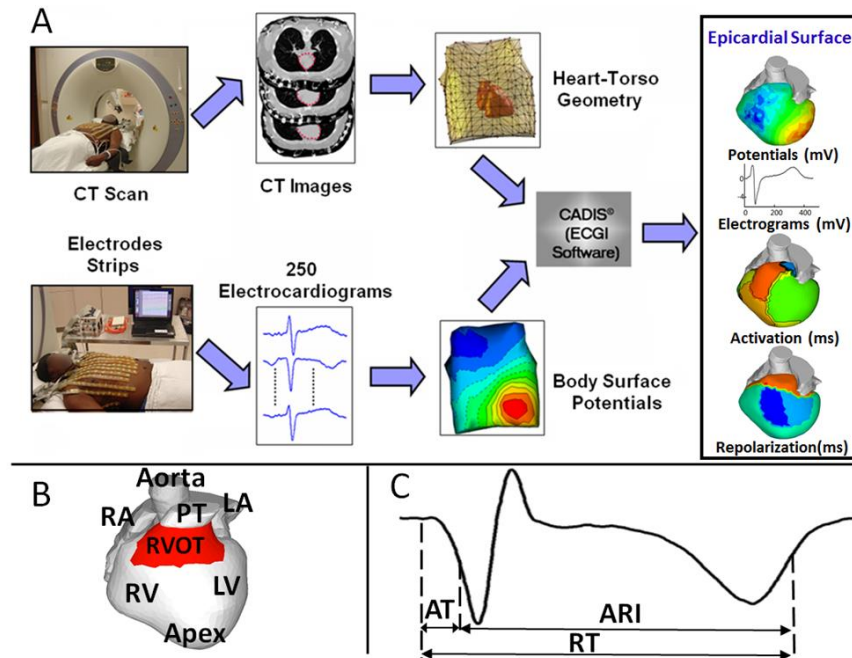


**Figure 4-1: ECGI Procedure and Parameters**

Panel A: The noninvasive ECGI procedure. Body surface potential recordings (250 electrodes) and gated, non-contrast thoracic computed tomography (CT) scan are processed mathematically to obtain epicardial potentials, 1500 unipolar electrograms, and maps of epicardial activation and repolarization. Panel B: The right ventricular outflow tract (RVOT) region in one patient's heart (shown in red) as determined from CT images. This representative image serves as an example. Panel C: Temporal fiducial points on electrograms. AT: activation time; RT: recovery time; ARI: activation recovery interval.

Spatial properties of the EP substrate were determined by dividing the epicardium into 6 segments based on CT images (the RVOT is depicted in Figure 4-1B). EGMs from valvular regions were excluded. On average, 1154 EGMs per patient were used for analysis.

EGMs were evaluated for morphology, magnitude and fractionation. EGM Brugada morphology was defined as STE followed by T-wave inversion. EGM magnitude (EMM) was measured peak-to-peak during the EGM QRS; for fractionated EGMs, the measurement was confined to the fractionated segment. Fractionation was expressed as number of low-amplitude deflections per EGM and displayed on epicardial EGM deflection maps (EDMs).<sup>16</sup> For the fractionation analysis, bipolar EGMs were approximated by time derivatives of unipolar EGMs.

Local activation time (AT, referenced to beginning of QRS in ECG lead II) was determined by the maximal negative slope of the EGM during QRS inscription (Figure 4-1C). From the ATs, epicardial activation isochrone maps were created. Slow conduction is represented by crowded isochrones. Regional activation duration (AD) was defined as the interval between the earliest and latest AT in a region, considering all EGMs in that region.

Local recovery time (RT) was determined from the maximal positive slope of the EGM T-wave (Figure 4-1C); it reflects the sum of local activation time and local action potential duration (APD). For a given activation sequence, RT determines spatial voltage gradients during repolarization, and underlies ST-T deflections. RT dispersion provides substrate for unidirectional block and reentry. Activation-recovery interval (ARI) was defined as the difference between RT and AT. ARI is independent of AT and a surrogate for local APD.<sup>71</sup> Epicardial RT and ARI gradients were computed as the difference between neighboring epicardial nodes, divided by the distance between them.

ECGI was conducted in 6 patients during increased heart rate (HR; 3 with exercise and 3 with isoprenaline). ECGI maps at baseline and during the faster HR were compared.

### **4.3.3 Simulation**

The O'Hara-Rudy (ORd) model of a human ventricular myocyte<sup>101</sup> was used in the simulations. Fast/late  $I_{Na}$  and  $I_{to}$  were replaced by formulations used previously to represent the prominent phase-1 repolarization notch characteristic of RVOT APs.<sup>102</sup> The model was paced to steady state at normal and slow rates (1,000 beats at 1 and 0.5 Hz, respectively) with various combinations of reduced  $I_{Na}$  and enhanced  $I_{to}$  conductances ( $G_{Na}$  and  $G_{to}$ ). Combinations were selected to span a virtual Brugada severity space. APD was measured at 90% repolarization (APD90 in ms).

### **4.3.4 Statistical Analysis**

For every subject, the mean values for EGM variables within each epicardial segment were computed. All statistical tests were performed at the level of epicardial segments. Differences in variables among epicardial segments were compared by one-way repeated measures ANOVA. When the assumption of sphericity was violated, Greenhouse-Geisser correction was performed. Using the Bonferroni method, pairwise comparisons between RVOT and other regions were conducted (5 tests in total). Continuous variables at baseline and increased HR were compared by paired t-test. Continuous variables between BrS and control, and between BrS and RBBB were compared by unpaired t-test. The Satterthwaite modified t-test was used for variables with unequal variances. All tests with  $P < 0.05$  were considered statistically significant. Statistical analysis was performed using SPSS v19.



	<b>RVOT</b>	<b>RV Free Wall</b>	<b>RV Apex</b>	<b>LV Base</b>	<b>LV Free Wall</b>	<b>LV Apex</b>
<b>Mean Peak STE (mV)</b>	2.21±0.67	0.13±0.09*	0*	0*	0.08±0.04*	0*
<b>Mean EGM Magnitude (mV)</b>	0.47±0.16 (Fractionated)	2.52±0.94*	3.77±0.85*	2.99±1.17*	3.14±0.81*	5.88±1.18*
<b>Mean EGM Fractionation (# of deflections)</b>	2.97±0.69	1.04±0.80*	0*	0*	0*	0*

**Table 4-3: EGM Properties for BrS Patients**

Variables presented as mean±SD. \*P<0.005 when comparing other segments to RVOT. EGM = Electrogram; STE = ST-segment elevation.

## 4.4 Results

### 4.4.1 BrS Abnormal EGM Characteristics and Localization

Table 4-3 summarizes values of EGM parameters in each epicardial segment for baseline HR. Pairwise multiple comparisons between the RVOT and other regions suggest that the abnormal substrate is localized in the RVOT. Figure 4-2 shows EGM characteristics and localization for representative examples in 3 BrS patients (normal maps are provided for reference). STE (examples in Panel A) was observed in RVOT of all 25 patients (2.21±0.67 vs. 0 mV in control, p<0.005), but rarely detected outside the RVOT. Three patients had low-magnitude STE in the RV free wall and two in the left ventricular (LV) free wall (range from 0.2 to 0.5 mV). ECG leads with STE for all patients are identified in Table 4-1. 59% of EGMs in RVOT had STE>1 mV. EGMs magnitude (Panel B) was lower in the RVOT (0.47±0.16 vs. 3.74±1.60 mV in control, p<0.005) than in other regions (>2.5mV). 46% of EGMs in the RVOT had voltage<2 mV. Four patients had low voltage in the RV free wall and 3 in the LV base. Fractionated EGMs (Panel C) were present in the RVOT (number of deflections =2.97±0.69 vs. 0 in control, p<0.005). 27% of EGMs in the RVOT had more than 2 deflections. Two patients had fractionated EGMs in the RV free wall. Panel D shows EGMs from locations marked by white dots in Panel C, representative

of abnormal morphology of RVOT EGMs. Red arrows indicate low voltage and fractionated EGMs.

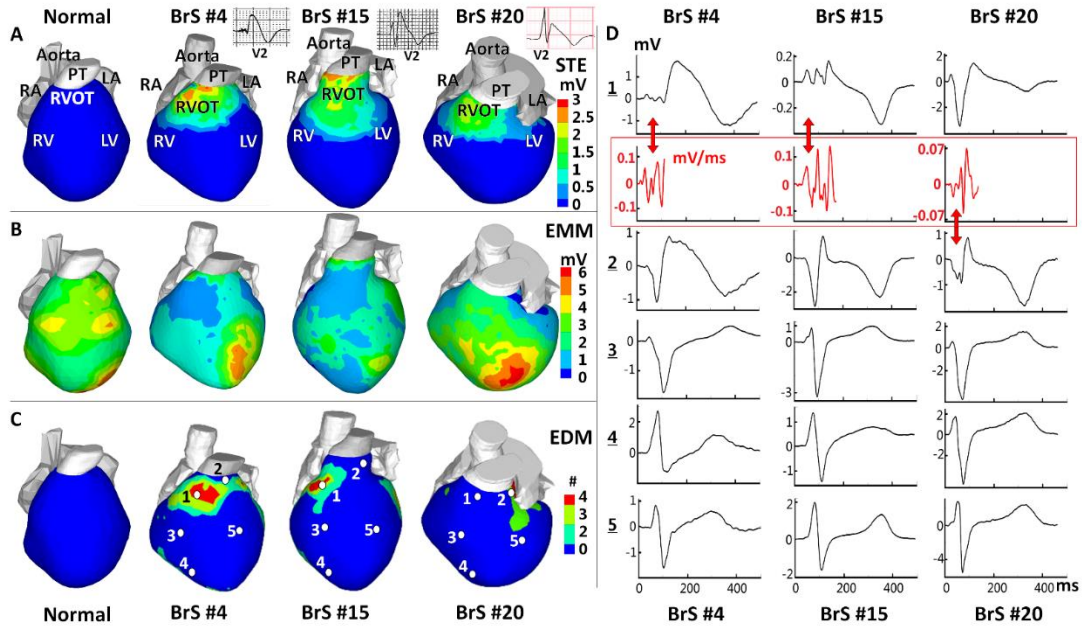


**Figure 4-2: Abnormal Epicardial Electrograms (EGMs) Characteristics and Localization**

Panel A: Peak ST Segment elevation (STE) magnitude map. Insets show ECG lead V2. Panel B: EGM magnitude map (EMM). Panel C: EGM deflection map (EDM) showing number (#) of low amplitude deflections. BrS maps are in 3 right columns; left column shows corresponding maps from a normal subject for reference. Panel D: Unipolar EGMs from locations marked by white dots in Panel C. 1-Anterior RVOT, 2-Lateral RVOT, 3-RV free wall, 4-RV apex, 5-LV free wall (EGMs from other LV sites are also normal). Red traces: time derivatives of fractionated QRS. The derivatives approximate bipolar EGMs and emphasize fractionation. Maps are shown in anterior view. Each BrS column shows maps/EGMs from one patient identified by BrS#. RA: right atrium, LA: left atrium, RV: right ventricle, LV: left ventricle, RVOT: right ventricular outflow tract, PT: pulmonary trunk. Red arrows point to low voltage and fractionated EGMs.

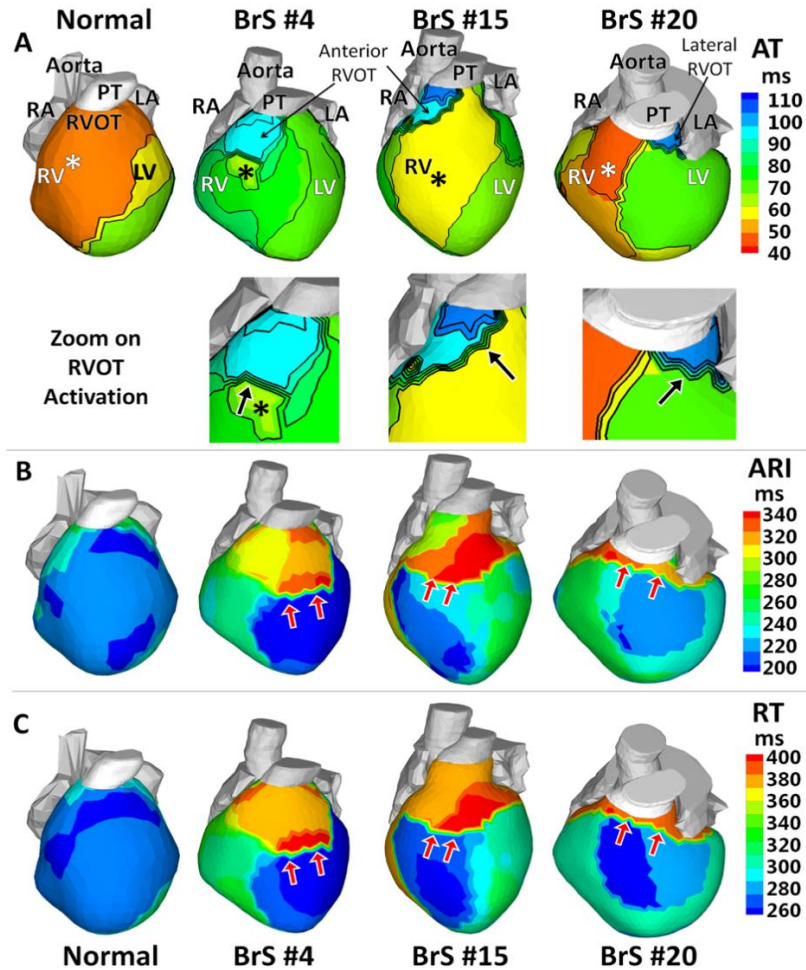


**Figure 4-3: Activation and Repolarization during Sinus Rhythm**

Panel A: Activation times isochrone maps (AT). Lower panels: zoom on the RVOT. Panel B: Activation-recovery interval maps (ARI). Panel C: Recovery time maps (RT). Epicardial breakthroughs are indicated by asterisks. Isochrones are depicted in thin black lines. Black arrows in the RVOT zoom maps of Panel A point to slow conduction indicated by crowded isochronal lines. Red arrows in Panels B-C point to regions with steep repolarization gradients.

#### 4.4.2 BrS Activation

Normal human epicardial activation patterns during SR were reported previously.<sup>13, 72</sup> In general, earliest epicardial activation occurs in anterior RV (although there are many variants of location),<sup>13, 72</sup> while lateral LV base is most commonly the latest region to activate. Activation isochrone maps in Figure 4-3A show examples of how SR epicardial activation patterns were altered by the presence of BrS EP substrate. Patient BrS#4 had earliest epicardial breakthrough

(asterisk) over the RV free wall, from which activation propagated slowly (crowded isochrones) across the RVOT-RV free wall border. RV free wall and LV activated first, leaving the anterior RVOT to activate last (light blue). Patient BrS#15 had a similar activation pattern, with a broader wavefront and faster activation of the RV free wall. Slow conduction occurred in the RVOT (crowded isochrones in the blue region). Patient BrS#20 had earliest activation in the anterior RV. Latest activation (dark blue) occurred at the lateral RVOT, nearly 65 ms after the anterior RV breakthrough.

Of the 25 BrS patients imaged during SR, 20 demonstrated altered or delayed epicardial activation at the RVOT. Table 4-4: Activation and Repolarization Parameters for BrS Patients Table 4-4 summarizes AT (mean  $\pm$  standard deviation) in each segment. AT in RVOT ( $82 \pm 18$  vs.  $37 \pm 11$  ms in control,  $p < 0.005$ ) was almost as late as that of LV base ( $80 \pm 16$  ms), and was much delayed compared to the other 4 segments. In specific RVOT locations, AT was as late as 150 ms. AD (the time needed for activation of a defined region) was calculated for the RVOT ( $36 \pm 16$  ms), the RV free wall ( $16 \pm 3$  ms), the entire RV ( $40 \pm 14$  ms), the entire LV ( $27 \pm 5$  ms) and both ventricles ( $51 \pm 10$  ms). RVOT activation took much longer than RV free wall or LV. AD of the RVOT accounted for about 71% of total AD in both ventricles, highlighting the slow activation of the RVOT.

	<b>RVOT</b>	<b>RV Free Wall</b>	<b>RV Apex</b>	<b>LV Base</b>	<b>LV Free Wall</b>	<b>LV Apex</b>
<b>Mean AT (ms)</b>	$82 \pm 18$	$52 \pm 12^*$	$57 \pm 7^*$	$80 \pm 16$	$62 \pm 8^*$	$58 \pm 10^*$
<b>Mean RT (ms)</b>	$381 \pm 30$	$272 \pm 42^*$	$263 \pm 30^*$	$317 \pm 38^*$	$279 \pm 31^*$	$272 \pm 31^*$
<b>Mean ARI (ms)</b>	$318 \pm 32$	$229 \pm 36^*$	$221 \pm 37^*$	$245 \pm 40^*$	$222 \pm 31^*$	$220 \pm 27^*$

**Table 4-4: Activation and Repolarization Parameters for BrS Patients**

Variables presented as mean  $\pm$  SD. \* $P < 0.005$  when comparing other segments to RVOT. ARI= Activation-Recovery Interval; AT=Activation Time; RT=Recovery Time.

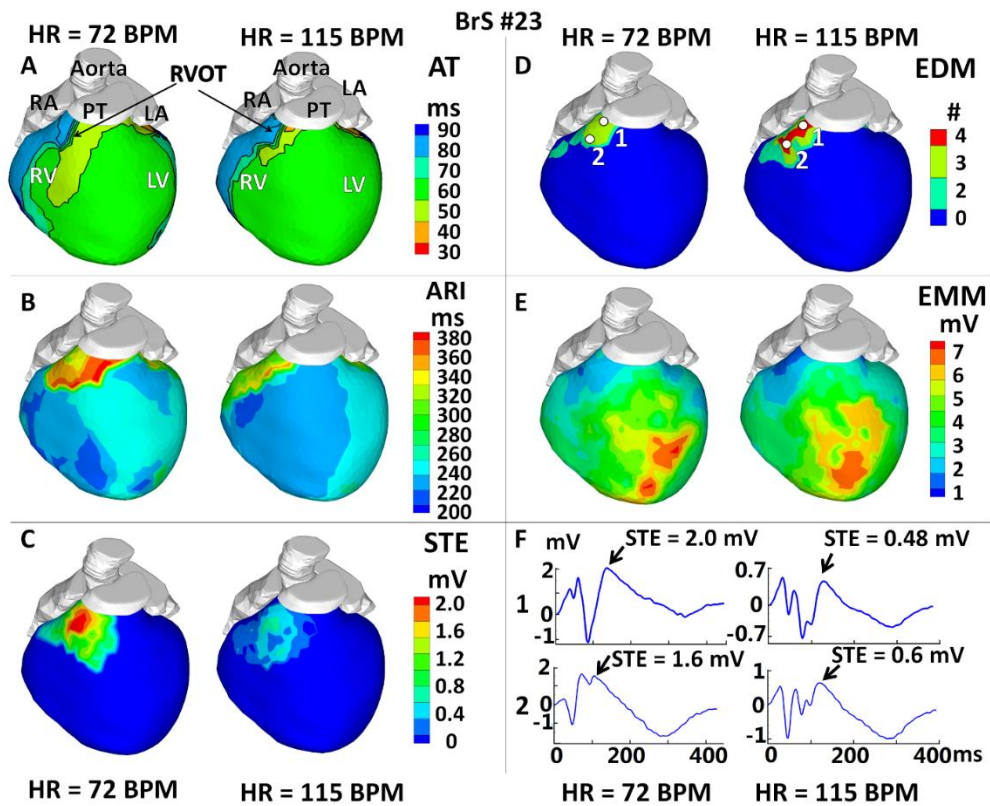
### 4.4.3 BrS Repolarization

Figure 4-3 Panel B and Panel C show representative ARI and RT maps from 3 BrS patients. Table 4-4 provides ARI and RT in each epicardial segment. ARI prolongation ( $318 \pm 32$  vs.  $241 \pm 27$  ms in control,  $p < 0.005$ ) and RT prolongation ( $381 \pm 30$  vs.  $311 \pm 34$  ms in control,  $p < 0.005$ ) were observed primarily in the RVOT, but also extended into adjacent neighboring regions of the RV free wall and the LV free wall. Steep epicardial ARI gradients and RT gradients (red arrows) occurred mostly at the RVOT-RV free wall or RVOT-LV free wall borders. These gradients also existed within the RVOT. Transitions of colors from blue to red across these regions reflect large differences in ARI and RT of 70-140 ms, leading to very steep localized ARI gradients ( $105 \pm 24$  vs.  $7 \pm 5$  ms/cm in control<sup>13</sup>,  $p < 0.005$ ) and RT gradients ( $96 \pm 28$  vs.  $7 \pm 6$  ms/cm in control,  $p < 0.005$ ). In patient BrS#15, the gradients between the anterior and lateral RVOT ARI map are not apparent in the RT map. This is because the anterior RVOT activated about 40 ms later than the lateral RVOT. This long delay masks the ARI differences between these two regions. However, in regions that activate without conduction delay (e.g., RV free wall) RTs and their dispersion are primarily determined by ARI and ARI dispersion, independent of conduction. The patterns in RT maps closely follow the ARI patterns in such cases.

### 4.4.4 Effects of Increased HR in BrS

ECGI was performed in 6 BrS patients during increased HR (mean increase from 71 to 133 BPM) Figure 4-4 shows the effects of increased HR (from 72 to 115 BPM) in one representative example. Although the activation sequence remained largely unchanged (Panel A), RVOT activation was further delayed with HR increase (AD: from  $32 \pm 7$  ms to  $38 \pm 10$  ms), and RVOT EGMs had more fractionation and lower voltage (Panels D-F). This change of RVOT EGMs was observed in 4 out of 6 patients (no significant change in the other 2 patients). When HR increased,

ARIs (Panel B, corrected for HR) were shorter over the entire heart, but the RVOT ARIs decreased more than in other regions (by 50 ms compared to 25 ms in RV free wall). The regions with steep ARI gradients persisted, but the magnitude of the ARI gradient decreased (from 117 ms/cm to 96 ms/cm). Reductions in RT and RT gradients were also observed during increased HR. STE (Panel C) in RVOT was significantly reduced (from 2.0 mV to 0.5 mV). Similar changes in ARI, RT and STE were observed in all 6 patients (Table 4-5).



**Figure 4-4: Effects of Increased Heart Rate (HR)**

Panel A: Activation isochrone maps (AT). Panel B: Activation-recovery interval maps (ARI). Panel C: Peak ST segment elevation magnitude maps (STE). Panel D: Electrogram deflection maps (EDM), showing number (#) of deflection on EGM. Panel E: Electrogram magnitude maps (EMM). Panel F: EGMs from RVOT locations marked by white dots in Panel D. Each panel shows the map at resting (75 BPM) and increased HR (115 BPM).

		<b>RVOT</b>	<b>RV Free Wall</b>	<b>RV Apex</b>	<b>LV Base</b>	<b>LV Free Wall</b>	<b>LV Apex</b>
<b>Mean AT (ms)</b>	Baseline HR	84±14	57±16	61±8	84±11	65±10	60±7
	Faster HR	81±19	56±15	63±7	84±10	63±8	58±8
<b>Mean RT (ms)</b>	Baseline HR	392±26	265±38	274±34	333±42	284±39	281±38
	Faster HR	358±30 <sup>§</sup>	251±35	265±29	320±36	275±33	274±37
<b>Mean ARI (ms)</b>	Baseline HR	328±35	222±41	224±42	256±44	229±37	231±24
	Faster HR	287±33 <sup>§</sup>	203±32	210±39	239±40	218±36	220±22
<b>Mean Peak STE (mV)</b>	Baseline HR	2.56±0.71	0.09±0.08	0	0	0.13±0.04	0
	Faster HR	0.84±0.26 <sup>§§</sup>	0.06±0.06	0	0	0.12±0.04	0
<b>Mean EGM Fractionation</b>	Baseline HR	2.73±0.53	0.87±0.54	0	0	0	0
	Faster HR	3.65±0.60 <sup>§§</sup>	1.09±0.41	0	0	0	0

**Table 4-5: Effects of Increased Heart Rate (HR) in BrS Patients**

Variables presented as mean±SD. <sup>§</sup>P<0.05 when compared to baseline HR; <sup>§§</sup>P<0.005 when compared to baseline HR. ARI= Activation-Recovery Interval; AT= Activation Time; EGM= Electrogram; RT= Recovery Time; STE= ST-segment Elevation.

#### 4.4.5 Comparison between BrS and Non-BrS RBBB

ECGI was conducted during sinus rhythm in 6 non-BrS patients with RBBB, without structural heart disease. Epicardial activation patterns, ARI maps and EGM morphologies were analyzed and compared to those of the BrS patients. This comparison is of clinical importance, because the diagnosis of BrS in the presence of an RBBB ECG could be challenging. This is demonstrated in Figure 4-5A, where the Brugada ECG pattern for BrS#10 is masked by an RBBB pattern. Figure 4-5 shows representative data from 4 patients (2 BrS and 2 RBBB). BrS#4 had a spontaneous Brugada ECG pattern, while the ECG of BrS#10 showed an atypical RBBB pattern. Table 4-6 summarizes the differences of ECGI parameters between all BrS and RBBB patients. In RBBB patients, activation of the entire RV was delayed, with a long conduction delay of 35 ms

across the interventricular septum (crowded isochrones; black arrow). In contrast, delayed activation was confined to the RVOT of BrS patients. Normal RV epicardial breakthrough (indicative of normal conduction system participation) was observed in all BrS patients, but not in any RBBB patient. BrS patients had a much longer AD in the RVOT than RBBB patients ( $36 \pm 16$  ms BrS vs.  $14 \pm 5$  ms RBBB;  $p < 0.005$ ), accounting for most of the AD in the entire RV ( $40 \pm 14$  ms BrS vs.  $24 \pm 6$  ms RBBB;  $p < 0.005$ ). Unlike BrS, RBBB T-wave inversion in the RVOT and RV was not accompanied by ARI prolongation (RBBB= $246 \pm 25$  ms, BrS= $326 \pm 30$  ms,  $p < 0.005$ ), steep ARI dispersion (RBBB= $8 \pm 4$  ms/cm, BrS= $105 \pm 24$  ms/cm,  $p < 0.005$ ) or steep RT gradients (RBBB= $6 \pm 3$  ms/cm, BrS= $96 \pm 28$  ms/cm,  $p < 0.005$ ); ARI and RT maps were uniform. This demonstrates that T-wave inversion *per-se* does not indicate the presence of repolarization gradients. The abnormal EGM characteristics specific for BrS (STE and low amplitude fractionation) were not observed in RBBB patients. It is of note that ECGI unmasked the presence of BrS in BrS#10, who had an RBBB pattern on the body surface ECG but BrS substrate in the RVOT, as revealed by ECGI.

	Activation Duration (ms)			EGM Fractionation (# of small deflections)		EGM Magnitude (mV)		ARI Dispersion (ms/cm)	RT Dispersion (ms/cm)
	RVOT†	RV free wall	Entire RV†	RVOT†	RV free wall†	RVOT†	RV free wall	RVOT†	RVOT†
<b>BrS</b>	$36 \pm 16$	$16 \pm 3$	$40 \pm 14$	$2.97 \pm 0.69$	$1.04 \pm 0.80$	$0.47 \pm 0.16$	$2.52 \pm 0.94$	$105 \pm 24$	$96 \pm 28$
<b>RBBB</b>	$14 \pm 5$	$16 \pm 6$	$24 \pm 6$	0	0	$3.74 \pm 0.65$	$3.53 \pm 0.60$	$8 \pm 4$	$6 \pm 3$

**Table 4-6: A Comparison of ECGI Parameters between BrS and Non-BrS RBBB Patients**

Variables presented as mean  $\pm$  SD. † Unpaired t-test:  $P < 0.05$ . ARI= Activation-Recovery Interval; EGM= Electrogram; RT= Recovery Time.



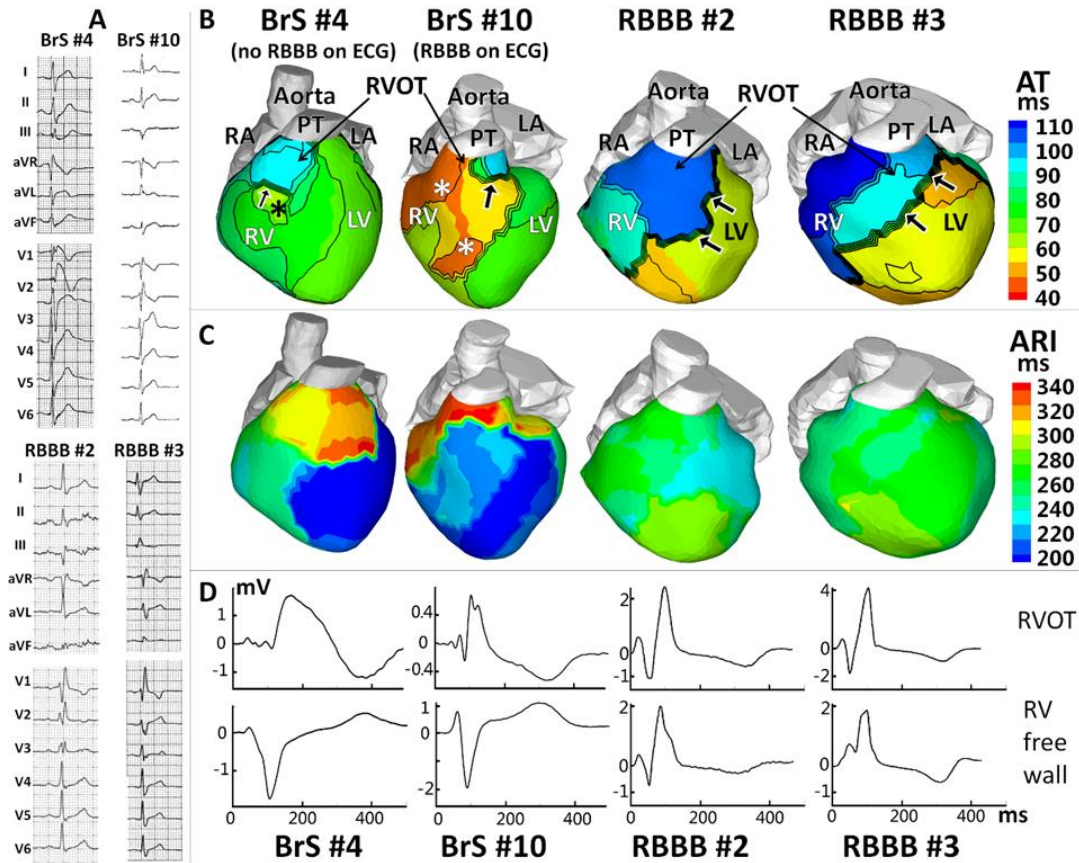


**Figure 4-5: Comparison between BrS and Non-BrS RBBB.**

Panel A: 12-lead ECGs. Panel B: Activation isochrone maps (AT). Panel C: Activation-recovery interval maps (ARI). Panel D: EGMs from the RVOT (top) and RV free wall (bottom). ECGs, maps and EGMs are shown for 4 representative examples (BrS#4: spontaneous Brugada ECG pattern. BrS#10: BrS patient with RBBB ECG pattern. RBBB#2 and RBBB#3: Non-BrS patients with RBBB ECG patterns). Epicardial breakthroughs are indicated by asterisks. Black arrows point to slow conduction in RVOT (BrS) or across the septum (RBBB).

## 4.5 Discussion

This is the first panoramic ventricular mapping study in BrS patients, made possible by ECGI. The panoramic mapping identified the RVOT as the region of abnormal EP substrate with the following properties: (1) Abnormal EGMs characterized by STE and inverted T-wave, reduced amplitude and fractionation; (2) Conduction delays and regions of slow conduction; (3) Prolonged repolarization and steep repolarization gradients; (4) Reduced STE, increased fractionation,

decreased RVOT ARI and RT, decreased ARI and RT gradients with increased HR. These properties are significantly different than in patients with RBBB.

#### **4.5.1 Abnormal EGM Characteristics and Localization**

The RVOT has been suggested as the origin of arrhythmic activity in BrS patients.<sup>93, 98-99, 103-104</sup> Our observation of substrate localization exclusively to the RVOT in BrS patients provides crucial evidence for the RVOT dominant role in clinical BrS. This is in contrast to a recent ECGI study of the long QT syndrome, where abnormal repolarization substrate was spread over the entire epicardium.<sup>19</sup> ECGI revealed RVOT EGMs with coved morphology similar to the typical Brugada ECG morphology in the body surface right precordial leads (Figure 4-2). Additionally, the EGMs were of low amplitude and fractionated. These EGM properties, reconstructed noninvasively by ECGI, were consistent with those obtained from invasive electroanatomical mapping.<sup>98, 103</sup> The ECGI panoramic mapping determined that the majority of these Brugada EGMs were confined to the RVOT; only rarely were they detected close to the RVOT, in adjacent neighboring regions of the RV or LV free wall. Therefore, our study adds insight to the observation from invasive epicardial mapping and ablation, that the Brugada morphology normalized following ablation in the anterior RVOT.<sup>98</sup> This EGMs localization confirms that the RVOT is the origin of the Brugada-type ECG morphology in the body surface right precordial leads.

#### **4.5.2 Substrate for Abnormal Conduction**

BrS has been considered a primary electrical disease, because structural abnormalities have not been detectable by noninvasive clinical imaging (e.g. echocardiography or MRI). Recently, RV interstitial derangements (fibrosis, fatty infiltration) have been found in endomyocardial biopsies of BrS patients,<sup>90</sup> as well as in the explanted heart of a BrS patient carrying an SCN5A

mutation.<sup>91</sup> Fibrosis and fatty infiltration have been associated with decreased electric coupling, discontinuous propagation and reduced conduction velocity.<sup>27</sup> In the normal heart, excitability and conduction are dominated by  $I_{Na}$ . In BrS, where  $I_{Na}$  is impaired,  $I_{to}$  becomes a significant determinant of excitability, opposing the depolarizing effect of  $I_{Na}$ . This is especially true in the RVOT, where  $I_{to}$  is expressed with very high density. In this region, the balance between reduced depolarizing  $I_{Na}$  and large repolarizing  $I_{to}$  results in a reduced excitatory current, which on the background of a structurally abnormal substrate, can support long localized conduction delays and discontinuous slow conduction, conditions that facilitate sustained reentrant arrhythmias.<sup>27</sup>

Experimental, theoretical, and clinical studies have shown that low-magnitude, fractionated and wide EGMs reflect slow, non-uniform and discontinuous conduction through a structurally heterogeneous substrate associated with separation and reduced coupling of myocardial fibers.<sup>38</sup> Previous studies demonstrated ECGI's ability to reconstruct EGMs with these properties.<sup>5, 16, 100</sup> In this study, ECGI reconstructed low-magnitude, fractionated and wide unipolar EGMs. The time derivatives ( $dV/dt$ ) of unipolar EGMs approximate bipolar EGMs and emphasize fractionation (Figure 4-2D, red). The reconstructed unipolar EGMs and the approximated bipolar EGMs are consistent with those measured directly by catheters in BrS patients,<sup>98, 103</sup> providing evidence for slow discontinuous conduction in the RVOT. The ECGI mapping of late RVOT activation, prolonged AD, presence of regions of slow conduction, and altered wavefront propagation compared to normal (Figure 4-3A) provides additional evidence supporting the conduction hypothesis. Similar observations were made with invasive mapping.<sup>98, 103</sup> Computer modeling of AP conduction in presence of BrS mutant  $I_{Na}$  also produced slow discontinuous conduction, causing spatial gradients of membrane potential during the AP plateau and/or early

repolarization phase and STE in the computed pseudo-ECG waveform.<sup>105</sup> Taken together, these data provide evidence for the presence of abnormal conduction in the RVOT of BrS patients.

Antzelevitch and colleagues used a canine RV wedge preparation, where  $I_{to}$  activator and sodium and calcium channel blockers were applied to pharmacologically simulate effects of BrS, and to explain EGM fractionation and late potentials.<sup>95-96</sup> This preparation did not include structural abnormalities and conduction disturbances; it investigated the mechanism of EGM fractionation in the setting of abnormal repolarization alone. It demonstrated the ability to generate secondary deflections on the epicardial EGMs based on differences in the AP morphology at different epicardial locations during the AP repolarization phase. Following the phase-1 notch (which underlies the STE), APs can differ by the presence/amplitude of a dome and by the time of complete repolarization. The associated gradients can result in 2 late deflections on the EGM.<sup>96</sup> Because the deflections occur during late repolarization, the shortest coupling interval to the main EGM deflection (generated by the AP upstroke) was 200 ms.<sup>96</sup>

In the patients studied here, and in patients studied using catheters,<sup>98</sup> EGM fractionation shows different properties; it includes more than 2 deflections (many show 4 deflections) that are tightly coupled to the main deflection (<50 ms) and even occur before the main deflection. Moreover, the fractionation is amplified with increased heart rate. All of these properties point to fragmented slow conduction as a major contributor to EGM fractionation. Of course, abnormal repolarization can also contribute to fractionation of the EGM,<sup>96</sup> but the augmentation with increased heart rate identifies conduction as the major mechanism.

### 4.5.3 Substrate for Abnormal Repolarization

$I_{to}$  expression is non-uniform in the ventricular myocardium. Expression is highest in the epicardium and diminishes transmurally towards the endocardium, creating a phase-1 notch in epicardial, but not endocardial AP. A particularly large  $I_{to}$  density is found in the epicardial RVOT. Reduced  $I_{Na}$  in BrS on the background of the large  $I_{to}$  exaggerates the phase-1 notch, and the resulting spatial gradients of membrane voltage can give rise to STE in ECG waveforms. The deep and wide notch delays the AP plateau and prolongs APD, potentially causing reversal of membrane voltage gradients and T wave inversion.<sup>95, 97</sup> In extreme cases (not recorded in this study), the membrane is repolarized to voltages that are too low for sufficient  $I_{Ca-L}$  activation during phase-1 of the AP and cells repolarize prematurely, losing the AP plateau.<sup>95</sup> This bi-phasic behavior (APD prolongation followed by APD shortening in conditions of extreme severity) is supported by the computer simulations of Figure 4-6. ECGI was validated to accurately map regions of altered repolarization and steep repolarization gradients.<sup>6</sup> The ECGI mapping in this study (Figure 4-3) demonstrated delayed repolarization and prolonged epicardial APDs (based on reconstructed ARIs) in the RVOT of BrS patients. Short ARIs, closely coupled extrasystoles, or VT were not recorded in any patient. Interestingly, direct recordings from endocardium and epicardium revealed longer ARIs in epicardium than in endocardium of BrS patients, suggesting prolongation of epicardial APD; ARI shortening was not reported.<sup>106</sup> A steep repolarization gradient existed at the RVOT borders, which could be due to non-uniform spatial expression of the mutation. However, even uniform spatial distribution of mutant-channel current can cause spatial ARI dispersion. APD is determined by a delicate balance of transmembrane currents and this dependence is non-linear. Therefore, spatially uniform mutant  $I_{Na}$  expression on the background of non-uniform electrophysiologic profile (heterogeneous  $I_{to}$ ) can cause large spatial variation of

the APD. It is also possible that reduced coupling and fiber separation in the BrS substrate limit electrical loading and help maintain the steep spatial repolarization gradients.

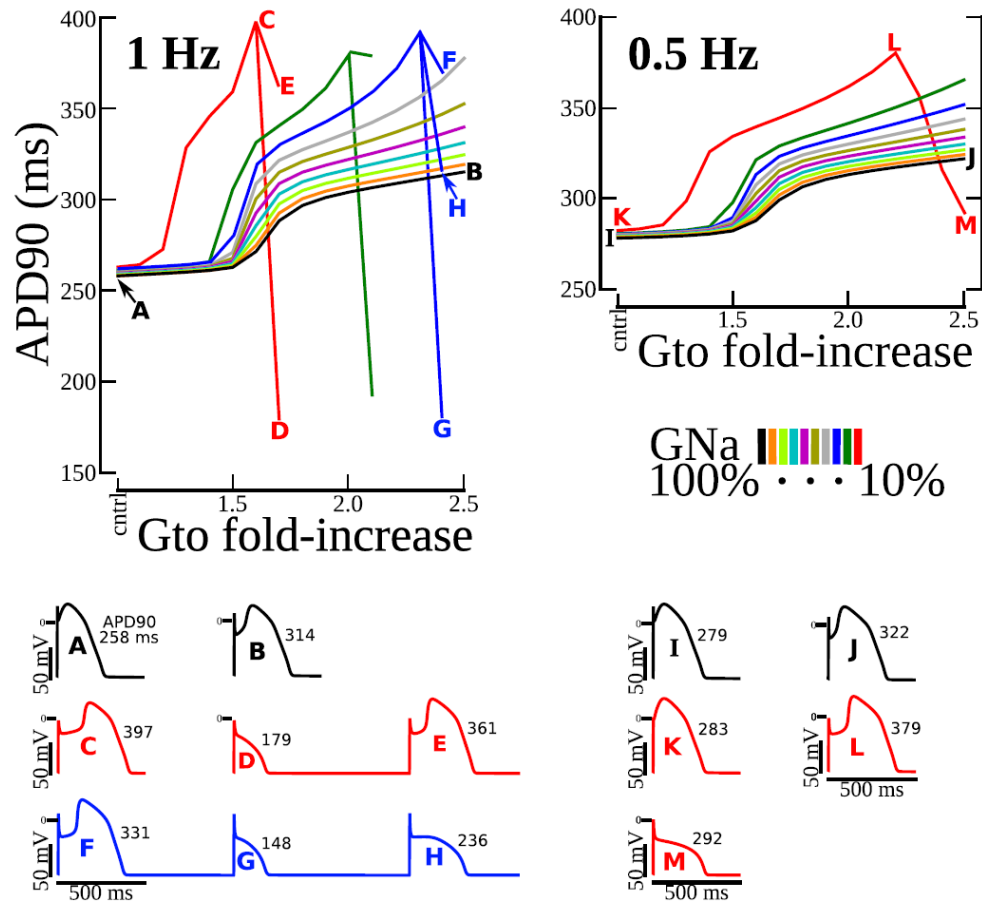


**Figure 4-6: Computer Simulation of BrS Effects on a Human RVOT Action Potential**

At pacing rate of 1 Hz and 0.5 Hz, APD90 (APD at 90% repolarization) was plotted versus  $I_{to}$  conductance increase ( $G_{to}$  from 1.0 to 2.5 fold). Colors indicate different amounts of  $I_{Na}$  conductance reduction ( $G_{Na}$  from 100 to 10%). APs and their duration are shown for  $G_{to}/G_{Na}$  pairings selected to illustrate the behaviors of interest: control— A and I; AP prolongation – B, C, E, F, J, and L; premature repolarization and AP shortening – D, G, H, and M; alternating AP prolongation and shortening – D, E, and F, G, H. Letters A through M relate the summary data above with each of the APs in the traces below. The simulations demonstrate bi-phasic changes of APD (prolongation followed by shortening). Prolongation was greater when  $I_{Na}$  was reduced. With  $I_{Na}$  loss, there was a critical degree of  $I_{to}$  enhancement beyond which APs fully repolarized prematurely at phase-1, causing loss of plateau and APD shortening. Just below this critical degree, APs could alternate between premature repolarization and prolongation.

#### **4.5.4 Examining the Coexistence of Conduction and Repolarization Substrates Using Increased HR**

The rate-dependence of STE and EGM fractionation in BrS may be helpful in unmasking the existence of abnormal repolarization and abnormal conduction, respectively, in the EP substrate. Decreased STE at increased HR supports the repolarization hypothesis, because it suppresses the AP phase-1 notch and associated voltage gradients. In this study, STE in the RVOT decreased in all 6 patients with increased HR. In contrast, increased EGM fractionation with increased HR reflects the presence of slow discontinuous conduction, consistent with the conduction hypothesis. Increased RVOT EGM fractionation was observed in 4 patients at faster HR. Taken together, the effects of increased HR on STE and EGM fractionation support coexistence of these two mechanisms in the BrS substrate. Repolarization abnormality is the major contributor to STE, while conduction abnormality is the major contributor to EGM fractionation.

From the arrhythmogenic perspective, the presence of steep repolarization gradients (dispersion) introduces asymmetry of excitability and thus conditions for unidirectional block.<sup>27</sup> Slow conduction shortens the wavelength of the reentrant AP, thus allowing for shorter reentry pathways and stabilizing reentry. Together, these two properties provide conditions for sustained reentrant excitation. Their coexistence in the substrate of BrS patients has been suggested by other recent studies;<sup>107-108</sup> it is consistent with the high incidence of arrhythmic SCD. Interestingly, most arrhythmic events occur during bradycardia. Reduced STE at increased HR reflects less steep repolarization gradients; it reduces arrhythmogenicity because the probability for unidirectional block is reduced.

#### **4.5.5 Comparison to Non-BrS RBBB**

BrS and RBBB differ greatly in their arrhythmogenicity, with BrS being highly arrhythmogenic. Therefore, a noninvasive method for distinguishing between these abnormalities is highly desirable. Despite the similarities in the 12-lead ECG, ECGI differentiated BrS from non-BrS RBBB in several aspects: (1) BrS EGMs with STE, low voltage and fractionation were not found in RBBB. (2) Non-delayed RV epicardial breakthrough was observed in all BrS patients, indicating involvement of a functioning RBB. RV breakthrough was absent in all RBBB patients, reflecting the defective conduction system. (3) In BrS, slow discontinuous conduction and delayed activation were confined to the RVOT and RVOT-RV border. In contrast, RBBB caused late activation of the entire RV because of a long conduction delay across the septum; there were no regional conduction delays within the RVOT/RV. (4) ARI prolongation and steep ARI gradients were observed in RVOT of BrS patients but not in RBBB patients. These differences could provide the basis for an ECGI-based differential diagnosis in the clinical setting. In addition, the BrS ECG pattern may be masked by an RBBB ECG pattern in some patients, causing difficulties in distinguishing between BrS and RBBB. This has led to invasive procedures (e.g., RV pacing in Chiale intervention<sup>109</sup>) that help unmask the Brugada phenotype in patients with RBBB. In this study, we demonstrated that ECGI can image the BrS substrate in such patients, providing a noninvasive method for the clinical diagnosis of BrS even when it is masked by an RBBB pattern on the body surface ECG.

#### **4.5.6 Limitations**

Being the first ECGI study of BrS patients, it does not differentiate between subgroups (genotype, symptoms, family history etc.) within the BrS population.



ECGI data for the normal controls were previously obtained with the same ECGI methodology; the data were not obtained at the time of this study.

This study is limited to characterizing the BrS substrate from data obtained during SR, and relating its properties to the BrS ECG and EGM phenotype. Results demonstrate the existence of substrate with steep dispersion of repolarization and slow conduction, conditions that facilitate reentrant arrhythmias. However, arrhythmias were not recorded in any of the patients and the study does not provide direct information about the mechanism of VT in BrS patients.

Typically, BrS  $I_{Na}$  is reduced to approximately 50% relative to control. Figure 4-6 shows simulated behavior for a large range of  $I_{Na}$  reduction, paired with a range of  $I_{to}$  to account for its high density in the RVOT. Deepening and broadening of the phase-1 notch, resulting in APD prolongation, is obtained for the entire range of  $I_{Na}$  with  $G_{to} \geq 1.5$  times control. The accentuated notch and resulting transmembrane voltage gradients contribute to STE in BrS EGMs. However, loss of the dome and APD shortening at 50%  $I_{Na}$  required  $G_{to} \geq 3.3$  times control (at 1 Hz pacing). A previously characterized BrS gain-of-function mutation in  $I_{to}$ , L450F, was associated with a similarly large degree (~3-fold) of current increase.<sup>110</sup> It should be mentioned that the simulations were conducted in an isolated cell. In the multicellular substrate of BrS hearts, electrical loading on the AP dome during localized conduction delays (due to structural derangement) can contribute to premature repolarization, loss of the dome and short APD. In the 25 patients studied here, short ARIs were never observed.

## 4.6 Conclusions

Noninvasive ECGI reveals that the abnormal EP substrate in BrS patients is localized in the RVOT. Both abnormal repolarization and abnormal conduction are present in the substrate,

leading to steep repolarization gradients and delayed activation. In addition, ECGI could differentiate BrS from RBBB based on differences in patterns of activation and repolarization, and EGM morphology.

## **Chapter 5: Concluding Remarks and Future Work**

### **5.1 Concluding Remarks**

The studies presented here focused on clinical application of ECGI in patients with ischemic cardiomyopathy (ICM), early repolarization syndrome (ERS) and Brugada syndrome (BrS). As a research tool, ECGI has provided insights into the abnormal electrophysiological (EP) substrate that underlies these pathologies. (1) In ICM patients, the EP substrate associated with previous myocardial infarction is characterized by the presence of low-voltage and fractionated electrograms, late potentials and altered activation pattern during sinus rhythm. These properties reflect structure-based abnormal conduction through the scar substrate. ECGI correlates scar-related arrhythmia patterns with high-resolution maps of spatial characteristics of the scar EP substrate. It also identifies key epicardial EP properties that may account for the difference in ventricular tachycardia (VT) incidence between VT and non-VT patients. (2) In ERS patients, regions with epicardial J-waves and steep repolarization gradients caused by regional shortening of action potential duration are identified. Conduction abnormalities are not present. These EP properties may account for the arrhythmogenicity in this syndrome. Activation maps during premature ventricular contractions (PVCs) show that the PVC sites of origin are located in an epicardial region (inferior and lateral left ventricle) with marked J-waves and steep repolarization gradients, indicating that the EP substrate plays an important role in the development of arrhythmias. (3) In BrS patients, the abnormal EP substrate is localized exclusively in the right ventricular outflow tract (RVOT). The RVOT displays delayed activation, prolonged repolarization and steep repolarization gradients. These findings reveal the existence of both, abnormal repolarization and slow discontinuous conduction in the BrS substrate.

ECGI also demonstrates its potential usefulness in pre-procedural guidance for catheter ablation of scar-related ventricular tachycardia, arrhythmic risk stratification (criteria for ICD implantation) in ICM patients, and differentiation between malignant BrS and benign right bundle branch block.

## **5.2 Future Work**

The present studies demonstrate that ECGI is an important research tool for understanding the underlying EP substrate that predisposes patients to arrhythmias in various pathologies that involve conduction abnormality, repolarization abnormality, or both. More importantly, ECGI can be a useful clinical tool for improved diagnosis, treatment and risk stratification.

Studies in patients with ERS, BrS and long QT syndrome<sup>19</sup> (conducted by R. Vijayakumar et al.) constitute the first series of ECGI studies investigating the mechanisms of arrhythmogenesis and sudden cardiac death in hereditary cardiac disorders. These studies are very important because many of these patients are relatively young, healthy individuals without apparent structural heart disease. The very first symptoms they experience may be ventricular fibrillation. As pilot studies, the differences between genotypic subgroups were not investigated. Future studies should examine the relationship between the properties of EP substrate and genotype within each disease population.

Several drugs (e.g. quinidine, isoproterenol etc.) have been shown to have ameliorative effects on the ER and Brugada ECG patterns. Future studies should characterize drug effects on epicardial activation and repolarization patterns. The changes in activation and repolarization could provide additional information on the EP substrate and arrhythmia mechanisms associated with these disorders.

Arrhythmic risk stratification could be one of the main directions of future ECGI application. ICD has been prescribed for patients at the risk of ventricular arrhythmias; it is the most effective measure for preventing sudden cardiac death. Despite this critical benefit, ICD therapy is costly and can be associated with procedural complications and diminished quality of life. Current clinical criteria for identifying ICD candidates rely heavily on nonspecific ECG markers or reduction in global ventricular function (ejection fraction <35%). Only a small percentage of patients who meet the criteria and thus undergo device implantation receive appropriate defibrillation shocks. Development of selection criteria of higher specificity requires knowledge of the properties of the myocardial substrate such as slow, discontinuous conduction and repolarization gradients. As shown in the present studies, ECGI is able to image conduction delays, electrograms indicative of slow, discontinuous conduction and spatial dispersion of repolarization. However, due to the research-oriented nature, the generalizability of present studies is limited by the relatively small number of patients. Future large-scale ECGI studies should be conducted to establish the potential of the approach for noninvasive arrhythmic risk stratification.

On the technical side, the usability and compatibility of ECGI have been enhanced over the past few years. Examples include application of ECGI during exercise test to examine the effects of heart rate change, improvements in the software graphical user interface for faster data analysis and adaptation of ECGI mapping procedure to achieve compatibility with MRI, etc. Current data analysis involving low-voltage and fractionated electrograms is still challenging and time consuming. With sophisticated signal processing and machine learning algorithms, ECGI should be able to handle electrogram fractionation/late potential analysis and far-field potential detection with faster computing and higher accuracy.

## References

1. Oster HS, Taccardi B, Lux RL, Ershler PR and Rudy Y. Noninvasive electrocardiographic imaging: Reconstruction of epicardial potentials, electrograms, and isochrones and localization of single and multiple electrocardiac events. *Circulation*. 1997;96:1012-1024.
2. Oster HS, Taccardi B, Lux RL, Ershler PR and Rudy Y. Electrocardiographic imaging - Noninvasive characterization of intramural myocardial activation from inverse-reconstructed epicardial potentials and electrograms. *Circulation*. 1998;97:1496-1507.
3. Rudy Y. Electrocardiographic imaging - A noninvasive imaging modality for characterization of intramural myocardial activation. *Journal of electrocardiology*. 1999;32:1-6.
4. Burnes JE, Taccardi B and Rudy Y. A noninvasive imaging modality for cardiac arrhythmias. *Circulation*. 2000;102:2152-2158.
5. Burnes JE, Taccardi B, MacLeod RS and Rudy Y. Noninvasive ECG imaging of electrophysiologically abnormal substrates in infarcted hearts: A model study. *Circulation*. 2000;101:533-540.
6. Ghanem RN, Burnes JE, Waldo AL and Rudy Y. Imaging dispersion of myocardial repolarization, II: Noninvasive reconstruction of epicardial measures. *Circulation*. 2001;104:1306-1312.
7. Burnes JE, Ghanem RN, Waldo AL and Rudy Y. Imaging dispersion of myocardial repolarization, I: comparison of body-surface and epicardial measures. *Circulation*. 2001;104:1299-305.
8. Burnes JE, Taccardi B, Ershler PR and Rudy Y. Noninvasive electrocardiogram imaging of substrate and intramural ventricular tachycardia in infarcted hearts. *Journal of the American College of Cardiology*. 2001;38:2071-2078.
9. Ramanathan C, Jia P, Ghanem R, Calvetti D and Rudy Y. Noninvasive electrocardiographic imaging (ECGI): Application of the generalized minimal residual (GMRes) method. *Annals of biomedical engineering*. 2003;31:981-994.
10. Ramanathan C, Ghanem RN, Jia P, Ryu K and Rudy Y. Noninvasive electrocardiographic imaging for cardiac electrophysiology and arrhythmia. *Nature medicine*. 2004;10:422-428.

11. Ghanem RN, Jia P, Ramanathan C, Ryu K, Markowitz A and Rudy Y. Noninvasive electrocardiographic imaging (ECGI): Comparison to intraoperative mapping in patients. *Heart Rhythm*. 2005;2:339-354.
12. Ghosh S and Rudy Y. Accuracy of quadratic versus linear interpolation in noninvasive electrocardiographic imaging (ECGI). *Annals of biomedical engineering*. 2005;33:1187-1201.
13. Ramanathan C, Jia P, Ghanem R, Ryu K and Rudy Y. Activation and repolarization of the normal human heart under complete physiological conditions. *Proceedings of the National Academy of Sciences*. 2006;103:6309-6314.
14. Jia P, Ramanathan C, Ghanem RN, Ryu K, Varma N and Rudy Y. Electrocardiographic imaging of cardiac resynchronization therapy in heart failure: observation of variable electrophysiologic responses. *Heart Rhythm*. 2006;3:296-310.
15. Ghosh S, Cooper DH, Vijayakumar R, Zhang JJ, Pollak S, Haissaguerre M and Rudy Y. Early repolarization associated with sudden death: Insights from noninvasive electrocardiographic imaging. *Heart Rhythm*. 2010;7:534-537.
16. Cuculich PS, Zhang J, Wang Y, Desouza KA, Vijayakumar R, Woodard PK and Rudy Y. The electrophysiological cardiac ventricular substrate in patients after myocardial infarction: Noninvasive characterization with electrocardiographic imaging. *Journal of the American College of Cardiology*. 2011;58:1893-1902.
17. Wang Y, Cuculich PS, Zhang J, Desouza KA, Vijayakumar R, Chen J, Faddis MN, Lindsay BD, Smith TW and Rudy Y. Noninvasive electroanatomic mapping of human ventricular arrhythmias with electrocardiographic imaging. *Science translational medicine*. 2011;3:98ra84.
18. Ghosh S, Silva JNA, Canham RM, Bowman TM, Zhang J, Rhee EK, Woodard PK and Rudy Y. Electrophysiologic substrate and intraventricular left ventricular dyssynchrony in nonischemic heart failure patients undergoing cardiac resynchronization therapy. *Heart Rhythm*. 2011;8:692-699.
19. Vijayakumar R, Silva JNA, Desouza KA, Abraham RL, Strom M, Sacher F, Van Hare GF, Haissaguerre M, Roden DM and Rudy Y. Electrophysiologic Substrate in Congenital Long QT Syndrome: Noninvasive Mapping with Electrocardiographic Imaging (ECGI). *Circulation*. 2014;130:1936-1943.
20. Zhang J, Sacher F, Hoffmayer K, O'Hara T, Strom M, Cuculich P, Silva J, Cooper D, Faddis M, Hocini M, Haissaguerre M, Scheinman M and Rudy Y. Cardiac electrophysiologic

substrate underlying the ECG phenotype and electrogram abnormalities in Brugada syndrome patients. *Circulation*. 2015;131:1950-1959.

21. Barr RC, Ramsey M and Spach MS. Relating Epicardial to Body-Surface Potential Distributions by Means of Transfer-Coefficients Based on Geometry Measurements. *Ieee Transactions on Biomedical Engineering*. 1977;24:1-11.

22. Tikhonov A and Arsenin V. Solution of Ill-Posed Problems. 1977.

23. Franzone PC, Guerri L, Taccardi B and Viganotti C. The Direct and Inverse Potential Problems in Electrocardiology. Numerical Aspects of Some Regularization Methods and Application to Data Collected in Isolated Dog Heart Experiments. *Lab Anal Numerica CNR*. 1979:222.

24. Saad Y and Schultz MH. Gmres - a Generalized Minimal Residual Algorithm for Solving Nonsymmetric Linear-Systems. *Siam Journal on Scientific and Statistical Computing*. 1986;7:856-869.

25. Janse MJ and Wit AL. Electrophysiological mechanisms of ventricular arrhythmias resulting from myocardial ischemia and infarction. *Physiological reviews*. 1989;69:1049-1169.

26. Ursell PC, Gardner PI, Albala A, Fenoglio J and Wit AL. Structural and electrophysiological changes in the epicardial border zone of canine myocardial infarcts during infarct healing. *Circulation Research*. 1985;56:436-451.

27. Kløber AG and Rudy Y. Basic mechanisms of cardiac impulse propagation and associated arrhythmias. *Physiological reviews*. 2004;84:431-488.

28. Dillon SM, Allessie MA, Ursell PC and Wit AL. Influences of anisotropic tissue structure on reentrant circuits in the epicardial border zone of subacute canine infarcts. *Circulation Research*. 1988;63:182-206.

29. de Bakker J, van Capelle F, Janse MJ, Tasseron S, Vermeulen JT, de Jonge N and Lahpor JR. Slow conduction in the infarcted human heart. 'Zigzag' course of activation. *Circulation*. 1993;88:915-926.

30. Gonska B-D, Cao K, Schaumann A, Dorszewski A, von zur Mühlen F and Kreuzer H. Catheter ablation of ventricular tachycardia in 136 patients with coronary artery disease: results and long-term follow-up. *Journal of the American College of Cardiology*. 1994;24:1506-1514.



31. Harada T, Stevenson WG, Kocovic DZ and Friedman PL. Catheter ablation of ventricular tachycardia after myocardial infarction: relation of endocardial sinus rhythm late potentials to the reentry circuit. *Journal of the American College of Cardiology*. 1997;30:1015-1023.
32. Zei PC and Stevenson WG. Epicardial catheter mapping and ablation of ventricular tachycardia. *Heart Rhythm*. 2006;3:360-363.
33. Oza S and Wilber DJ. Substrate-based endocardial ablation of postinfarction ventricular tachycardia. *Heart Rhythm*. 2006;3:607-609.
34. Moss AJ, Zareba W, Hall WJ, Klein H, Wilber DJ, Cannom DS, Daubert JP, Higgins SL, Brown MW and Andrews ML. Prophylactic Implantation of a Defibrillator in Patients with Myocardial Infarction and Reduced Ejection Fraction. *New England Journal of Medicine*. 2002;346:877-883.
35. Haqqani HM, Kalman JM, Roberts-Thomson KC, Balasubramaniam RN, Rosso R, Snowdon RL, Sparks PB, Vohra JK and Morton JB. Fundamental differences in electrophysiologic and electroanatomic substrate between ischemic cardiomyopathy patients with and without clinical ventricular tachycardia. *Journal of the American College of Cardiology*. 2009;54:166-173.
36. de Bakker JM and van Rijen HV. Electrocardiographic manifestation of anatomical substrates underlying post-myocardial infarction tachycardias. *Journal of electrocardiology*. 2007;40:S21-S25.
37. Gardner PI, Ursell PC, Fenoglio JJ and Wit AL. Electrophysiologic and anatomic basis for fractionated electrograms recorded from healed myocardial infarcts. *Circulation*. 1985;72:596-611.
38. Wit AL and Josephson ME. Fractionated electrograms and continuous electrical activity: Fact or artifact. *Cardiac Electrophysiology and Arrhythmias*. 1985:343-351.
39. Vergara P, Trevisi N, Ricco A, Petracca F, Baratto F, Cireddu M, Bisceglia C, Maccabelli G and Della Bella P. Late potentials abolition as an additional technique for reduction of arrhythmia recurrence in scar related ventricular tachycardia ablation. *Journal of Cardiovascular Electrophysiology*. 2012;23:621-627.
40. Tsiachris D, Silberbauer J, Maccabelli G, Oloriz T, Baratto F, Mizuno H, Bisceglia C, Vergara P, Marzi A, Sora N, Guarracini F, Radinovic A, Cireddu M, Sala S, Gulletta S, Paglino G, Mazzone P, Trevisi N and Della Bella P. Electroanatomical Voltage and Morphology Characteristics in Post-Infarction Patients Undergoing Ventricular Tachycardia Ablation: A

Pragmatic Approach Favoring Late Potentials Abolition. *Circulation: Arrhythmia and Electrophysiology*. 2015:CIRCEP. 114.002551.

41. Jais P, Maury P, Khairy P, Sacher F, Nault I, Komatsu Y, Hocini M, Forclaz A, Jadidi AS, Weerasoorya R, Shah A, Derval N, Cochet H, Knecht S, Miyazaki S, Linton N, Rivard L, Wright M, Wilton SB, Scherr D, Pascale P, Roten L, Pederson M, Bordachar P, Laurent F, Kim SJ, Ritter P, Clementy J and Haissaguerre M. Elimination of Local Abnormal Ventricular Activities A New End Point for Substrate Modification in Patients With Scar-Related Ventricular Tachycardia. *Circulation*. 2012;125:2184-2196.

42. Silberbauer J, Oloriz T, Maccabelli G, Tsiachris D, Baratto F, Vergara P, Mizuno H, Bisceglia C, Marzi A, Sora N, Guarracini F, Radinovic A, Cireddu M, Sala S, Gulletta S, Paglino G, Mazzone P, Trevisi N and Della Bella P. Noninducibility and Late Potential Abolition A Novel Combined Prognostic Procedural End Point for Catheter Ablation of Postinfarction Ventricular Tachycardia. *Circulation: Arrhythmia and Electrophysiology*. 2014;7:424-435.

43. Baldinger SH, Nagashima K, Kumar S, Barbhaiya CR, Choi E-K, Epstein LM, Michaud GF, John R, Tedrow UB and Stevenson WG. Electrogram Analysis and Pacing Are Complimentary for Recognition of Abnormal Conduction and Far - Field Potentials during Substrate Mapping of Infarct - Related Ventricular Tachycardia *Circulation: Arrhythmia and Electrophysiology*. 2015:CIRCEP.114.002714.

44. Irie T, Yu R, Bradfield JS, Vaseghi M, Buch EF, Ajjola O, Macias C, Fujimura O, Mandapati R, Boyle NG, Shivkumar K and Tung R. Relationship Between Sinus Rhythm Late Activation Zones and Critical Sites for Scar-Related Ventricular Tachycardia: A Systematic Analysis of Isochronal Late Activation Mapping. *Circulation: Arrhythmia and Electrophysiology*. 2015:CIRCEP. 114.002637.

45. Cassidy DM, Vassallo JA, Miller JM, Poll DS, Buxton AE, Marchlinski FE and Josephson M. Endocardial catheter mapping in patients in sinus rhythm: relationship to underlying heart disease and ventricular arrhythmias. *Circulation*. 1986;73:645-652.

46. Wiener I, Mindich B and Pitchon R. Determinants of ventricular tachycardia in patients with ventricular aneurysms: results of intraoperative epicardial and endocardial mapping. *Circulation*. 1982;65:856-861.

47. Izquierdo M, Sanchez-Gomez JM, Loma-Osorio AFd, Martínez A, Bellver A, Pelaez A, Núñez J, Nuñez C, Chorro FJ and Ruiz-Granell R. Endo-Epicardial versus Only-Endocardial Ablation as a First Line Strategy for the Treatment of Ventricular Tachycardia in Patients with

Ischemic Heart Disease *Circulation: Arrhythmia and Electrophysiology*. 2015;CIRCEP.115.002827

48. Klatsky AL, Oehm R, Cooper RA, Udaltsova N and Armstrong MA. The early repolarization normal variant electrocardiogram: Correlates and consequences. *American Journal of Medicine*. 2003;115:171-177.
49. Tikkanen JT, Anttonen O, Junttila J, Aro AL, Kerola T, Rissanen HA, Reunanen A and Huikuri HV. Long-Term Outcome Associated with Early Repolarization on Electrocardiography. *New England Journal of Medicine*. 2009;361:2529-2537.
50. Gussak I and Antzelevitch C. Early repolarization syndrome: Clinical characteristics and possible cellular and ionic mechanisms. *Journal of electrocardiology*. 2000;33:299-309.
51. Kambara H and Phillips J. Long-Term Evaluation of Early Repolarization Syndrome (Normal Variant Rs-T Segment Elevation). *American Journal of Cardiology*. 1976;38:157-161.
52. Wasserburger RH and Alt WJ. The Normal RS-T Segment Elevation Variant. *The American journal of cardiology*. 1961;8:184-192.
53. Shu J, Zhu T, Yang L, Cui C and Yan G-X. ST-segment elevation in the early repolarization syndrome, idiopathic ventricular fibrillation, and the Brugada syndrome: cellular and clinical linkage. *Journal of electrocardiology*. 2005;38:26-32.
54. Otto CM, Tauxe RV, Cobb LA, Greene HL, Gross BW, Werner JA, Burroughs RW, Samson WE, Weaver WD and Trobaugh GB. Ventricular-Fibrillation Causes Sudden-Death in Southeast Asian Immigrants. *Annals of Internal Medicine*. 1984;101:45-47.
55. Garg A, Finneran W and Feld GK. Familial sudden cardiac death associated with a terminal QRS abnormality on surface 12-lead electrocardiogram in the index case. *Journal of Cardiovascular Electrophysiology*. 1998;9:642-647.
56. Kalla H, Yan GX and Marinchak R. Ventricular fibrillation in a patient with prominent J (Osborn) waves and ST segment elevation in the inferior electrocardiographic leads: A Brugada syndrome variant? *Journal of Cardiovascular Electrophysiology*. 2000;11:95-98.
57. Takeuchi T, Sato N, Kawamura Y, Takahashi F, Sato M, Kikuchi K, Akasaka N, Go K, Fujimoto K and Hasebe N. A case of a short-coupled variant of Torsades de Pointes with electrical storm. *Pace-Pacing and Clinical Electrophysiology*. 2003;26:632-636.

58. Boineau JP. The early repolarization variant--normal or a marker of heart disease in certain subjects. *J Electrocardiol.* 2007;40:3 e11-6.
59. Boineau JP. The early repolarization variant--an electrocardiographic enigma with both QRS and J-STT anomalies. *J Electrocardiol.* 2007;40:3 e1-10.
60. Haissaguerre M, Derval N, Sacher F, Jesel L, Deisenhofer I, de Roy L, Pasquie J, Nogami A, Babuty D, Yli-Mayry S, De Chillou C, Scanu P, Mabo P, Matsuo S, Probst V, Le Scouarnec S, Defaye P, Schlaepfer J, Rostock T, Lacroix D, Lamaison D, Lavergne T, Aizawa Y, Englund A, Anselme F, O'Neill M, Hocini M, Lim KT, Knecht S, Veenhuyzen GD, Bordachar P, Chauvin M, Jais P, Coureau G, Chene G, Klein GJ and Clementy J. Sudden cardiac arrest associated with early repolarization. *New England Journal of Medicine.* 2008;358:2016-2023.
61. Rosso R, Kogan E, Belhassen B, Rozovski U, Scheinman MM, Zeltser D, Halkin A, Steinvil A, Heller K, Glikson M, Katz A and Viskin S. J-point elevation in survivors of primary ventricular fibrillation and matched control subjects - Incidence and clinical significance. *Journal of the American College of Cardiology.* 2008;52:1231-1238.
62. Nam GB, Kim YH and Antzelevitch C. Augmentation of J waves and electrical storms in patients with early repolarization. *New England Journal of Medicine.* 2008;358:2078-2079.
63. Derval N, Simpson CS, Birnie DH, Healey JS, Chauhan V, Champagne J, Gardner M, Sanatani S, Yee R, Skanes AC, Gula LJ, Leong-Sit P, Ahmad K, Gollob MH, Haissaguerre M, Klein GJ and Krahn AD. Prevalence and Characteristics of Early Repolarization in the CASPER Registry Cardiac Arrest Survivors With Preserved Ejection Fraction Registry. *Journal of the American College of Cardiology.* 2011;58:722-728.
64. Aizawa Y, Chinushi M, Hasegawa K, Naiki N, Horie M, Kaneko Y, Kurabayashi M, Ito S, Imaizumi T, Aizawa Y, Takatsuki S, Joo K, Sato M, Ebe K, Hosaka Y, Haissaguerre M and Fukuda K. Electrical Storm in Idiopathic Ventricular Fibrillation Is Associated With Early Repolarization. *Journal of the American College of Cardiology.* 2013;62:1015-1019.
65. Tikkanen JT, Junttila MJ, Anttonen O, Aro AL, Luttinen S, Kerola T, Sager SJ, Rissanen HA, Myerburg RJ, Reunanen A and Huikuri HV. Early Repolarization Electrocardiographic Phenotypes Associated With Favorable Long-Term Outcome. *Circulation.* 2011;123:2666-2673.
66. Nam GB, Ko KH, Kim J, Park KM, Rhee KS, Choi KJ, Kim YH and Antzelevitch C. Mode of onset of ventricular fibrillation in patients with early repolarization pattern vs. Brugada syndrome. *European heart journal.* 2010;31:330-339.

67. Yan GX and Antzelevitch C. Cellular basis for the electrocardiographic J wave. *Circulation*. 1996;93:372-379.
68. Antzelevitch C and Yan GX. J wave syndromes. *Heart Rhythm*. 2010;7:549-558.
69. Haissaguerre M, Shoda M, Jais P, Nogami A, Shah DC, Kautzner J, Arentz T, Kalushe D, Lamaison D, Griffith M, Cruz F, de Paola A, Gaita F, Hocini M, Garrigue S, Macle L, Weerasooriya R and Clementy J. Mapping and ablation of idiopathic ventricular fibrillation. *Circulation*. 2002;106:962-967.
70. Haissaguerre M, Sacher F, Nogami A, Komiya N, Bernard A, Probst V, Yli-Mayry S, Defaye P, Aizawa Y, Frank R, Mantovan R, Cappato R, Wolpert C, Leenhardt A, de Roy L, Heidebuchel H, Deisenhofer I, Arentz T, Pasquie JL, Weerasooriya R, Hocini M, Jais P, Derval N, Bordachar P and Clementy J. Characteristics of Recurrent Ventricular Fibrillation Associated With Inferolateral Early Repolarization. *Journal of the American College of Cardiology*. 2009;53:612-619.
71. Coronel R, de Bakker JM, Wilms-Schopman FJ, Opthof T, Linnenbank AC, Belterman CN and Janse MJ. Monophasic action potentials and activation recovery intervals as measures of ventricular action potential duration: Experimental evidence to resolve some controversies. *Heart Rhythm*. 2006;3:1043-1050.
72. Durrer D, Van Dam RT, Freud G, Janse M, Meijler F and Arzbaecher R. Total excitation of the isolated human heart. *Circulation*. 1970;41:899-912.
73. Koncz I, Gurabi Z, Patocsikai B, Panama BK, Szel T, Hu D, Barajas-Martinez H and Antzelevitch C. Mechanisms underlying the development of the electrocardiographic and arrhythmic manifestations of early repolarization syndrome. *Journal of molecular and cellular cardiology*. 2014;68:20-28.
74. Topaz O and Edwards JE. Pathologic Features of Sudden-Death in Children, Adolescents, and Young-Adults. *Chest*. 1985;87:476-482.
75. Kramer MR, Drori Y and Lev B. Sudden-Death in Young Soldiers - High-Incidence of Syncope Prior to Death. *Chest*. 1988;93:345-347.
76. Rosso R, Glikson E, Belhassen B, Katz A, Halkin A, Steinvil A and Viskin S. Distinguishing "benign" from "malignant early repolarization": The value of the ST-segment morphology. *Heart Rhythm*. 2012;9:225-229.

77. Rollin A, Maury P, Bongard V, Sacher F, Delay M, Duparc A, Mondoly P, Carrie D, Ferrieres J and Ruidavets JB. Prevalence, Prognosis, and Identification of the Malignant Form of Early Repolarization Pattern in a Population-Based Study. *American Journal of Cardiology*. 2012;110:1302-1308.
78. Obeyesekere MN, Klein GJ, Nattel S, Leong-Sit P, Gula LJ, Skanes AC, Yee R and Krahn AD. A Clinical Approach to Early Repolarization. *Circulation*. 2013;127:1620-1629.
79. Mahida S, Derval N, Sacher F, Leenhardt A, Deisenhofer I, Babuty D, Schlapfer J, de Roy L, Frank R, Yli-Mayry S, Mabo P, Rostock T, Nogami A, Pasquie JL, de Chillou C, Kautzner J, Jesel L, Maury P, Berte B, Yamashita S, Roten L, Lim HS, Denis A, Bordachar P, Ritter P, Probst V, Hocini M, Jais P and Haissaguerre M. Role of Electrophysiological Studies in Predicting Risk of Ventricular Arrhythmia in Early Repolarization Syndrome. *Journal of the American College of Cardiology*. 2015;65:151-159.
80. Haissaguerre M, Chatel S, Sacher F, Weerasooriya R, Probst V, Loussouarn G, Horlitz M, Liersch R, Schulze-Bahr E, Wilde A, Kaab S, Koster J, Rudy Y, Le Marec H and Schott JJ. Ventricular Fibrillation with Prominent Early Repolarization Associated with a Rare Variant of KCNJ8/K-ATP Channel. *Journal of Cardiovascular Electrophysiology*. 2009;20:93-98.
81. Medeiros-Domingo A, Tan BH, Crotti L, Tester DJ, Eckhardt L, Cuoretti A, Kroboth SL, Song CH, Zhou Q, Kopp D, Schwartz PJ, Makielski JC and Ackerman MJ. Gain-of-function mutation S422L in the KCNJ8-encoded cardiac K-ATP channel Kir6.1 as a pathogenic substrate for J-wave syndromes. *Heart Rhythm*. 2010;7:1466-1471.
82. Barajas-Martinez H, Hu D, Ferrer T, Onetti CG, Wu YS, Burashnikov E, Boyle M, Surman T, Urrutia J, Veltmann C, Schimpf R, Borggreffe M, Wolpert C, Ibrahim BB, Sanchez-Chapula JA, Winters S, Haissaguerre M and Antzelevitch C. Molecular genetic and functional association of Brugada and early repolarization syndromes with S422L missense mutation in KCNJ8. *Heart Rhythm*. 2012;9:548-555.
83. Burashnikov E, Pfeiffer R, Barajas-Martinez H, Delpon E, Hu D, Desai M, Borggreffe M, Haissaguerre M, Kanter R, Pollevick GD, Guerchicoff A, Laino R, Marieb M, Nademanee K, Nam GB, Robles R, Schimpf R, Stapleton DD, Viskin S, Winters S, Wolpert C, Zimmern S, Veltmann C and Antzelevitch C. Mutations in the cardiac L-type calcium channel associated with inherited J-wave syndromes and sudden cardiac death. *Heart Rhythm*. 2010;7:1872-1882.
84. Watanabe H, Nogami A, Ohkubo K, Kawata H, Hayashi Y, Ishikawa T, Makiyama T, Nagao S, Yagihara N, Takehara N, Kawamura Y, Sato A, Okamura K, Hosaka Y, Sato M, Fukae S, Chinushi M, Oda H, Okabe M, Kimura A, Maemura K, Watanabe I, Kamakura S, Horie M,

Aizawa Y, Shimizu W and Makita N. Electrocardiographic Characteristics and SCN5A Mutations in Idiopathic Ventricular Fibrillation Associated With Early Repolarization. *Circulation-Arrhythmia and Electrophysiology*. 2011;4:874-881.

85. Noma A. Atp-Regulated K<sup>+</sup> Channels in Cardiac-Muscle. *Nature*. 1983;305:147-148.

86. Nichols CG, Ripoll C and Lederer WJ. ATP-Sensitive Potassium Channel Modulation of the Guinea-Pig Ventricular Action-Potential and Contraction. *Circulation Research*. 1991;68:280-287.

87. Nichols CG and Lederer WJ. Adenosine Triphosphate-Sensitive Potassium Channels in the Cardiovascular-System. *American Journal of Physiology*. 1991;261:H1675-H1686.

88. Shaw RM and Rudy Y. Electrophysiologic effects of acute myocardial ischemia: a theoretical study of altered cell excitability and action potential duration. *Cardiovascular research*. 1997;35:256-272.

89. Antzelevitch C and Yan G-X. J-wave syndromes: Brugada and early repolarization syndromes (in press). *Heart Rhythm*. 2015;doi:10.1016/j.hrthm.2015.04.014.

90. Frustaci A, Priori SG, Pieroni M, Chimenti C, Napolitano C, Rivolta I, Sanna T, Bellocci F and Russo MA. Cardiac histological substrate in patients with clinical phenotype of Brugada syndrome. *Circulation*. 2005;112:3680-3687.

91. Coronel R, Casini S, Koopmann TT, Wilms-Schopman FJ, Verkerk AO, de Groot JR, Bhuiyan Z, Bezzina CR, Veldkamp MW, Linnenbank AC, van der Wal AC, Tan HL, Brugada P, Wilde AA and de Bakker JM. Right ventricular fibrosis and conduction delay in a patient with clinical signs of Brugada syndrome: A combined electrophysiological, genetic, histopathologic, and computational study. *Circulation*. 2005;112:2769-2777.

92. Mahida S, Derval N, Sacher F, Berte B, Yamashita S, Hooks DA, Denis A, Lim H, Amraoui S, Aljefairi N, Hocini M, Jais P and Haissaguerre M. History and clinical significance of early repolarization syndrome. *Heart Rhythm*. 2015;12:242-249.

93. Antzelevitch C, Brugada P, Borggrefe M, Brugada J, Brugada R, Corrado D, Gussak I, LeMarec H, Nademanee K, Riera ARP, Shimizu W, Schulze-Bahr E, Tan HL and Wilde AA. Brugada syndrome: Report of the second consensus conference endorsed by the Heart Rhythm Society and the European Heart Rhythm Association. *Circulation*. 2005;111:659-670.

94. Brugada P and Brugada J. Right bundle branch block, persistent ST segment elevation and sudden cardiac death: A distinct clinical and electrocardiographic syndrome. A multicenter report. *Journal of the American College of Cardiology*. 1992;20:1391-1396.
95. Antzelevitch C. Cellular basis and mechanism underlying normal and abnormal myocardial repolarization and arrhythmogenesis. *Annals of medicine*. 2004;36:5-14.
96. Szé T and Antzelevitch C. Abnormal repolarization as the basis for late potentials and fractionated electrograms recorded from epicardium in experimental models of Brugada syndrome. *Journal of the American College of Cardiology*. 2014;63:2037-2045.
97. Aiba T, Shimizu W, Hidaka I, Uemura K, Noda T, Zheng C, Kamiya A, Inagaki M, Sugimachi M and Sunagawa K. Cellular Basis for Trigger and Maintenance of Ventricular Fibrillation in the Brugada Syndrome Model High-Resolution Optical Mapping Study. *Journal of the American College of Cardiology*. 2006;47:2074-2085.
98. Nademanee K, Veerakul G, Chandanamattha P, Chaothawe L, Ariyachaipanich A, Jirasirojanakorn K, Likittanasombat K, Bhuripanyo K and Ngarmukos T. Prevention of ventricular fibrillation episodes in Brugada syndrome by catheter ablation over the anterior right ventricular outflow tract epicardium. *Circulation*. 2011;123:1270-1279.
99. Tukkier R, Sogaard P, Vleugels J, de Groot IK, Wilde AA and Tan HL. Delay in right ventricular activation contributes to Brugada syndrome. *Circulation*. 2004;109:1272-1277.
100. Rudy Y. Noninvasive electrocardiographic imaging of arrhythmogenic substrates in humans. *Circulation Research*. 2013;112:863-874.
101. O'Hara T, Virág L, Varró A and Rudy Y. Simulation of the undiseased human cardiac ventricular action potential: Model formulation and experimental validation. *PLoS computational biology*. 2011;7:e1002061.
102. Clancy CE and Rudy Y. Na<sup>+</sup> channel mutation that causes both Brugada and Long-QT syndrome phenotypes: A simulation study of mechanism. *Circulation*. 2002;105:1208-1213.
103. Postema PG, van Dessel PF, de Bakker JM, Dekker LR, Linnenbank AC, Hoogendijk MG, Coronel R, Tijssen JG, Wilde AA and Tan HL. Slow and discontinuous conduction conspire in Brugada syndrome: A right ventricular mapping and stimulation study. *Circulation: Arrhythmia and Electrophysiology*. 2008;1:379-386.
104. Yokokawa M, Takaki H, Noda T, Satomi K, Suyama K, Kurita T, Kamakura S and Shimizu W. Spatial distribution of repolarization and depolarization abnormalities evaluated by body



surface potential mapping in patients with Brugada syndrome. *Pacing and clinical electrophysiology*. 2006;29:1112-1121.

105. Bójarov M, O'Hara T, Geelen JL, Jongbloed RJ, Timmermans C, Arens YH, Rodriguez L-M, Rudy Y and Volders PG. Subepicardial phase 0 block and discontinuous transmural conduction underlie right precordial ST-segment elevation by a SCN5A loss-of-function mutation. *American journal of physiology Heart and circulatory physiology*. 2008;295:H48-H58.

106. Nagase S, Kusano KF, Morita H, Nishii N, Banba K, Watanabe A, Hiramatsu S, Nakamura K, Sakuragi S and Ohe T. Longer repolarization in the epicardium at the right ventricular outflow tract causes type 1 electrocardiogram in patients with Brugada syndrome. *Journal of the American College of Cardiology*. 2008;51:1154-1161.

107. Tokioka K, Kusano K, Morita H, Miura D, Nishii N, Nagase S, Nakamura K, Kohno K, Ito H and Ohe T. Electrocardiographic parameters and fatal arrhythmic events in patients with Brugada syndrome: Combination of depolarization and repolarization abnormalities. *Journal of the American College of Cardiology*. 2014;63:2131-2138.

108. Lambiase P, Ahmed A, Ciaccio E, Brugada R, Lizotte E, Chaubey S, Ben-Simon R, Chow A, Lowe M and McKenna W. High-density substrate mapping in Brugada syndrome: Combined role of conduction and repolarization heterogeneities in arrhythmogenesis. *Circulation*. 2009;120:106-117.

109. Chiale PA, Garro HA, Fernández PA and Elizari MV. High-degree right bundle branch block obscuring the diagnosis of Brugada electrocardiographic pattern. *Heart Rhythm*. 2012;9:974-976.

110. Giudicessi JR, Ye D, Tester DJ, Crotti L, Mugione A, Nesterenko VV, Albertson RM, Antzelevitch C, Schwartz PJ and Ackerman MJ. Transient outward current (I<sub>to</sub>) gain-of-function mutations in the KCND3-encoded Kv4.3 potassium channel and Brugada syndrome. *Heart Rhythm*. 2011;8:1024-1032.

111. Auger D, Bleeker GB, Bertini M, Ewe SH, van Bommel RJ, Witkowski TG, Ng ACT, van Erven L, Schalij MJ and Bax JJ. Effect of cardiac resynchronization therapy in patients without left intraventricular dyssynchrony. *European Heart Journal*. 2012;33:913-920.

112. Silva JNA, Ghosh S, Bowman TM, Rhee EK, Woodard PK and Rudy Y. Cardiac resynchronization therapy in pediatric congenital heart disease: insights from noninvasive electrocardiographic imaging. *Heart Rhythm*. 2009;6:1178-1185.

## Appendix: Case Reports

### A1. Continuous ECGI Mapping of Spontaneous VT Initiation, Continuation and Termination with Antitachycardia Pacing

A 40-year-old woman with nonischemic cardiomyopathy and a left ventricular (LV)

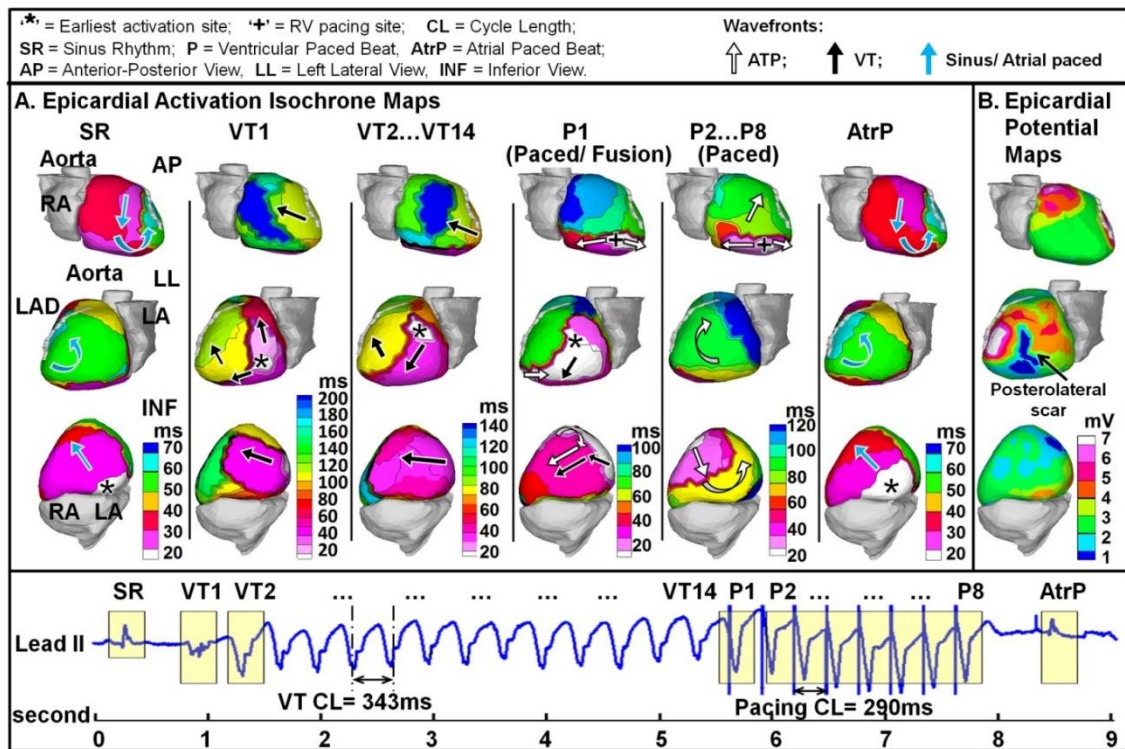


**Figure A- 1: Continuous ECGI Mapping of Spontaneous VT Initiation, Continuation and Termination with Antitachycardia Pacing**

Panel A: Epicardial Activation Isochrone Maps. Panel B: Epicardial Potential Maps.

ejection fraction of 35% was referred for recurrent ventricular tachycardia (VT). She experienced 248 VT episodes treated by antitachycardia pacing (ATP) over 14 days. In 2005, she received an implantable cardioverter defibrillator for an episode of syncope and nonsustained VT. She later underwent an invasive electrophysiology study (EPS) with inducible VT and an ablation of the AV nodal reentrant tachycardia. Since then, she experienced symptomatic VT, terminated by ATP.

Her VT was unresponsive to sotalol and mexiletine. Two EPS in early 2010 failed to induce VT despite intravenous isoproterenol and triple extrastimuli at two right ventricular (RV) sites; therefore, no ablations were performed.

Upon admission, the patient underwent noninvasive Electrocardiographic Imaging (ECGI).<sup>14, 18</sup> Movie A-1 (available in the attached CD) shows a continuous reconstruction of epicardial activation during initiation, continuation and termination by ATP of spontaneous VT during ECGI procedure. The images in Figure A-1 summarize the events. Note that the VT triggering beat differed in origin and activation sequence from the following beats of the sustained monomorphic VT. This first VT beat (VT1) originated from the inferolateral LV base, while subsequent VT beats (VT2...VT14) originated from the superolateral LV base with a cycle length (CL) of 343 ms. After 14 VT beats, ATP started pacing at 85% of VT CL. The first ATP beat (P1) was a fusion beat of the VT and right RV pacing wavefronts. The remainder ATP beats (P2...P8) captured the ventricles and showed exclusive RV pacing pattern. The recovered atrial paced beat following ATP was identical to the sinus beat before VT onset. ECGI identified a low-voltage zone (scar) on posterolateral LV (Figure A-1, Panel B, dark blue).

Following ECGI, monomorphic VT with a CL of 341 ms was induced with LV programmed stimulation in EPS. Pacing from the posterolateral LV scar yielded a QRS with a near-perfect match to the induced VT. Ablation in this region rendered the tachycardia noninducible. The patient has been arrhythmia-free during follow-up.

**Video File (available in the attached CD):**

Movie A-1: Wavefront propagation during VT initiation, continuation and termination by ATP. The activation wavefront is shown in red. An asterisk (\*) indicates the earliest epicardial activation site. A plus sign (+) indicates the right ventricular pacing site.

## **A2. Electrophysiologic Mechanism of Deteriorating Cardiac Function in a Patient with Inappropriate CRT Indication and Frequent Ventricular Ectopy**

An 84 y/o man had worsened symptoms (NYHA class III, LVEF 25%) following implant of a biventricular (BiV) cardioverter defibrillator (Biotronik, Lumax 540) at another institution. He also had frequent premature ventricular contractions (PVCs, 35%) that interfered with cardiac resynchronization therapy (CRT) and triggered BiV pacing. At electrophysiology (EP) study, the left ventricular (LV) lead was discovered to be within the anterior interventricular vein. His native QRS (113 ms) was much narrower than during CRT; thus, BiV pacing was disabled to allow for native conduction. The dominant clinical PVC was mapped and successfully ablated from the coronary cusps. His symptoms improved dramatically within days of the procedure and programming change. Prior to ablation, Electrocardiographic Imaging (ECGI)<sup>14, 18</sup> was applied to noninvasively map and study the mechanisms of pacing induced dyssynchrony (Figure A-2) and ineffectiveness of PVC-triggered pacing (Figure A-3).

This patient had a narrow QRS and consequently a predictable lack of benefit from CRT and inappropriate CRT indication. Moreover, his LV lead was anterior, which several studies have demonstrated not to be optimal for CRT. Inappropriate CRT in patients with synchronous LV activation could cause pacing induced dyssynchrony, leading to deteriorating LV function.<sup>18, 111</sup> In the context of heart failure, ECGI has been used to map the EP substrate,<sup>14</sup> to identify potential responders/nonresponders to CRT,<sup>18</sup> and to guide electrode placement.<sup>112</sup> Unlike the global body-surface QRSd, the ECGI derived cardiac electrical dyssynchrony (ED) index, computed as the standard deviation of all activation times on the LV, quantifies the spatial dispersion of activation over the LV (ED>28 ms is a marker of electrical dyssynchrony<sup>18</sup>).

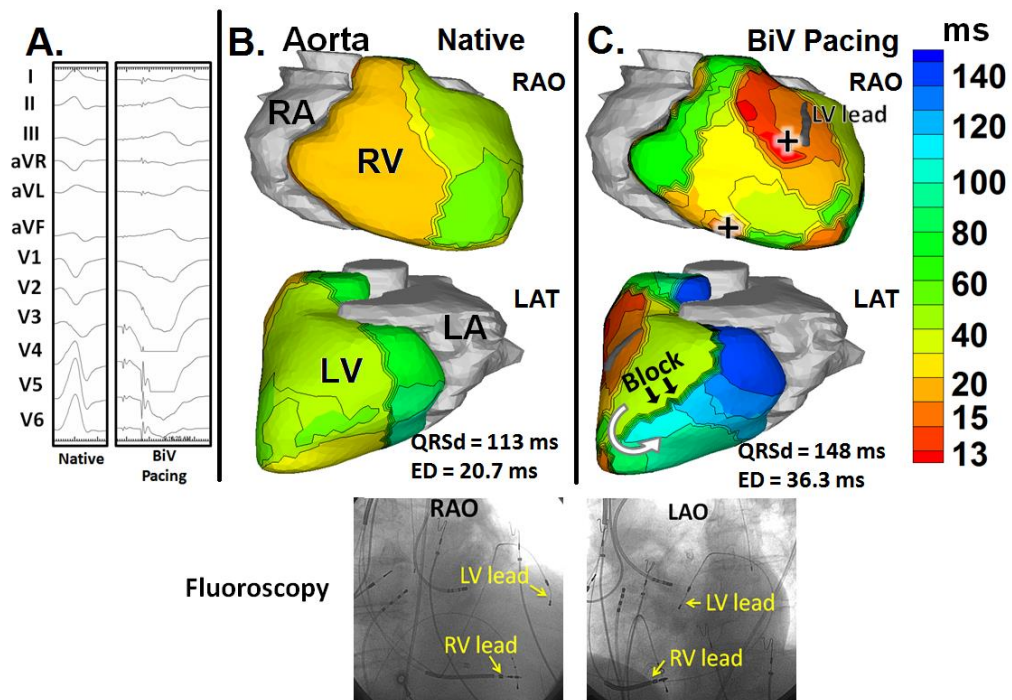


**Figure A- 2: Activation Isochrone Maps during Native Sinus Rhythm and BiV Pacing**

Panel A: QRS morphologies (12-lead ECG). Panel B: ECGI-reconstructed epicardial activation isochrones under native sinus rhythm. Panel C: Activation isochrones during BiV Pacing. Note that QRS in native sinus rhythm is much narrower than for BiV pacing. The activation maps are shown in right anterior oblique (top, RAO) and lateral (bottom, LAT) views. Pacing sites are indicated by plus signs(+). QRSd and ED index are computed for each rhythm. The white arrow highlights the U-shaped propagation pattern around a functional line of block (black arrows) during BiV Pacing, which induced dyssynchrony. Inset: Fluoroscopy images showing the pacing lead positions in RAO and left anterior oblique (LAO) views. RA= right atrium; LA= left atrium; RV= right ventricle; LV= left ventricle.

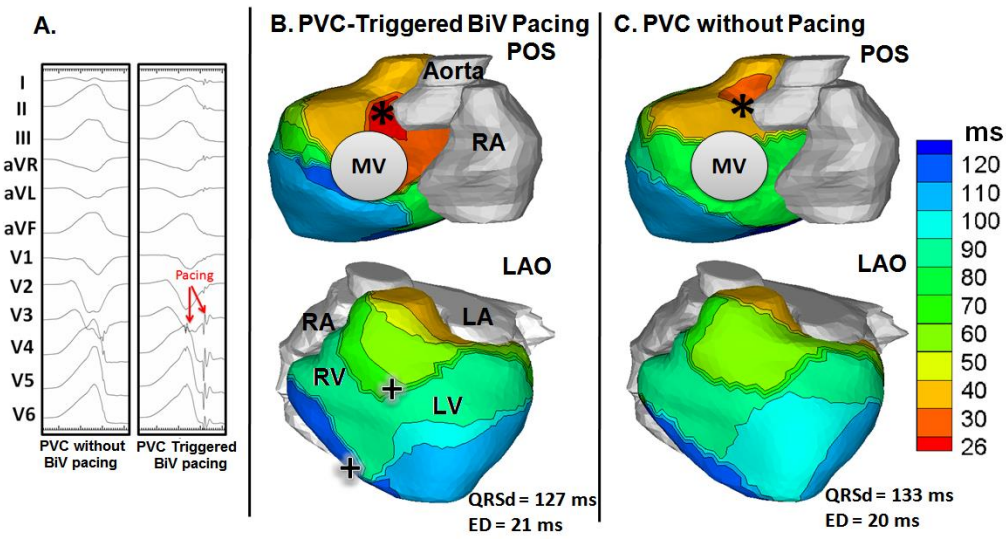


**Figure A- 3: PVC Activation Isochrone Maps with and without Pacing**

Panel A: QRS morphologies (12-lead ECG). Panel B: ECGI activation Isochrone maps during PVC-triggered BiV pacing. Panel C: ECGI activation Isochrone maps during spontaneous PVC without pacing. The activation maps are shown in posterior (top, POS) and left anterior oblique (bottom, LAO) views. Pacing sites are indicated by plus signs (+). The earliest epicardial activation is marked with an asterisk (\*). RA= right atrium; LA= left atrium; MV= mitral valve. PVC-triggered BiV pacing did not change the QRS morphology of the PVC (pacing occurred during the PVC, too late to capture). There was no appreciable effect of pacing on the PVC (Panel B, compare to Panel C). Both rhythms had identical activation patterns and similar ED and QRSd values.

As shown in the ECGI image of Figure A-2, pacing from the early-activated LV anterior wall during BiV created a functional line-of-block. This forced the activation front to propagate in a U-shaped pattern around the line-of-block, causing late dyssynchronous activation of the lateral LV base. The image in Figure A-3 shows that during PVC-triggered pacing, the PVC site of origin was in close proximity to the anterior LV lead, but far from the RV sensing lead, which caused delayed sensing and pacing. Thus, BiV pacing triggered by PVC failed to capture the (already activated) ventricles and was ineffective. Because in many similar cases PVCs can impede the effective delivery of continuous CRT, PVC treatment (catheter ablation or antiarrhythmic drugs) to ensure high percentage of effective BiV pacing might be considered.

# Curriculum Vitae

Junjie Zhang

Department of Biomedical Engineering

Washington University in St. Louis,

One Brookings Drive,

St. Louis, MO 63130

Office: 314-935-8163

Email: [zhangjunjie@go.wustl.edu](mailto:zhangjunjie@go.wustl.edu)

## Education

Ph.D. in Biomedical Engineering

Washington University in St. Louis, December 2015

B.S. in Biomedical Engineering

Zhejiang University, China, July 2008

## Award

Second prize in the research poster and presentation competition at Gordon Research Conference on Cardiac Arrhythmia Mechanisms, Galveston, TX, February 2011

## Publication and Abstract

### Peer-Reviewed Journals

1. S. Ghosh, D.H. Cooper, R. Vijayakumar, **J. Zhang**, S. Pollack, M. Haïssaguerre, Y. Rudy, Early "Repolarization Associated with Sudden Death: Insights From Noninvasive Electrocardiographic Imaging." *Heart Rhythm* 2010;7:534-537
2. Y. Wang, P.S. Cuculich, **J. Zhang**, K.A. Desouza, R. Vijayakumar, J. Chen, M.N. Faddis, B.D. Lindsay, T.W. Smith, Y. Rudy, "Noninvasive Electroanatomic Mapping of Human Ventricular Arrhythmias Using ECG Imaging (ECGI)." *Science Translational Medicine* 2011;3:98ra84
3. P.S. Cuculich, **J. Zhang\***, Y. Wang, K.A. Desouza, R. Vijayakumar, P.K. Woodard, Y. Rudy, "The Electrophysiologic Cardiac Ventricular Substrate in Patients after Myocardial Infarction: Noninvasive Characterization with ECG Imaging (ECGI)." *Journal of the American College of Cardiology* 2011;58:1893-1902
4. **J. Zhang**, K.A. Desouza, P.S. Cuculich, D.H. Cooper, J. Chen, Y. Rudy, "Continuous ECGI Mapping of Spontaneous VT Initiation, Continuation and Termination with Antitachycardia Pacing." *Heart Rhythm* 2012;10:1244-1245
5. **J. Zhang**, D.H. Cooper, Y. Rudy, "Electrophysiologic Mechanism of Deteriorating Cardiac Function in a Patient with Inappropriate CRT Indication and Frequent Ventricular Ectopy." *Pacing and Clinical Electrophysiology* 2013;36:1024-1026
6. **J. Zhang**, F. Sacher, K. Hoffmayer, T. O'Hara, M. Strom, P.S. Cuculich, J.N. Silva, D.H. Cooper, M.N. Faddis, M. Hocini, M. Haïssaguerre, M. Scheinman, Y. Rudy, "Cardiac Electrophysiologic Substrate Underlying the ECG Phenotype and Electrogram Abnormalities in Brugada Syndrome Patients." *Circulation* 2015;131:1950-1959
7. **J. Zhang**, D.H. Cooper, K.A. Desouza, P.S. Cuculich, P.K. Woodard, T.W. Smith, Y. Rudy, "Noninvasive High-Resolution Cardiac Mapping in Ischemic Cardiomyopathy Patients: the Electrophysiological Substrate in Relation to Ventricular Arrhythmias and Arrhythmic Risk." *Circulation: Arrhythmia and Electrophysiology* 2015 (submitted)

---

\* Joint first authorship with P.S.C. and Y.W.



8. **J. Zhang**, F. Sacher, M. Strom, P.S. Cuculich, D.H. Cooper, M. Hocini, M. Haïssaguerre, Y. Rudy, "The Electrophysiological Substrate of Early Repolarization Syndrome: Noninvasive Mapping in Patients" (in preparation)

## Abstracts

1. **J. Zhang**, P.S. Cuculich, Y. Wang, K.A. Desouza, R. Vijayakumar, P.K. Woodard, Y. Rudy, "Characterization of Electrophysiologic Substrate in Post-Myocardial Infarction Patients using Noninvasive Electrocardiographic Imaging (ECGI)." Gordon Research Conference on Cardiac Arrhythmia Mechanisms, Galveston, TX, February 2011
2. **J. Zhang**, D.H. Cooper, K.A. Desouza, S.B. Marrus, D.R. Fansler, P.S. Cuculich, T.W. Smith, Y. Rudy, "ECG Imaging (ECGI) of Electrophysiologic Substrate in Ischemic Cardiomyopathy: Differences in Patients with and without Ventricular Tachycardia (VT)." Heart Rhythm Society 32nd Annual Scientific Sessions, San Francisco, California, May 2011. Heart Rhythm 2011;8, issue 5S: S480
3. **J. Zhang**, K.A. Desouza, P.S. Cuculich, D.H. Cooper, J. Chen, Y. Rudy, "Noninvasive Electrocardiographic Imaging of Spontaneous Ventricular Tachycardia Initiation and Termination with Antitachycardia Pacing." Heart Rhythm Society 32nd Annual Scientific Sessions, San Francisco, California, May 2011. Heart Rhythm 2011;8, issue 5S: S341
4. **J. Zhang**, F. Sacher, K. Hoffmayer, M. Strom, P. Cuculich, J. Silva, D. Cooper, M. Faddis, M. Hocini, M. Haïssaguerre, M. Scheinman, Y. Rudy, "ECG Imaging of Electrophysiologic Substrate in Brugada Syndrome Patients." Heart Rhythm Society 35th Annual Scientific Sessions, San Francisco, California, May 2014. Heart Rhythm 2014;11, issue 5S: S161.